1-1-2017

Specimen-Specific Natural, Pathological, and Implanted Knee Mechanics Using Finite Element Modeling

Azhar Akber Ali
University of Denver

Specimen-Specific Natural, Pathological, and Implanted Knee Mechanics Using Finite Element Modeling

Abstract

There is an increasing incidence of knee pain and injury among the population, and increasing demand for higher knee function in total knee replacement designs. As a result, clinicians and implant manufacturers are interested in improving patient outcomes, and evaluation of knee mechanics is essential for better diagnosis and repair of knee pathologies. Common knee pathologies include osteoarthritis (degradation of the articulating surfaces), patellofemoral pain, and cruciate ligament injury and/or rupture. The complex behavior of knee motion presents unique challenges in the diagnosis of knee pathology and restoration of healthy knee function. Quantifying knee mechanics is essential for developing successful rehabilitation therapies and surgical treatments. Researchers have used in-vitro and in-vivo experiments to quantify joint kinematics and loading, but experiments can be costly and time-intensive, and contact and ligament mechanics can be difficult to measure directly. Computational modeling can complement experimental studies by providing cost-effective solutions for quantifying joint and soft tissue forces. Musculoskeletal models have been used to measure whole-body motion, and predict joint and muscle forces, but these models can lack detail and accuracy at the joint-level. Finite element modeling provides accurate solutions of the internal stress/strain behavior of bone and soft tissue using subject-specific geometry and complex contact and material representations. While previous FE modeling has been used to simulate injury and repair, models are commonly based on literature description or average knee behavior. The research presented in this dissertation focused on developing subject-specific representations of the TF and PF joints including calibration and validation to experimental data for healthy, pathological, and implanted knee conditions. A combination of in-vitro experiment and modeling was used to compare healthy and cruciate-deficient joint mechanics, and develop subject-specific computational representations. Insight from in-vitro testing supported in-vivo simulations of healthy and implanted subjects, in which PF mechanics were compared between two common patellar component designs and the impact of cruciate ligament variability on joint kinematics and loads was assessed. The suite of computational models developed in this dissertation can be used to investigate knee pathologies to better inform clinicians on the mechanisms surrounding injury, support the diagnosis of at-risk patients, explore rehabilitation and surgical techniques for repair, and support decision-making for new innovative implant designs.

Document Type

Dissertation

Degree Name

Ph.D.

Department

Mechanical Engineering

First Advisor

Paul J. Rullkoetter, Ph.D.

Second Advisor

Kevin Shelburne

Third Advisor

Chadd Clary

Keywords
Biomechanics, Finite element, Knee, Modeling

Subject Categories
Biomechanics and Biotransport

Specimen-Specific Natural, Pathological, and Implanted Knee Mechanics Using Finite Element Modeling

---

A Dissertation

Presented to

the Faculty of the Daniel Felix Ritchie School of Engineering and Computer Science

University of Denver

In Partial Fulfillment

of the Requirements for the Degree

Doctor of Philosophy

---

by

Azhar Ali

August 2017

Advisor: Paul J. Rullkoetter

Author: Azhar Ali
Title: Specimen-Specific Natural, Pathological, and Implanted Knee Mechanics Using Finite Element Modeling
Advisor: Paul J. Rullkoetter
Degree date: August 2017

ABSTRACT

There is an increasing incidence of knee pain and injury among the population, and increasing demand for higher knee function in total knee replacement designs. As a result, clinicians and implant manufacturers are interested in improving patient outcomes, and evaluation of knee mechanics is essential for better diagnosis and repair of knee pathologies. Common knee pathologies include osteoarthritis (degradation of the articulating surfaces), patellofemoral pain, and cruciate ligament injury and/or rupture. The complex behavior of knee motion presents unique challenges in the diagnosis of knee pathology and restoration of healthy knee function. Quantifying knee mechanics is essential for developing successful rehabilitation therapies and surgical treatments. Researchers have used in-vitro and in-vivo experiments to quantify joint kinematics and loading, but experiments can be costly and time-intensive, and contact and ligament mechanics can be difficult to measure directly. Computational modeling can complement experimental studies by providing cost-effective solutions for quantifying joint and soft tissue forces. Musculoskeletal models have been used to measure whole-body motion, and predict joint and muscle forces, but these models can lack detail and accuracy at the joint-level. Finite element modeling provides accurate solutions of the internal stress/strain behavior of bone and soft tissue using subject-specific geometry and complex contact and material representations. While previous FE modeling has been

used to simulate injury and repair, models are commonly based on literature description or average knee behavior. The research presented in this dissertation focused on developing subject-specific representations of the TF and PF joints including calibration and validation to experimental data for healthy, pathological, and implanted knee conditions. A combination of in-vitro experiment and modeling was used to compare healthy and cruciate-deficient joint mechanics, and develop subject-specific computational representations. Insight from in-vitro testing supported in-vivo simulations of healthy and implanted subjects, in which PF mechanics were compared between two common patellar component designs and the impact of cruciate ligament variability on joint kinematics and loads was assessed. The suite of computational models developed in this dissertation can be used to investigate knee pathologies to better inform clinicians on the mechanisms surrounding injury, support the diagnosis of at-risk patients, explore rehabilitation and surgical techniques for repair, and support decision-making for new innovative implant designs.

TABLE OF CONTENTS

LIST OF FIGURES VII

ACKNOWLEDGEMENTS X

CHAPTER 1 – INTRODUCTION 1
1.1 INTRODUCTION 1
1.2 DISSERTATION OVERVIEW 5

CHAPTER 2 – BACKGROUND & MOTIVATION 8
2.1 QUADRICEPS MECHANISM 8
2.2 PATELLOFEMORAL PATHOLOGY 10
2.3 CRUCIATE INJURY AND FUNCTION 11
2.4 INTERDEPENDENCE OF TIBIOFEMORAL AND PATELLOFEMORAL JOINTS 12
2.5 PASSIVE CONSTRAINT 14
2.6 TOTAL KNEE ARTHROPLASTY 15
2.7 TECHNIQUES FOR EVALUATION OF KNEE BIOMECHANICS 17
2.7.1 In-Vivo Experiments 17
2.7.2 In-Vitro Experiments 19
2.7.3 Musculoskeletal Modeling 22
2.7.4 Finite Element Modeling 24

CHAPTER 3 – VALIDATION OF PREDICTED PATELLOFEMORAL MECHANICS IN A FINITE ELEMENT MODEL OF THE HEALTHY AND CRUCIATE-DEFICIENT KNEE 39
3.1 ABSTRACT 39
3.2 INTRODUCTION 40
3.3 METHODS 44
3.3.1 Experimental Testing 44
3.3.2 Computational Modeling 45
3.4 RESULTS 48
3.4.1 PF Kinematics 48
3.4.2 Quadriceps Forces 49
3.4.3 Patellar Tendon Moment Arm 49
3.4.4 Patellar Tendon Angle 50

3.4.5 Patellar Force Ratio....50
3.4.6 PF Contact....51
3.5 Discussion....51

CHAPTER 4 – COMBINED MEASUREMENT AND MODELING OF SPECIMEN-SPECIFIC KNEE MECHANICS FOR HEALTHY AND ACL-DEFICIENT CONDITIONS....64
4.1 Abstract....64
4.2 Introduction....65
4.3 Methods....68
4.3.1 Summary....68
4.3.2 Experimental Setup....69
4.3.3 Computational Modeling....70
4.4 Results....74
4.4.1 TF Kinematics....74
4.4.2 PF Kinematics....75
4.4.3 Quadriceps Force....75
4.4.4 Contact Force....76
4.4.5 Ligament Forces....76
4.5 Discussion....77

CHAPTER 5 – EVALUATION OF IN-VIVO MECHANICS FOR MEDIALIZED DOME AND ANATOMIC PATELLOFEMORAL GEOMETRIES DURING KNEE EXTENSION AND LUNGE....90
5.1 Abstract....90
5.2 Introduction....91
5.3 Methods....95
5.3.1 Data Collection....96
5.3.2 Musculoskeletal Modeling....97
5.3.3 Finite Element Modeling....98
5.4 Results....101
5.4.1 PF Kinematics....101
5.4.2 Quadriceps Force....102
5.4.3 Contact Force and Force Ratio....102
5.4.4 Patellar Force Ratio....103
5.4.5 Patellar Tendon Moment Arm....103
5.4.6 Patellar Tendon Angle....104
5.5 Discussion....104

CHAPTER 6 – AN EXPERIMENTAL AND COMPUTATIONAL MODELING FRAMEWORK FOR EVALUATION OF IN-VIVO KNEE MECHANICS DURING KNEE EXTENSION AND LUNGE....117
6.1 Introduction....117
6.2 Methods....121
6.2.1 Data Collection....121

6.2.2 Musculoskeletal Modeling 122
6.2.3 Finite Element Modeling 123
6.3 RESULTS 129
6.3.1 Experimental kinematics 129
6.3.2 Quadriceps and Hamstrings Forces 129
6.3.3 Knee Extension Model Kinematics 130
6.3.4 Lunge Model Kinematics 130
6.3.5 Joint Contact Forces 131
6.3.6 Ligament Forces 131
6.3.7 Sensitivity Analysis 132
6.4 DISCUSSION 133

CHAPTER 7 – CONCLUSIONS & RECOMMENDATIONS 145
7.1 CONCLUSION 145
7.2 RECOMMENDATIONS 149
7.3 CLOSING 155

LIST OF REFERENCES 157

APPENDIX A: SUBJECT-SPECIFIC PREDICTIONS OF MECHANICS FOR MEDIALIZED DOME AND ANATOMIC PATELLAE 173

LIST OF FIGURES

Figure 2.1 Free body diagram of the patellar mechanism from (Buff et al., 1988) illustrating the forces acting on the patella. Fq=quadriceps force, Fp=patellar tendon force, and PFJR=patellofemoral joint reaction force 30
Figure 2.2 Patellar shape and alignment characteristics correlated to patellar maltracking by (Pal et al., 2012): patellar tilt, bisect offset (BO) 31
Figure 2.3 The effect of q-angle on lateral patellar maltracking. Q-angle is measured as the frontal plane angle between the quadriceps line of action and patellar tendon line of action. Increased q-angle leads to increased lateral forces on the patella. (Powers, 2003) 32
Figure 2.4 Passive joint laxity experiments performed by (Harris et al., 2016) for evaluation of TF soft tissue constraint and for calibration of finite element representations of ligament structures 33
Figure 2.5 Illustration of total knee arthroplasty components aligned to the native bone geometry. Implant components include femoral, patellar button, tibial tray and insert components. 34
Figure 2.6 Three-dimensional rendering of high-speed stereo radiographic measurement of joint kinematics for total knee replacement patients. 3D implant geometry is simultaneously aligned to bi-plane 2D radiography images for computation of relative joint motions. 35
Figure 2.7 In-vitro experimental knee simulators designed to apply dynamic loading using muscle-actuated forces. (Amis et al., 2006; Baldwin et al., 2012; Mizuno et al., 2001; Shalhoub and Maletsky, 2014) 36
Figure 2.8 Musculoskeletal model of the lower limb and knee joint developed by (Shelburne et al., 2004a) for evaluation of ligament forces during walking. 37
Figure 2.9 Open Knee: a detailed finite element representation of the knee joint with subject-specific geometry and complex material and contact definitions. ... 38

Figure 3.1 Knee cadaver mounted in muscle loading rig (MLR) (right) and its computational representation (left) 57
Figure 3.2 Experimental TF kinematics for the intact, ACL-deficient, and PCL deficient conditions (VV: varus(+)/valgus(-), IE: internal(+)/external(-), ML: medial(-)/lateral(+), AP: anterior(+)/posterior(-), SI: superior(+)/inferior(-)) 58
Figure 3.3 a) Comparison of experimental and model predicted PF kinematics in the intact (left), ACL-deficient (middle), and PCL-deficient (right) conditions averaged across specimens. b) Uncertainty in model PF kinematics (F-E, I-E, and M-L) shown for 3 intact specimens with experimental (solid line), model (dashed line),

and bounds of uncertainty (shaded region). (FE: flexion(+)/extension(-), VV: varus(+)/valgus(-), IE: internal(+)/external(-), ML: medial(-)/lateral(+), AP: anterior(+)/posterior(-), SI: superior(+)/inferior(-)) 59
Figure 3.4 Model predicted quadriceps forces in the intact (left), ACL-deficient (middle), PCL-deficient (right) conditions 60
Figure 3.5 a) Patellar tendon moment arm, b) patellar tendon angle, c) patellar force ratio, and d) contact to quadriceps force ratio presented for intact and cruciate-deficient conditions. Shaded regions represent the span of experimental data from literature sources (Ahmed et al., 1987; Buff et al., 1988; Grood et al., 1984; Yamaguchi and Zajac, 1989) 61
Figure 3.6 a) PF contact pressure distributions shown in a representative specimen at knee flexion angles of 0°, 30°, 60°, and 90°. b) PF contact center of pressure through the flexion activity and c) contact distribution at ~90° is shown for a representative specimen in intact and cruciate-deficient conditions. 62

Figure 4.1 Knee cadaver mounted in the Kansas Knee Simulator (KKS) (left), and its computational representation (middle) with specimen-specific TF and PF soft tissue structures (right): anterior cruciate ligament (**ACLam**, **ACLpl**), posterior cruciate ligament (**PCLal**, **PCLpm**), lateral collateral ligament (**LCL**), popliteofibular ligament (**PFL**), medial collateral ligament (**MCL**), superficial medial collateral ligament (**DMCL**), posterior oblique ligament (**POL**), anterolateral structure (**ALS**), posterior capsule (**PCAPM**, **PCAPL**) 84
Figure 4.2 Comparison of model (dashed) and experimental (solid) TF kinematics in the KKS simulator for intact and ACL-resected conditions in two specimens .. 85
Figure 4.3 Comparison of model (dashed) and experimental (solid) PF kinematics in the KKS simulator for intact and ACL-resected conditions in two specimens .. 86
Figure 4.4 Comparison of model (dashed) and experimental (solid) quadriceps force in the KKS simulator for intact and ACL-resected conditions in two specimens87
Figure 4.5 Total TF and PF contact force (left) and contact center of pressure with force vectors (right) shown for two specimens in intact and ACL-deficient conditions 88
Figure 4.6 Ligament recruitment as a function of knee flexion (left), and total ligament shear and tensile forces (right) for intact (solid) and ACL-deficient (dashed) conditions in two specimens 89

Figure 5.1 Workflow for the current study describing a) HSSR measurements of the knee extension and lunge activities, b) motion capture and force plate data used to drive musculoskeletal simulations, and c) subject-specific finite element modeling for the evaluation of PF mechanics 111
Figure 5.2 Comparison of average +/- 1 standard deviation experimental (-) and model (--) PF kinematics for medialized anatomic and medialized dome implants.. 112
Figure 5.3 Average (line) ± 1 standard deviation (shaded) of patellotibial flexion-extension for natural knees, and medialized dome and medialized anatomic implants during lunge 113

Figure 5.4 Average +/- 1 standard deviation of quadriceps force predictions from musculoskeletal modeling for knee extension and lunge..... 114
Figure 5.5 Comparison of mean (line) and ± 1 standard deviation (shaded) of a) contact force ratio and b) patellar force ratio between medialized dome, medialized anatomic, and natural subjects (Ahmed et al., 1987). Force ratios (right) shown for the lunge activity: Fc = contact force, Fq = quadriceps force, Fpt = patellar tendon force. 115

Figure 6.1 Experiment and computational modeling workflow including a) data collection of HSSR images, motion capture, and ground reaction forces, b) whole-body musculoskeletal modeling, and c) detailed, subject-specific finite element modeling for knee extension and lunge activities 139
Figure 6.2 Comparison of model and experimental TF and PF kinematics for the knee extension activity: experiment (-), initial estimate of soft tissue properties from (Harris et al., 2016) (--), ACL-deficient, PCL-deficient, and calibrated model predictions 141
Figure 6.3 a) Comparison of model and experimental TF kinematics for the lunge activity: a) experiment and calibrated model predictions, b) sensitivity analysis comparing the impact of mean ± 1 standard deviation of ligament stiffness (K) and reference strain (EREF) on TF internal-external and anterior-posterior kinematics. Mean and standard deviations obtained from the literature (see Table 1). . 142
Figure 6.4 a) Total TF contact force, b) PF contact force (middle), and c) comparison of TF contact forces between calibrated, mean, and ±1 standard deviation of ligament stiffness and reference strain analyses during the lunge activity. 143
Figure 6.5 a) Total tensile and shear ligament forces, b) individual ligament forces, and c) comparison of total ligament force between calibrated, mean, and standard deviation of ligament stiffness and reference strain analyses during the lunge activity. 144

Figure A.1 Comparison of average +/- 1 standard deviation of experimental PF kinematics for medialized dome and anatomic subjects performing the knee extension and lunge. Subject-specific PF kinematics are shown using thin solid lines. 174
Figure A.2 Comparison of average +/- 1 standard deviation of experimental TF low point kinematics for medialized dome and anatomic subjects performing the knee extension and lunge. Subject-specific low point data are shown using thin solid lines. 175
Figure A.3 Subject-specific quadriceps force predictions from musculoskeletal modeling for knee extension and lunge 176
Figure A.4 Comparison of a) contact force ratio and b) patellar force ratio between medialized dome and anatomic subjects. Force ratios (right) shown for the lunge activity: Fc = contact force, Fq = quadriceps force, Fpt = patellar tendon force. 176
Figure A.5 Comparison of a) patellar tendon moment arm and b) patellar tendon angle between medialized dome and anatomic subjects. Results shown for knee extension only..... 177

ACKNOWLEDGEMENTS

I would like to thank, first and foremost, my advisors and committee members Dr. Kevin Shelburne, Dr. Paul Rullkoetter, Dr. Peter Laz, and Dr. Chadd Clary for their support and guidance throughout my time at the University of Denver. Dr. Rullkoetter and Dr. Laz, thank you for the opportunity to work in the Computational Biomechanics Lab since my sophomore undergraduate year, it inspired my passion for orthopaedic biomechanics. Dr. Shelburne was a part of my first project in the Computational Biomechanics Lab, and he served as my primary advisor for my PhD: thank you for your support on the research projects, and for sharing your knowledge and experience over the years. Dr. Clary and Dr. Clare Fitzpatrick, thank you for teaching me the technical skills necessary to be successful in the orthopaedics industry.

I would also like to thank my parents, Akber and Nasim Ali, and my siblings, Anil and Anita, for their unwavering support. In particular, I would like to thank my parents for the tremendous sacrifices that they have made towards my success.

Finally, I am grateful to all friends, graduate students, and post-doctorates for the encouraging words and memorable moments during my time at DU.

CHAPTER 1 – INTRODUCTION

1.1 Introduction

Biomechanics is the study of the mechanical laws governing the motion of an organism, including the kinematics and kinetics associated with that motion. The focus of this dissertation work is in the biomechanics of the human knee due to the over 65% increase in prevalence of knee pain and injury in the last 20 years and the increase in total knee replacement (TKR) surgeries (Arendt and Dick, 1995; Nguyen et al., 2011). When compared to different joints in the human body, the knee is uniquely complex in its behavior due to the combination of rolling and sliding movement, and substantial weight-bearing joint loads; as a result, repair of the knee joint from damaged tissue, and restoration of natural kinematics and range of motion present significant challenges.

Damage to the cruciates (anterior cruciate ligament-ACL and posterior cruciate ligament-PCL) is one of the most common injuries among the population. The ACL is the most frequently ruptured ligament in the U.S. with over 100,000 cases per year in the United States (Beynnon et al., 2005). The ACL plays an important role in the restraint of excessive anterior translation of the tibia with respect to the femur (Girgis et al., 1975).

Additionally, the ACL prevents excessive internal-external rotation and varus-valgus angulation. The PCL plays an important role during deep flexion, in preventing posterior translation of the tibia and excessive internal-external rotation. Given the high incidence of cruciate injuries and complex function, the current dissertation work focuses on pathologies associated with cruciate injury. Researchers are interested in studying knee biomechanics to improve rehabilitation from injuries by developing new innovative therapies, and developing surgical techniques for repair of damaged/worn tissue. Soft tissue injuries often lead to the progression of cartilage wear and onset of osteoarthritis.

For cases in which cartilage degradation in the knee joint has become severe, total knee arthroplasty (TKA) is a common surgical procedure to relieve pain and restore knee function. TKA procedures have drastically increased by more than 50% from 1990-2002, totaling to approximately half a million surgeries by 2002 (Kurtz et al., 2005). TKA is most commonly performed by replacing damaged bone and cartilage on the articulating surfaces with a combination of metal and polyethylene/ceramic components. The success of TKA is dependent on the design of the implant, relative alignment of the implant components, patient anatomy, and tensioning/balancing of the ligament structures during surgery. Characterizing the influence of these factors on knee mechanics is critical for improving patient outcomes post-TKA.

There are two primary sources of experimental data for which to study knee biomechanics: in-vivo studies of living patients and in-vitro cadaveric work. In-vivo

studies are a great source of experimental data since they can be performed on the subset of patients in need of repair/therapy. In-vivo studies typically include image-based measurements of joint kinematics and anatomical measurements such as patellar tendon angle and moment arm (Kellis and Baltzopoulos, 1999; Price et al., 2004). These metrics are useful in identifying abnormal motion, and estimating changes in contact location at the knee. However, direct measurement of internal loads such as joint contact, muscle and ligament forces are impractical to quantify in in-vivo studies due to the limited access of the internal structures in the knee. Recently, researchers have used telemetric implants to directly measure knee joint forces and loads, but these studies have shown only moderate success, and the technique can be very costly and time-intensive (Bergmann et al., 2014; Komistek et al., 2005; Morris et al., 2001). In-vitro studies allow direct measurement of the internal loads and soft tissue forces through the use of load cells in knee simulators, and pressure transducers embedded within the soft tissue (Cyr et al., 2015; Maletsky and Hillberry, 2005), but similar to telemetry, in-vitro studies, which involve the construction of knee simulators and the purchase of cadavers, can be expensive and time-consuming. Cadaveric studies also typically apply an idealized set of loading and boundary constraints that may not be representative of physiological loading conditions and are not able to reproduce adaptions in movement present in-vivo. Computational modeling can complement experimental studies by enabling prediction of joint loads, contact mechanics, and internal stress/strains, which would otherwise be challenging to measure experimentally.

Computational models present an efficient and cost-effective method for investigating multiple activities/loading conditions, pathologies, and implant design iterations for evaluation of natural, pathological, and implanted knee mechanics. Whole-body, dynamic musculoskeletal models have been used to quantify whole-body motion, and predict joint loads and muscle forces using inverse dynamics and static optimization techniques (Delp et al., 2007; Sharma et al., 2008). For additional accuracy at the joint-level, finite element modeling incorporates subject-specific geometry, complex contact interactions and material representations for detailed evaluations of knee mechanics (Baldwin et al., 2012; Guess et al., 2010). While several musculoskeletal and finite element models have been created to investigate a variety of biomechanics research questions, there is a lack of a single framework that combines whole-body representations and sophisticated joint-level models. Computational models are an effective complement to experimental studies, but they are limited by their ability to represent physiological conditions. Additionally, computational models require extensive calibration and validation to experimental data to ensure confidence in model predictions, and to allow their use as tools for diagnosis and evaluation of repair. While the overall objective was to create a combined musculoskeletal and finite element modeling framework, the objective of the current dissertation work was primarily in the development of joint-level simulations, specifically creating subject-specific tibiofemoral and patellofemoral soft tissue representations to evaluate knee mechanics across healthy, pathological, and implanted knee conditions. Quantifying natural knee mechanics provided a baseline of healthy activity for comparisons to pathological conditions, such

as cruciate injury, and the performance of TKR-implanted subjects. Subject-specific models developed in this dissertation are separately calibrated and validated for each subject, activity, and knee condition to provide a robust and comprehensive set of tools for evaluation of joint mechanics.

1.2 Dissertation Overview

A general description of the contents of this dissertation is outlined in this section. Each chapter includes an introduction with specific background and motivation for the research question, literature review, and description of methods, results, and discussion of the significance of the results. In general, Chapters 3 and 4 combine in-vitro measurement and finite element modeling for evaluation of TF and PF mechanics in healthy and cruciate-deficient specimens. The final chapters of the dissertation transition insight on soft tissue properties developed from cadaveric experiments to in-vivo evaluations of healthy and implanted joint mechanics.

Chapter 2 provides the background and motivation for this work, and highlights the previous research in knee biomechanics using computational modeling. Additionally, Chapter 2 discusses previous and current methodology employed for evaluations of knee kinematics and mechanics.

Chapter 3 compares patellofemoral mechanics in healthy and cruciate-deficient conditions, and develops computational representations of the patellofemoral soft tissue. Chapter 3 utilizes the muscle loading rig (MLR), which is an experimental testing frame from the University of Kansas, to isolate the quadriceps mechanism for evaluation of natural patellofemoral mechanics. Cadaveric specimens are subjected to a deep knee bend in the MLR under intact, ACL-deficient, and PCL-deficient conditions. Finite element models of the experiment are developed to reproduce the experimental motions and predict loading in the patellar construct. In addition to contact mechanics, measurements of quadriceps efficiency such as patellar tendon angle and moment arm are calculated to describe the changes in PF mechanics following cruciate resection.

Chapter 4 continues the development of specimen-specific finite element models by incorporating tibiofemoral soft tissue into simulations of patellofemoral mechanics developed in Chapter 3. Knee laxity experiments are performed at multiple flexion angles and resection levels to characterize the tibiofemoral passive constraint. Tibiofemoral soft tissue alignment and material properties are optimized to match the experimental laxity response. Cadaveric specimens are mounted in the Kansas Knee Simulator to simulate knee motion during dynamic activity. Specimen-specific finite element models of the KKS predict experimental knee kinematics, contact mechanics, and ligament forces for healthy and ACL-deficient conditions.

In Chapter 5, patellofemoral soft tissue representations developed in Chapter 3 are integrated into in-vivo evaluations of TKR-implanted subjects. Chapter 5 compares PF mechanics between medialized dome and anatomic patellofemoral geometries for subjects performing a seated knee extension and a single-leg lunge. A computational modeling framework is developed that combines in-vivo high-speed stereo radiography measurement, musculoskeletal modeling, and finite element modeling for evaluation of subject-specific PF mechanics.

Chapter 6 applies the modeling approach developed in Chapter 5 to in-vivo evaluations of TF and PF mechanics for a healthy subject. A subject-specific finite element model is developed using in-vivo motion, predicted muscle forces from musculoskeletal modeling, and calibrated tibiofemoral and patellofemoral soft tissue representations developed in previous cadaveric modeling. The computational framework reproduces subject-specific in-vivo joint mechanics, and allows implant manufacturers to test and develop new innovative implant designs and investigate surgical techniques and rehabilitation protocols.

The final chapter summarizes the findings of the studies presented in this dissertation, highlights continuing challenges within the biomechanics community, and provides recommendations for future work.

CHAPTER 2 – BACKGROUND & MOTIVATION

This chapter provides the background and motivation for the studies presented in this dissertation, including description of the tibiofemoral (TF) and patellofemoral (PF) joints, knee pathologies, such as patellar maltracking and cruciate injury, and description of previous experiment and modeling performed to study these disorders.

2.1 Quadriceps Mechanism

Healthy patellofemoral mechanics are critical for optimal performance of the knee, which requires healthy function of the quadriceps mechanism. The quadriceps mechanism includes the patella bone, rectus-femoris, vastus-lateralis, vastus-medialis, and vastus-intermedius muscle groups, the patellar ligament/tendon, and medial and lateral patellofemoral (PF) ligaments. The primary function of the patella, as part of the extensor mechanism, is to efficiently distribute load from the quadriceps tendons to the patellar ligament, and allow extension of the knee (Buff et al., 1988). The patella increases the effective moment arm of the knee by increasing the distance from the joint center of rotation to the converged quadriceps tendon attachments. By increasing the knee moment arm, the patella reduces the quadriceps forces required to extend the knee.

A simple free body diagram of the patella illustrates the function of the extensor mechanism, and the forces acting on the patella (Figure 2.1) (Buff et al., 1988; Huberti et al., 1984). The distribution of forces, from the quadriceps to the patellar tendon and joint contact, can vary as a function of knee flexion. Previous cadaveric experiments and mathematical determinations of the forces acting on the patella indicate the ratio of force in the patellar tendon to quadriceps force decreases as a function of flexion (Ahmed et al., 1987; Buff et al., 1988; Huberti and Hayes, 1984). In contrast, the patellofemoral contact force increases as the knee is flexed (Besier et al., 2005). In Figure 2.1, the angle β represents the patellar tendon angle, which is measured between the mechanical "long" axis of the tibia and the patellar tendon line of action. The patellar tendon angle is an important metric for determining the distribution of forces from the quadriceps to the patellar tendon, and also significantly influences the shear forces at the knee (Buff et al., 1988; Yamaguchi and Zajac, 1989).

Measurements of moment arm, patellar tendon angle, and the ratio of forces distributed across the patellar mechanism are critical for quantifying healthy knee function. For example, researchers have found that the ratio of patellar tendon force to quadriceps force can exceed one at flexion angles less than 45°, which suggests that knee exercises near full extension should be avoided due to the large knee moments and patellar tendon loads (Huberti and Hayes, 1984). Similarly, large weight-bearing exercises in deep flexion can be harmful to the PF cartilage due to the increased joint contact forces. The moment arm of the knee has been measured extensively in the

literature to quantify knee performance, and is typically measured as the perpendicular distance from the knee joint center and the patellar tendon line of action (Krevolin et al., 2004). In some cases, the effective moment arm was measured as a function of distance and the ratio of load in the patellar tendon and quadriceps force; Meff = Fpt*Marm/Fq, where Meff = effective moment arm, Fpt = patellar tendon force, Fq = quadriceps force, Marm = 'traditional' moment arm (Grood et al., 1984).

2.2 Patellofemoral Pathology

Quantifying measures of quadriceps efficiency is important for establishing a baseline of healthy knee function, and for evaluation of pathological conditions. Patellofemoral pain is one of the most common disorders of the knee with one in every four of the general population affected by anterior knee pain (Powers, 1998). Patellar maltracking is commonly attributed to PF pain, and represents abnormal motion of the patella with respect to the femur. Maltracking can lead to PF pain due to excessive strain of the patellar tendon, which can innervate nociceptive (pain) fibers in the bone, retinaculum, and synovium (Fulkerson, 2002; Post et al., 2002). In extreme cases, maltracking can lead to patellar dislocation from excessive medial-lateral translation and internal-external rotation. In addition to increased ligament strains, patellar maltracking may lead to increased reaction loads and pressures on the articulating cartilage. Large PF contact forces could increase the risk of cartilage wear, bone abnormalities, and eventually the development of osteoarthritis (Fulkerson and Shea, 1990; Zhang et al.,

2007). Measurements of patellar force ratios are important for understanding how kinematic variations in the PF joint affect the distribution of joint loading, especially considering that large patellar tendon loads and contact forces can lead to PF pain and cartilage wear (Ahmed et al., 1987). Quantifying PF joint loading is critical for diagnosis of at-risk patients. For example, previous studies have demonstrated that an imbalance in the activation of the vastus medialis and vastus lateralis could lead to lateral maltracking and PF pain (Pal et al., 2011). Also, researchers have correlated patellar shape and alignment characteristics, such as bisect offset, patellar tilt, and patella alta, to higher incidence of PF pain (Pal et al., 2013b; Pal et al., 2012) (Figure 2.2). Although PF pain can originate from a variety of sources ranging from extended activity to trauma, the mechanical causes of PF joint dysfunction are not well understood.

2.3 Cruciate Injury and Function

Rupture of the anterior cruciate ligament (ACL) is one of the most common soft tissue injuries in the U.S. with an estimated incidence rate of 1 injury per 3500 people, resulting in over 100,000 cases per year (Beynnon et al., 2005). Sports related activities account for a significant portion of knee ligament injuries (Gianotti et al., 2009). Although PCL injuries are less prevalent than ACL injuries, damage to the ACL and PCL can substantially reduce the quality of life with research suggesting long-term knee pain, cartilage degeneration, and occasional swelling of the joint (Boynton and Tietjens, 1996; Lohmander et al., 2007).

The anterior cruciate ligament (ACL) primarily prevents excessive anterior translation of the tibia with respect to the femur, and acts as a secondary restraint to valgus and internal rotation of the tibia (Girgis et al., 1975). The posterior cruciate ligament primarily provides stability of the knee joint at deeper flexion angles, and prevents posterior translation of the tibia.

2.4 Interdependence of Tibiofemoral and Patellofemoral Joints

The kinematics and kinetics of the tibiofemoral and patellofemoral joints are strongly interdependent, such that injury and/or altered motion in the TF joint can affect the PF mechanics and vice versa. For example, differences in TF internal-external rotations affect the coronal and transverse plane orientation of the patellar tendon, and the anterior-posterior position of the patellar tendon in the sagittal plane (Varadarajan et al., 2010). Additionally, the angle between the quadriceps tendon and patellar tendon in the frontal plane or the "q-angle" significantly affects both the TF and PF kinematics; a decrease in q-angle has been shown to increase lateral tilt of the patella, while also increasing external and varus rotation of the tibia (Mizuno et al., 2001). Patients with large q-angle could be at-risk of lateral patellar dislocation, or early onset of osteoarthritis due to increased contact forces in the medial TF cartilage (Powers, 2003) (Figure 2.3). Quantifying the relationships between the TF and PF joints is critical for prevention and diagnosis of knee pathologies, and the development of rehabilitation and surgical treatments.

Given the interaction between the TF and PF joints, PF pain and maltracking is prevalent following cruciate injury. In a 35-year follow-up study of high-level athletes with ACL-deficiency, clinicians found significant (>95% of cases) degradation of the TF cartilage and meniscus with several patients requiring menisectomies and total knee arthroplasty in the decades following injury (Nebelung and Wuschech, 2005). Additionally, the ACL-deficient athletes suffered from patellofemoral pain due to malalignment and PF cartilage wear. (Van de Velde et al., 2008) evaluated the effect of ACL-deficiency and reconstruction on the mechanics of the PF joint; eight patients with acute ACL injury and/or subsequent reconstruction demonstrated altered patellar kinematics, specifically decrease in flexion range of motion and increase in patellar tilt and spin. Altered patellar kinematics resulted in a proximal and lateral shift of the PF contact location, which resulted in contact forces on thinner cartilage regions. This altered loading could predispose the PF cartilage to degenerative conditions associated with osteoarthritis.

Similar to subjects with ACL-deficiency, PCL-deficient patients also demonstrated altered TF and PF kinematics, specifically posterior translation of the tibia with respect to the femur at 90° knee flexion, which led to a lateral patellar tilt and shift when compared to healthy subjects (von Eisenhart-Rothe et al., 2012). Due to the high incidence of cruciate injuries (Beynnon et al., 2005) and patellofemoral pain (Powers, 1998), and the interdependence of the TF and PF joints, the current dissertation work compares joint mechanics in healthy and cruciate-deficient subjects to understand the

mechanisms surrounding injury and to develop new treatment pathways for better restoration of natural knee function.

2.5 Passive Constraint

Quantifying the mechanics of passive structures in the knee is critical for understanding pathology, and developing successful rehabilitation protocols. Knee injuries are most commonly associated with the passive components of the knee and involve strain or wear of the soft tissue. Joint contact, muscle, and ligament forces are impractical to quantify in-vivo due to the limited access of the internal structures. However, in-vitro experiments provide access to the passive structures in the knee, allowing measurement of joint contact and tissue forces during simulations of everyday activity (Maletsky and Hillberry, 2005).

Passive experiments have been used to characterize soft tissue constraint in the TF joint (Figure 2.4). There are two primary methodologies for quantifying soft tissue properties: resection and measurement of individual ligament structures, and whole-joint, passive laxity experiments. When focusing on the material characteristics of an individual ligament, uniaxial testing of the ligament structure can be useful for identifying its material behavior. For example, in-situ measurement and uniaxial testing of eight cadaveric medial collateral ligaments (MCL) was performed to derive subject-specific transversely, isotropic, hyperelastic material properties (Gardiner and Weiss,

2003; Gardiner et al., 2001). Alternatively, passive laxity tests have been used to quantify the net constraint from soft tissue structures by measuring the resulting motions from fixed applied loads or measuring the resulting loads from fixed motions (Godest et al., 2000; Kiapour et al., 2014; Mootanah et al., 2014). Optimization techniques can be used to tune the material properties of individual structures by matching the experimental and computational load-displacement behavior. Since passive laxity experiments provide a holistic representation of joint stiffness, laxity tests, following subsequent resections, could be used to derive the mechanical contribution from individual ligaments. Passive experiments are an important step to quantifying joint stiffness and identifying ligament properties, but additional experiments and/or simulations are necessary to evaluate the performance of the healthy and repaired knee in representative daily activities.

2.6 Total Knee Arthroplasty

Total knee arthroplasty (TKA) is a surgical procedure that restores healthy knee function by replacing damaged articulating surfaces with artificial components (Figure 2.5). TKA is a common solution for patients suffering from osteoarthritis, which is a degenerative knee condition resulting in the loss of cartilage at the joint interface and the development of osteophytes and bone abnormalities. Osteoarthritis most often occurs in the elderly population due to regular "wear-and-tear" of the articulating surfaces. In general, TKA has been a successful solution for osteoarthritic patients with 8% or fewer requiring revision, but the number of total knee replacements and the demand for higher

knee functionality and performance is continuing to increase (Kurtz et al., 2005; Kurtz et al., 2007).

Functional limitations and altered knee kinematics have been well documented in patients following TKA. In a pre- and post-operative evaluation of TKA patients, clinicians found decreased strength in the quadriceps and hamstring muscles when compared to the non-operative/healthy control leg (Silva et al., 2003; Stevens-Lapsley et al., 2010). Loss of quadriceps strength after TKA has been attributed to failure of voluntary muscle activation and muscle atrophy (Mizner et al., 2005). Additionally, quadriceps weakness following TKA has significantly impacted joint loading and knee kinematics in everyday activities such as walking and rising from a chair (Mizner and Snyder-Mackler, 2005). Approximately 50% of TKA patients have reported substantial difficulty in performing higher demand activities, such as squatting and kneeling (Noble et al., 2005). While TKA has effectively reduced knee pain and restored healthy range of motion, quadriceps deficiency and altered knee motion are still present following TKA. Further investigation of TKA-implanted joint mechanics is necessary to improve performance of the current implant designs and functional outcomes post-TKA.

2.7 Techniques for Evaluation of Knee Biomechanics

2.7.1 In-Vivo Experiments

In-vivo evaluations of knee mechanics typically utilize motion capture and/or image-based techniques to quantify joint kinematics, measure anatomical variability, and estimate cartilage contact area and position. Passive and active marker-based motion capture is a common technique for measuring whole-body motion, but presents significant limitations in accuracy (primarily due to skin surface motion artifact) when measuring joint-level kinematics (Stagni et al., 2005). Imaging techniques can alleviate some of the challenges in accuracy from traditional motion capture methods. These techniques include x-ray photogrammetry, computed tomography (CT), static and dynamic magnetic resonance imaging (MRI), and single- and dual-plane fluoroscopy (Katchburian et al., 2003). For example, MRI has been used to compare PF sagittal plane motions and contact area between natural, posterior-cruciate- retaining, and bi-cruciate-retaining TKA subjects (Carpenter et al., 2009); however, predictions of contact location using MRI have limited accuracy. The current state-of-the-art in accurate dynamic measurement of joint kinematics is high-speed, dual-plane fluoroscopic/radiographic measurement, which can be accurate to within 1° and 1 mm of joint motion (Ivester et al., 2015). Due to the limited field of view in dual-plane stereo radiography systems, a combination of motion capture and stereo radiography are the suggested methods for in-vivo evaluations (Miranda et al., 2013; Stagni et al., 2005). In general for stereo radiography systems, 3D geometric representations of the bone geometry are

reconstructed using CT and MRI imaging, which are, then, positioned onto the 2D radiography images to describe the 3D joint kinematics and alignment (Figure 2.6).

Researchers have used dynamic fluoroscopy to quantify joint kinematics in natural (Nha et al., 2008) and implanted (Price et al., 2004; Stiehl et al., 2001) subjects. (Price et al., 2004) compared sagittal plane kinematics between healthy and TKA subjects, and found significantly altered TF kinematics post-TKA; TKA subjects demonstrated an anterior shift in the tibia with respect to the femur resulting in a decrease in the patellar tendon angle near full extension. Smaller patellar tendon angles near full extension could adversely affect quadriceps strength and alter shear loading at the knee. (Stiehl et al., 2001) evaluated PF kinematics and contact location for healthy, ACL-deficient, and TKR-implanted subjects, and found more superior PF contact in implanted patients; altered knee kinematics and PF contact locations suggested a reduction in the effective extensor moment arm. In addition to describing joint motions, in-vivo studies can use imaging to quantify anatomical features of the bone and cartilage (Nha et al., 2008); correlating shape and alignment characteristics to joint kinematics could be useful for identifying patients at-risk of pathologies such as patellar dislocation and maltracking.

While in-vivo studies are useful for measuring joint kinematics and estimating contact locations, internal joint, muscle, and tissue forces are impossible to quantify using non-invasive methods. Telemetry is an experimental approach that places load sensors into total knee replacement implants for recording real-time joint loads. Telemetric

implants have been used to measure in-vivo forces and moments in both the hip (Bergmann et al., 1993; Taylor et al., 1997) and the knee (Morris et al., 2001; Taylor et al., 1998). Although telemetric implants provide real-time accurate measurement of the internal joint forces, the cost of such an implant is expensive, which limits the numbers in studies, and the data can be unreliable as the device could malfunction after implantation (Komistek et al., 2005). Also, telemetric implants are an option for evaluation of TKR-implanted mechanics, but not healthy knee mechanics. Quantifying joint and soft tissue forces are important to understanding healthy knee function and the mechanical sources of pathology. Since measurement of internal loads is impractical using in-vivo methods, researchers must rely on in-vitro experiment and/or computational modeling for evaluation of joint, muscle, and tissue forces.

2.7.2 In-Vitro Experiments

In-vitro experimental testing applies a repeatable, controlled set of loading conditions for evaluation of TF and PF kinematics and internal joint and soft tissue forces. Experimental knee simulators have been developed to replicate the loading conditions for activities of daily living, such as gait and squat (DesJardins et al., 2000; Godest et al., 2000; Maletsky and Hillberry, 2005). In-vitro tests simulate joint motion in knee cadavers using a combination of motor-actuated muscle forces and loads directly applied to the bone geometry (Amis et al., 2006; Katchburian et al., 2003; Mizuno et al., 2001) (Figure 2.7). Joint kinematics can be measured using the output motions from experimental simulators or using anatomically defined local coordinate systems on the

bones that are tracked using motion capture systems (Grood and Suntay, 1983; Kwak et al., 2000; Maletsky et al., 2007). For evaluation of PF mechanics, researchers have applied motor-actuated quadriceps forces to simulate a knee extension task, and have measured the forces in the quadriceps and patellar tendon using an attached load cell and spring balance (Ahmed et al., 1987; Buff et al., 1988). In-vitro cadaveric experiments have been used to quantify soft tissue forces in the TF joint such as ACL, PCL, and meniscus loads by attaching pressure transducers along the ligament fiber direction (Draganich and Vahey, 1990; Li et al., 2004b; Markolf et al., 1990; Markolf et al., 2012). For measurement of joint contact, researchers have placed TekScan sensors (thin film sensor that records contact pressure distributions under applied loading) on the articulating surfaces (Elias et al., 2004; Fregly et al., 2003).

Due to the consistent set of loading conditions, in-vitro tests are an excellent platform for isolating the role of patient anatomy, pathology, implant design, and surgical technique on joint mechanics. For example, the influence of q-angle on tibiofemoral and patellofemoral kinematics was evaluated in six knee cadavers by changing the quadriceps line of action in the frontal plane (Mizuno et al., 2001) (Figure 2.7); results indicated an increase in q-angle could lead to lateral patellar dislocation, and a decrease in q-angle could lead to increased TF contact forces in the medial condyle. (Li et al., 2002a) studied the influence of PCL-deficiency on TF mechanics for eight cadaveric specimens during a simulated deep flexion cycle from full extension to 120° knee flexion. PCL injury resulted in increased posterior tibial translation and external tibial rotation, which was

hypothesized to increase PF contact forces. In-vitro experiments have also been used to evaluate implant design (Baldwin et al., 2012; Halloran et al., 2010) and surgical alignment variability, such as the effect of varus tibial alignment on joint contact mechanics (Green et al., 2002). Due to the many reports on quadriceps deficiency in TKA patients (Stevens-Lapsley et al., 2010), researchers have used in-vitro testing to quantify quadriceps forces in healthy and implanted knee cadavers (Ostermeier et al., 2004); results suggested substantial increases (>10%) in quadriceps forces required to extend the knee following implantation.

In-vitro experimental testing has been used extensively to quantify TF and PF kinematics, contact mechanics, ligament forces, and evaluate joint laxity for natural and implanted knee conditions (Baldwin et al., 2012; Cyr et al., 2015; Shalhoub and Maletsky, 2014), but these experiments can be costly and time-intensive. Due to the expense and labor, the total number of specimens in cadaveric studies is small. Also, simulation of multiple loading conditions and activities is difficult as it may require substantial modifications to the experimental setup. There are some advanced knee simulators, such as the Kansas Knee Simulator, that are capable of simulating multiple activities (Maletsky and Hillberry, 2005). However, simulated joint motions do not capture patient variability in the performance of activities, and cannot reproduce compensation strategies or adaptations in movement that may be present in vivo. While significant care is placed on the maintenance of knee cadavers during experimental testing, bone and tissue geometry may not be representative of healthy in vivo conditions.

In-vitro testing can be used to directly measure joint and soft tissue forces, but measurement of some soft tissue structures can be challenging due to size and limited access; also, collection of all tissue forces in the knee joint is impractical. Computational modeling provides an alternative method for evaluation of knee joint loads that would otherwise be challenging or impossible to measure experimentally.

2.7.3 Musculoskeletal Modeling

Musculoskeletal modeling is a computational approach for prediction of whole-body joint motions and loads, and muscle forces. For efficient and cost-effective evaluation of joint mechanics, researchers have combined data from experimental testing with musculoskeletal simulations for prediction of joint contact and soft tissue forces. Passive and active marker motion capture data, EMG muscle activity, and ground reaction force plate data have been integrated into musculoskeletal simulations for prediction of joint mechanics during a variety of activities such as step-up, gait, and chair-rise (Delp et al., 1998; Navacchia et al., 2016b; Piazza and Delp, 2001). In general, geometry and material properties for generic models of the lower limb are scaled to match subject geometry using anthropometrics, marker positions from motion capture and EMG maximum isometric forces (Delp et al., 2007) (Figure 2.8). Marker-based motion capture data is used to derive joint angles and motions using inverse kinematics. The corresponding joint loads can be obtained using inverse dynamics, which utilize the joint motions from inverse kinematics, and ground reaction forces simultaneously measured using force plates. Static and dynamic optimization techniques can be

employed to quantify the contribution of individual muscles in the simulation of the activity.

Combined in-vivo experiment and musculoskeletal modeling have been used to estimate in-vivo joint loads, muscle, and ligament forces for evaluation of natural, pathological and implanted knee conditions. (Lloyd and Besier, 2003) developed an EMG-driven musculoskeletal model for prediction of knee moments and muscle forces during running and cutting tasks. Musculoskeletal models have been used to estimate ligament forces, such as ACL and PCL forces during walking (Moissenet et al., 2014; Shelburne et al., 2004a) (Figure 2.8). The influence of pathology on shear forces and ligament loading in the knee has been evaluated using simulations of the healthy and ACL-deficient knee; researchers found that the medial collateral ligament (MCL) can play a significant role in anterior tibial translation and changes in patellar tendon angle can reduce the total anterior shear force at the knee (Shelburne et al., 2004b). In addition to evaluations of the natural knee, musculoskeletal models of the implanted knee have been developed to study joint kinematics and TF contact forces during knee extension, gait, and pivot activities, with model validation performed using comparisons to telemetric data (Marra et al., 2015). The musculoskeletal modeling framework can be used to investigate the mechanisms surrounding pathology, and explore the influence of implant design and alignment factors on the performance of TKR-implanted subjects.

While musculoskeletal modeling provides an efficient method for prediction of in-vivo joint kinematics and loads, these models generally lack accurate, subject-specific detail in the knee joint, which may be necessary for capturing the variability in patient-specific knee mechanics. Musculoskeletal models typically utilize generic geometry that is scaled to match subject size, but scaling does not account for important shape characteristics in the bone and cartilage, such as tibial slope and cartilage conformity, that may impact joint loading. Subject-specific articular geometry is important for evaluations of contact mechanics, however, contact is modeled using rigid body constraints and simulations do not consider the deformable characteristics of soft tissue. Also, ligament representations are most commonly defined using literature description and may not represent subject-specific attachment locations and material properties. Since joint loading and soft tissue mechanics are highly dependent on patient anatomy, computer models for evaluation of subject-specific knee mechanics require advanced description of knee geometry, material behavior, and contact definitions.

2.7.4 Finite Element Modeling

Finite element (FE) analysis is a computational modeling technique that incorporates subject-specific geometry and accurate solutions of the internal stress/strains at the joint level. FE modeling can include complex material representations and contact interactions for accurate and detailed description of joint behavior (Erdemir, 2016) (Figure 2.9). For example, researchers have developed depth-dependent, viscoelastic representations of articular cartilage and contact (Halonen et al., 2013), and transversely,

isotropic, hyperelastic material behavior for the ACL (Limbert et al., 2004). Computationally efficient representations of the quadriceps mechanism have also been developed, which include non-linear geometric and material representations of the vasti, rectus femoris, patellar tendon, and medial and lateral PF ligaments, and a simplified estimate of deformable contact (linear pressure-overclosure relationship) (Fitzpatrick et al., 2010). FE models are typically validated using comparison to six degree-of-freedom kinematics from similarly loaded experimental tests (Guess et al., 2010; Heegard et al., 1995).

Integrating in-vitro experimental data into FE models provides a comprehensive, cost-effective evaluation of knee mechanics. In evaluations of joint laxity or soft tissue mechanics, FE modeling is an excellent complement to in-vitro experiments due to the challenge of measuring and quantifying soft tissue properties. Previous studies have developed validated FE models of the knee with anatomically accurate description of TF soft tissue; geometry and material property representations are supported through comparisons of knee kinematics, ligament strains, and articular cartilage pressures obtained from static and dynamic in-vitro cadaveric testing (Kiapour et al., 2014). In-vitro laxity assessments of joint stiffness have been used to tune 3D representations of TF ligaments by minimizing kinematic differences between experiment and FE model outputs (Mootanah et al., 2014). Similarly, (Baldwin et al., 2012) performed in-vitro laxity testing and FE modeling of TKR-implanted cadavers for evaluation of implanted knee mechanics. While in-vitro experiments are ideally suited to support FE

representations, in-vivo experiments are more challenging to translate to the FE framework. In-vivo experiments provide measurement of whole-body and joint motions, but do not provide the necessary detail and accuracy of internal forces to effectively calibrate FE models. The current dissertation explores a novel methodology for integrating in-vivo experiment, musculoskeletal and finite element modeling for evaluation of in-vivo joint mechanics.

Validated FE models can easily be modified to evaluate multiple loading conditions and investigate a variety of knee conditions, making it an effective tool for studying knee pathology and repair. Several models have been developed to investigate the influence of anatomic variability on knee mechanics to better understand patient factors leading to pathology. For example, (Mesfar and Shirazi-Adl, 2005) simulated knee flexion under various magnitudes and locations of quadriceps forces to investigate the impact of quadriceps loading variability on knee torque, ligament forces, and contact mechanics. Similarly, researchers have used FE models to explore the sensitivity of ligament material properties on knee kinematics and contact forces (Barry et al., 2010; Dhaher et al., 2010; Mesfar and Shirazi-Adl, 2006a); uncertainty in ACL material properties significantly affected PF kinematics and contact stresses (Dhaher et al., 2010). (Mesfar and Shirazi-Adl, 2006a) established that forces in the ACL and PCL are highly interdependent such that the forces will increase as either cruciate ligament becomes tense. Investigating the influence of cruciate pre-tension/initial strain on joint loading is important for understanding cruciate injury and repair, for example, the appropriate

amount of pre-tension to apply in an ACL graft to maintain healthy ligament and joint loading (Barry et al., 2010; Halonen et al., 2016; Mesfar and Shirazi-Adl, 2006a). In addition to simulating anatomic variability, predictive FE models have been developed as clinical tools for diagnosis of pathology. (Cohen et al., 2003b) developed a FE model for identifying regions most likely to sustain cartilage damage. These models can be used in the diagnosis of patients at-risk of injury or cartilage degeneration, which could allow clinicians to employ preventative therapies.

FE models have been used to directly simulate pathology by removing or altering soft tissue structures in the analysis. (Tanska et al., 2015) predicted and compared cartilage stresses in normal and medial menisectomy knee joints. Removing the medial meniscus from the FE model resulted in an approximate 30% increase in cartilage contact pressure and up to 60% increase in the maximum principal strains in the medial cartilage. The increased contact pressures and principal strains are consistent with cellular degeneration associated with the onset of osteoarthritis. Similarly, researchers have used FE modeling to simulate rupture of the ACL. (Li et al., 2002a) simulated the effect of ACL injury on knee joint function by removing and lowering the ACL stiffness. (Mesfar and Shirazi-Adl, 2006b) simulated ACL injury by altering the TF constraint in the anterior-posterior direction, which effectively changed the net shear force at the knee.

In addition to investigating pathology, FE models have been used to simulate knee repair including modeling TKR-implanted conditions and simulations of surgical

techniques. For example, (Cohen et al., 2003a) simulated four variations of tibial tuberosity transfer in 20 patient-specific FE models (with geometry diagnosed as at-risk of patellar subluxation and osteoarthritis) to identify the optimal procedure for each subject. Subject-specific FE modeling of surgical techniques, such as tibial tuberosity transfer, can be used to identify optimal treatments on a patient-by-patient basis. Several FE models have been created to study knee mechanics in TKR-implanted subjects (Abo-Alhol et al., 2014; Baldwin et al., 2012; Clary et al., 2013; Fitzpatrick et al., 2014; Fitzpatrick et al., 2012a; Halloran et al., 2005; Rullkoetter et al., 2017). Recently, the role of implant design and surgical alignment factors on implanted knee mechanics was investigated to determine the most sensitive parameters in the restoration of healthy knee function (Fitzpatrick et al., 2012b). Features of the implant design, such as femora radius of curvature (Clary et al., 2013) and insert conformity (Fitzpatrick et al., 2012b), can have a substantial impact on reproducing healthy TF anterior-posterior kinematics and contact mechanics. Surgical alignment factors, such as restoration of the natural TF joint line and coronal plane alignment, have a significant effect on ligament and contact load balancing in the knee. Probabilistic FE models can be a useful design tool for implant manufacturers attempting to identify the influence of design and surgical alignment characteristics on knee mechanics.

The studies presented in this dissertation utilize the explicit finite element method in Abaqus (SIMULIA, Providence, RI). Abaqus/Explicit solutions are well suited for problems with large displacements/relative motions and highly non-linear contact

conditions. "Explicit" implies that the solution for one increment is only a function of the state of the previous increment. Also, explicit solutions assume the accelerations are constant from one increment to the next increment, which substantially reduces the complexity of the dynamic equations of motion. As a result, the computational cost of an explicit solution is significantly smaller than the implicit solution, which requires the storage and computation of a large strain-displacement matrix through every increment of the analysis. Since explicit solutions assume a constant acceleration during the increment, the stable time increment must be sufficiently small to satisfy that condition, which also increases the total number of iterations. Given the complex contact conditions, highly non-linear geometry, and large relative motions in the models developed in this dissertation, Abaqus/Explicit was used to efficiently simulate dynamic knee motion.

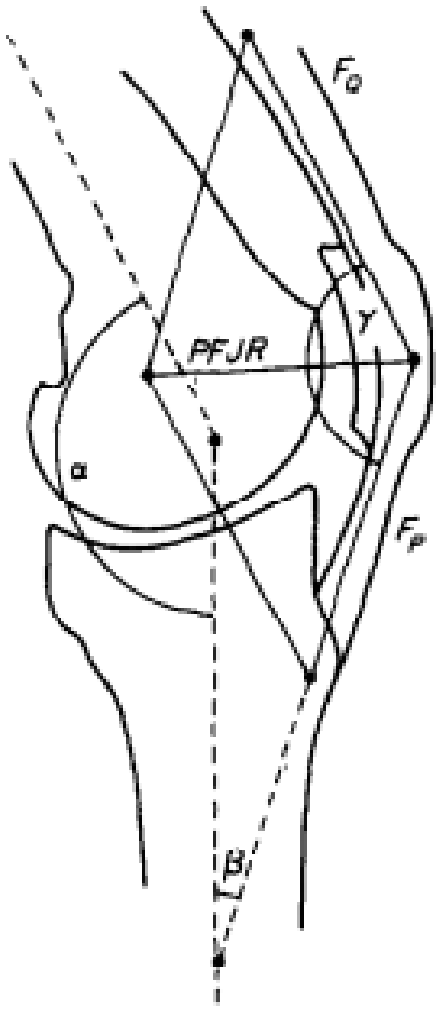

Figure 2.1 Free body diagram of the patellar mechanism from (Buff et al., 1988) illustrating the forces acting on the patella. Fq=quadriceps force, Fp=patellar tendon force, and PFJR=patellofemoral joint reaction force

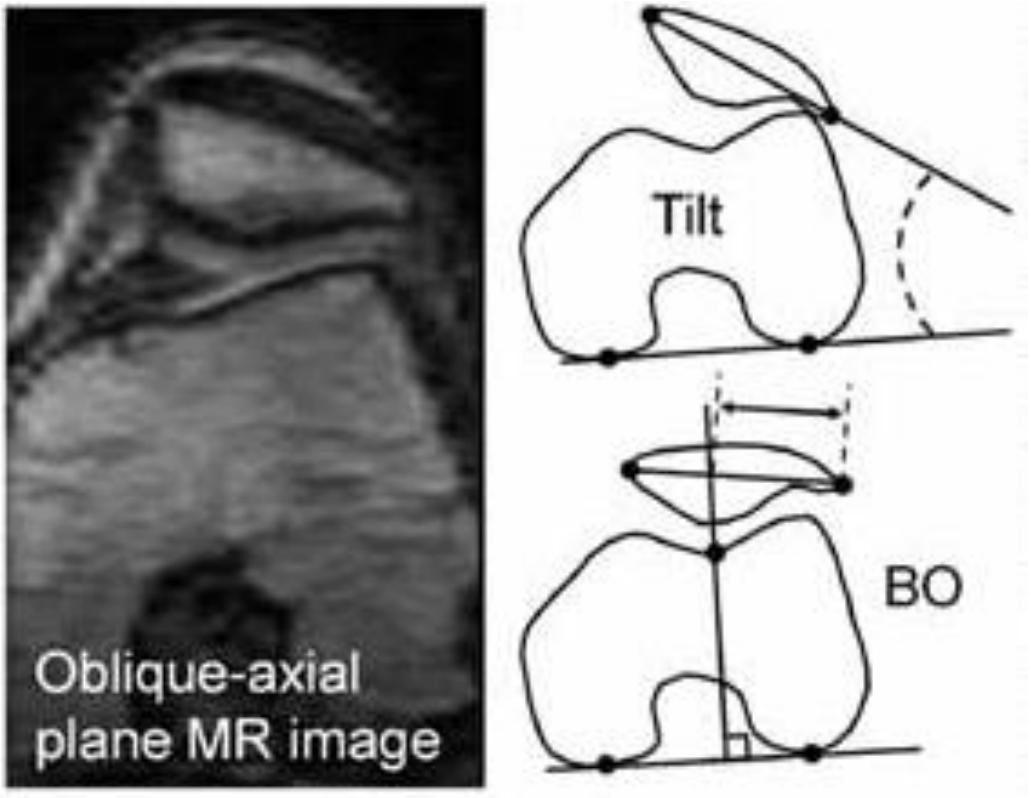

Figure 2.2 Patellar shape and alignment characteristics correlated to patellar maltracking by (Pal et al., 2012): patellar tilt, bisect offset (BO)

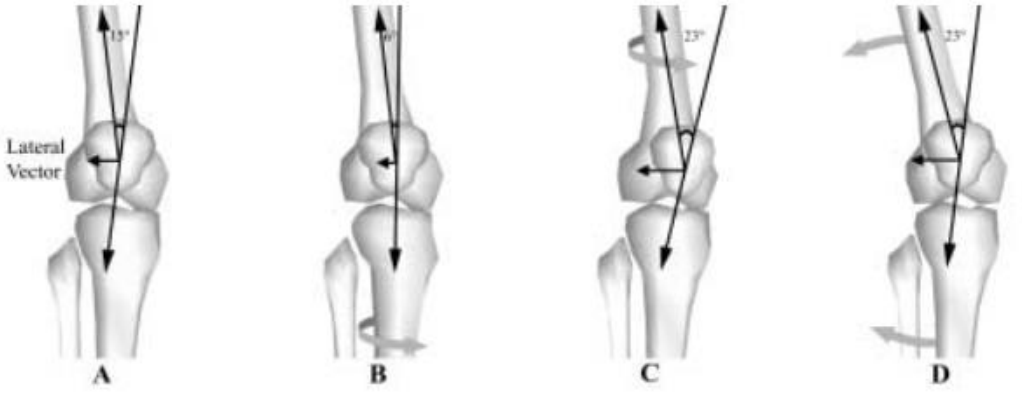

Figure 2.3 The effect of q-angle on lateral patellar maltracking. Q-angle is measured as the frontal plane angle between the quadriceps line of action and patellar tendon line of action. Increased q-angle leads to increased lateral forces on the patella. (Powers, 2003)

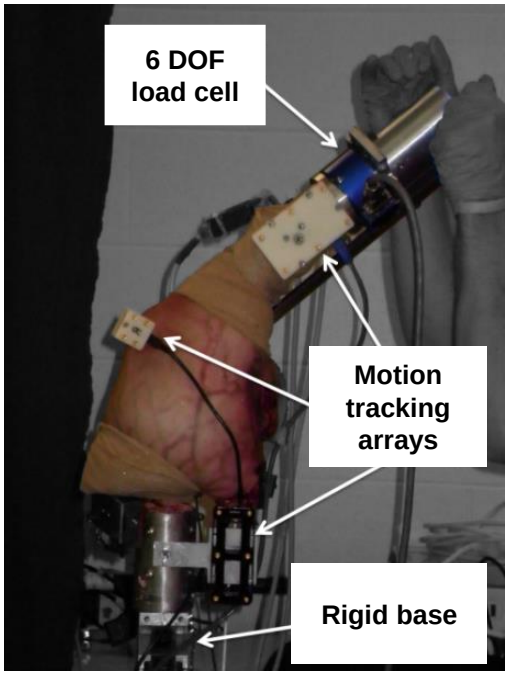

Figure 2.4 Passive joint laxity experiments performed by (Harris et al., 2016) for evaluation of TF soft tissue constraint and for calibration of finite element representations of ligament structures

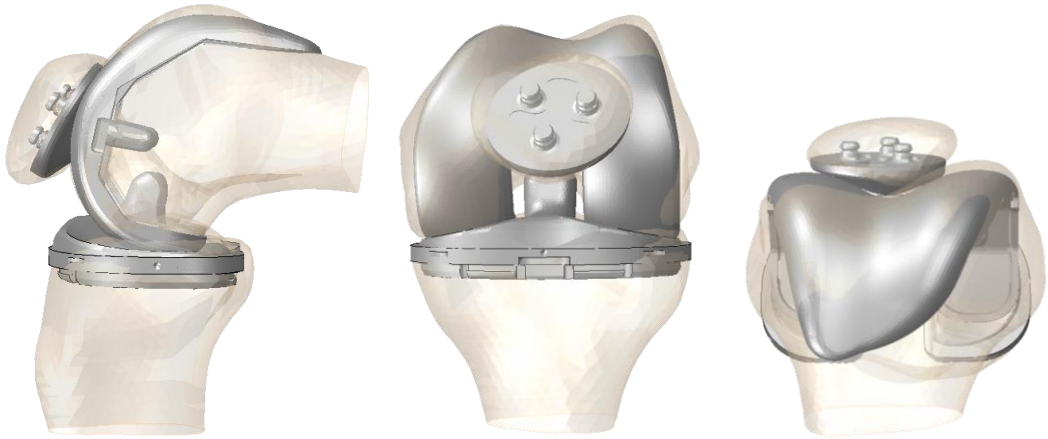

Figure 2.5 Illustration of total knee arthroplasty components aligned to the native bone geometry. Implant components include femoral, patellar button, tibial tray and insert components.

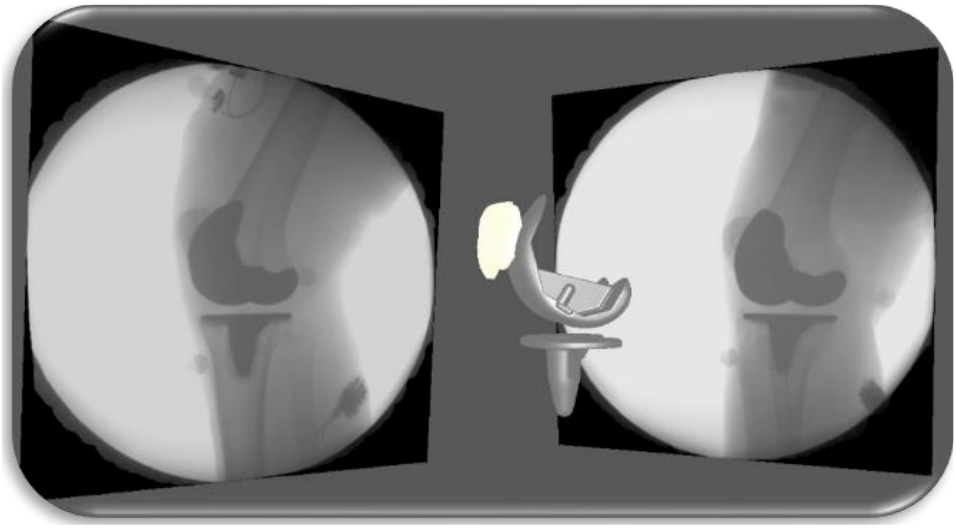

Figure 2.6 Three-dimensional rendering of high-speed stereo radiographic measurement of joint kinematics for total knee replacement patients. 3D implant geometry is simultaneously aligned to bi-plane 2D radiography images for computation of relative joint motions.

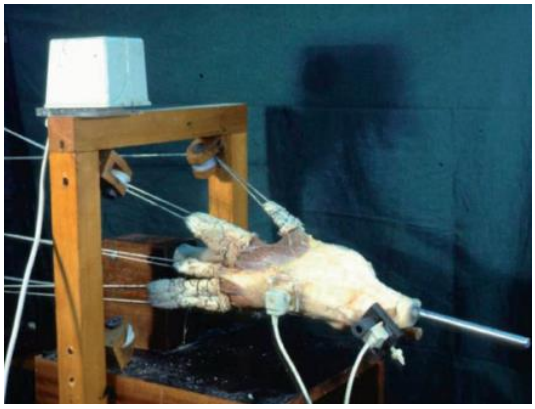

(Amis et al., 2006)

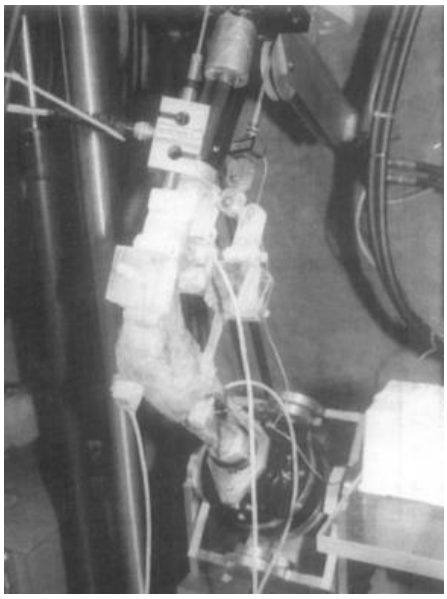

(Mizuno et al., 2001)

(Shalhoub et al., 2014)

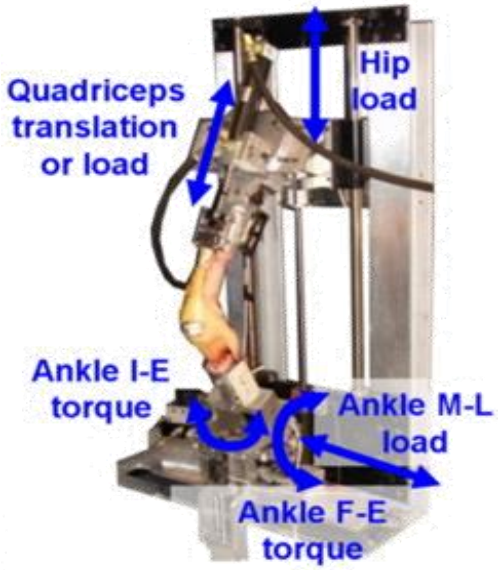

(Baldwin et al., 2012)

Figure 2.7 In-vitro experimental knee simulators designed to apply dynamic loading using muscle-actuated forces. (Amis et al., 2006; Baldwin et al., 2012; Mizuno et al., 2001; Shalhoub and Maletsky, 2014)

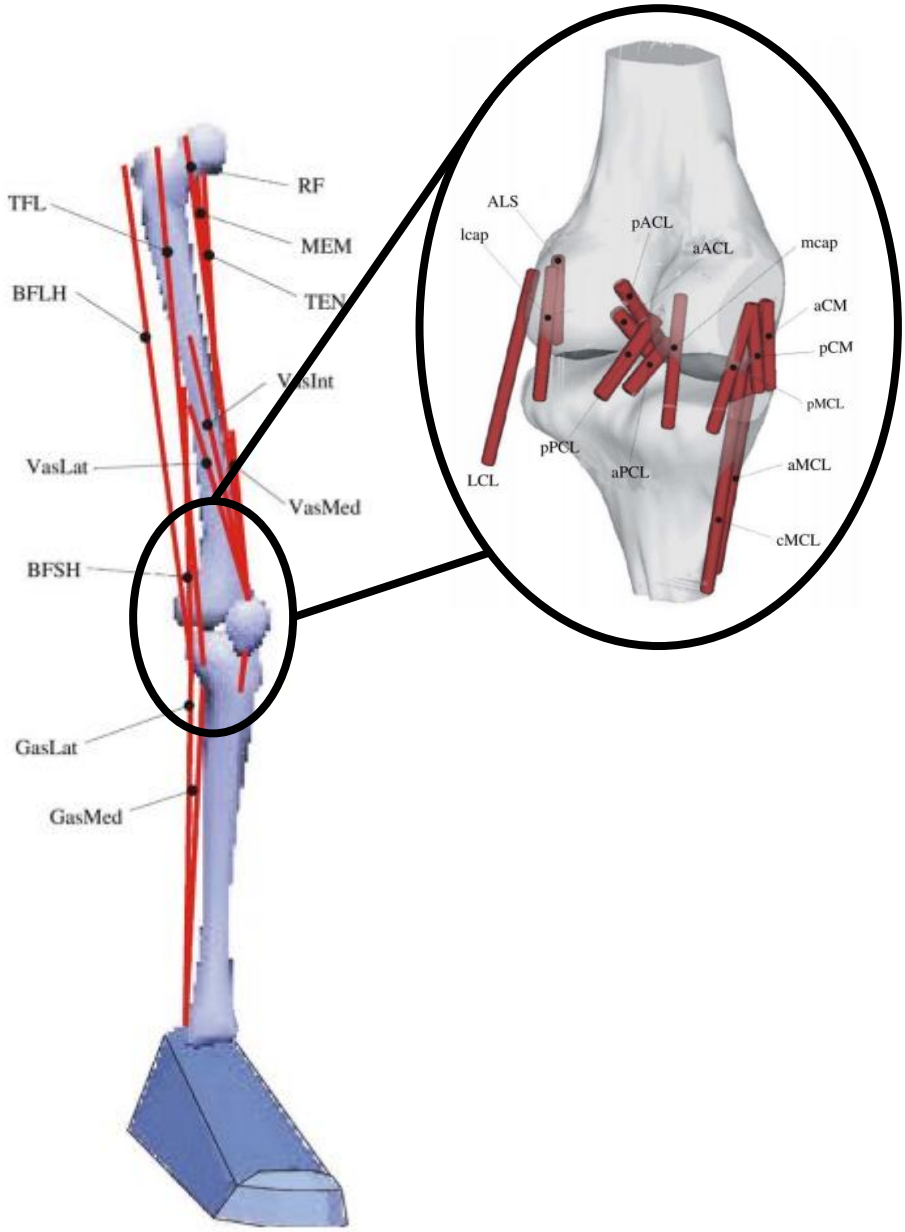

Figure 2.8 Musculoskeletal model of the lower limb and knee joint developed by (Shelburne et al., 2004a) for evaluation of ligament forces during walking.

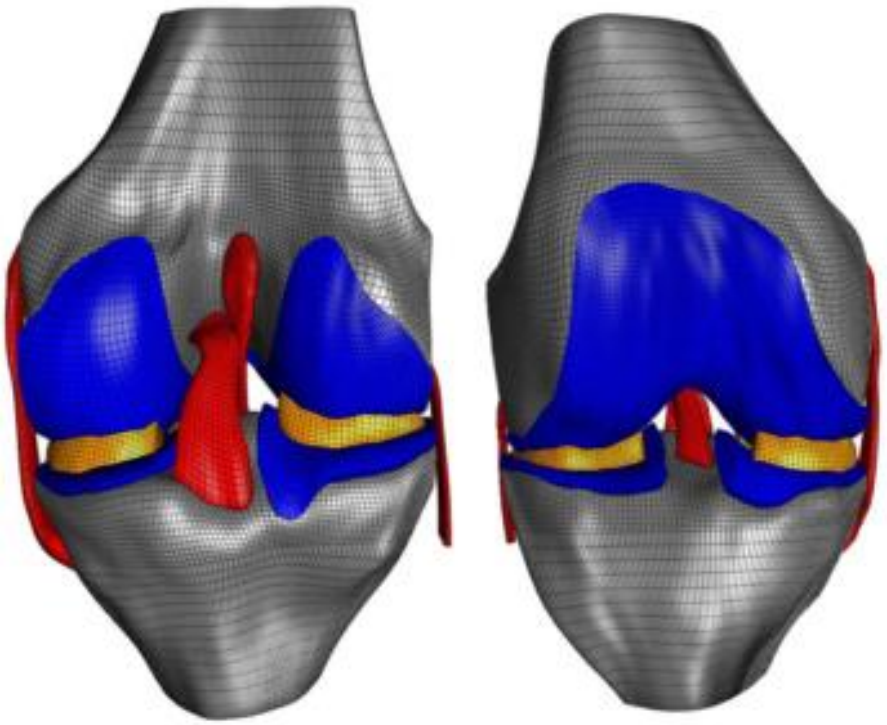

Figure 2.9 Open Knee: a detailed finite element representation of the knee joint with subject-specific geometry and complex material and contact definitions.

CHAPTER 3 – VALIDATION OF PREDICTED PATELLOFEMORAL MECHANICS IN A FINITE ELEMENT MODEL OF THE HEALTHY AND CRUCIATE-DEFICIENT KNEE

3.1 Abstract

Healthy patellofemoral (PF) joint mechanics are critical to optimal function of the knee joint. Patellar maltracking may lead to large joint reaction loads and high stresses on the articular cartilage, increasing the risk of cartilage wear and the onset of osteoarthritis. While the mechanical sources of PF joint dysfunction are not well understood, links have been established between PF tracking and abnormal kinematics of the tibiofemoral (TF) joint, specifically following cruciate ligament injury and repair. The objective of this study was to create a validated finite element (FE) representation of the PF joint in order to predict PF kinematics and quadriceps force across healthy and pathological specimens. Measurements from a series of dynamic in-vitro cadaveric experiments were used to develop finite element models of the knee for three specimens. Specimens were loaded under intact, ACL-resected, and both ACL and PCL-resected conditions. Finite element models of each specimen were constructed and calibrated to the outputs of the intact knee condition, and subsequently used to predict PF kinematics, contact mechanics, quadriceps force, patellar tendon moment arm, and patellar tendon

angle of the cruciate resected conditions. Model results for the intact and cruciate resected trials successfully matched experimental kinematics (avg. RMSE 4.0°, 3.1 mm) and peak quadriceps forces (avg. difference 5.6%). Cruciate resections demonstrated either increased patellar tendon loads or increased joint reaction forces. The current study advances the standard for evaluation of PF mechanics through direct validation of cruciate-resected conditions including specimen-specific representations of PF anatomy.

3.2 Introduction

Healthy patellofemoral (PF) joint mechanics are critical to optimal function of the knee joint. The main function of the patella is to distribute quadriceps load to efficiently extend the knee (Buff et al., 1988; Huberti et al., 1984). Patellar maltracking creates increased PF ligament strains, soft tissue injury and/or knee pain (Fulkerson, 2002; Post et al., 2002). In addition, maltracking may lead to large joint reaction loads and high stresses on the articular cartilage; these factors increase the risk of cartilage wear and development of bone abnormalities which ultimately contribute to osteoarthritis (Han et al., 2005; Wu et al., 2000; Zhang et al., 2007). While the mechanical sources of PF joint dysfunction are not well understood, links have been established between PF tracking and soft-tissue pathologies and abnormal kinematics of the tibiofemoral (TF) joint (Li et al., 2004a; Mizuno et al., 2001; Powers, 2003). Due to the interaction between TF and PF mechanics, PF dysfunction is prevalent following cruciate ligament injury and repair. The anterior cruciate ligament (ACL) of the knee is the primary restraint to anterior

translation of the tibia relative to the femur, a secondary restraint to varus/valgus and internal/external rotations of the tibia, and a key guide to the screw-home mechanism at full extension (Girgis et al., 1975). Follow-up studies of ACL-deficient patients have found altered patellar tracking and PF contact mechanics (Van de Velde et al., 2008), including signs of knee instability, pain, and patellar dislocation (Nebelung and Wuschech, 2005). The posterior cruciate ligament (PCL) of the knee is the primary restraint to posterior translation of the tibia relative to the femur, and contributes more generally to tibiofemoral stability at higher flexion angles. Like those with ACL-deficiency, subjects with posterior cruciate ligament (PCL) deficiency exhibit altered patellar mechanics, particularly in deep knee flexion (von Eisenhart-Rothe et al., 2012). Understanding the interaction between cruciate injury and PF mechanics is important in determining optimal treatment pathways to better restore extensor mechanism function.

While in vivo and in vitro experiments may be used to compare patellar kinematics and quadriceps extensor function between healthy control subjects and cruciate-deficient patients, there are some limitations associated with these studies. Joint loads are impractical to quantify in-vivo and in-vitro studies may allow measurement of contact pressure and joint contact (Elias et al., 2004), but are typically costly and time-intensive so that only small numbers of specimens can be evaluated. Due to the challenges of quantifying patellar function using in vitro and in vivo experiments, computational models of PF mechanics have been developed to understand patellar function and treatment (Barry et al., 2010; Halonen et al., 2015; Mesfar and Shirazi-Adl,

2005, 2006a, b). Prior models incorporated muscle and ligament forces, and the interaction of PF and TF mechanics including contact stresses in cartilage and the menisci. These models were used to study the kinematics and kinetics of the PF joint through simulation of gait (Barry et al., 2010; Halonen et al., 2015) and knee flexion (Mesfar and Shirazi-Adl, 2005, 2006a, b). Furthermore, probabilistic analyses were used to simulate PF pathology due to variability in ligament material properties (Barry et al., 2010; Dhaher et al., 2010; Mesfar and Shirazi-Adl, 2006a), muscle loading (Mesfar and Shirazi-Adl, 2005), and kinematics (Mesfar and Shirazi-Adl, 2006b). While most prior models were based on specimen or subject specific geometry, they may be limited because they were not calibrated or validated with combined experimental measurements of PF kinematics of the same subject or specimen.

Computational models are an ideal complement to experimental simulations (Beillas et al., 2004; Blankevoort and Huiskes, 1996). Sophisticated PF computational models can be validated using six degree of freedom (DOF) PF motion from identically loaded cadaveric tests (Baldwin et al., 2012; Guess et al., 2010; Heegard et al., 1995). Validated computational models can be used to overcome some of the limitations of in vivo and in vitro experiments; multiple procedures can be virtually performed on the same knee and compared under repeated loading conditions. Similar models have been used to evaluate cartilage damage in osteoarthritic patients (Cohen et al., 2003b), and simulate PF joint surgery (Cohen et al., 2003a), but typically are not validated under both healthy and altered conditions.

Restoration of normal patellar function is difficult to achieve once it has been compromised by injury or disease. To support clinicians and engineers, a reliable model for evaluation of PF joint mechanics is crucial to understanding patellar function and testing conservative and surgical therapies. The objective of this study was to create a validated finite element (FE) representation of the PF joint in order to predict PF kinematics and quadriceps force across healthy and pathological specimens. Specifically, given the relationship between PF dysfunction and cruciate ligament injury, intact, anterior cruciate ligament (ACL)-deficient and both ACL and posterior cruciate ligament (PCL)-deficient models were developed. While prior computational studies have modeled healthy PF mechanics and simulated injured/altered knee conditions, the current study advances the state of the art by recreating specimen-specific PF mechanics in healthy knees and directly validating cruciate-deficient conditions. A secondary objective was to assess the variability of PF mechanics to uncertainty in experimental measurement accuracy. The PF model was calibrated and validated through comparison to measured kinematics and quadriceps loads obtained from in-vitro simulations. Model calibrations were performed on the intact knee, while the subsequent ACL-deficient and PCL-deficient models predicted kinematics, quadriceps forces, and extensor function. Validated FE models may be used for the evaluation of cruciate injury and repair though parametric analyses assessing the variability in ligament/tendon stiffness, geometric shape and alignment, kinematics and muscle forces.

3.3 Methods

3.3.1 Experimental Testing

Three fresh frozen cadavers (all male, mean age of 55.3 years (range 44-72), mean height of 180.3 cm (range 175-183), mean weight of 91.5 kg (range 70-127)) were thawed at room temperature and, femur and tibia bones were sectioned approximately 20 cm from the knee joint line. All soft tissue beyond 10 cm of the joint was removed from the bones except quadriceps and hamstring muscles. Knees were examined and found to have no visible signs of injury. Following computed tomography (CT) and magnetic resonance (MR) imaging, a series of dynamic in-vitro tests were performed on the cadavers in the MLR as described by (Shalhoub and Maletsky, 2014). The MLR mounted the knee joint in an inverted position, such that the femur was rigidly attached and the tibia was allowed to move freely (Figure 3.1). Quadriceps and hamstring tendons were clamped and passed through a series of pulleys to maintain a physiological orientation to the joint. A stepper motor (Nema 34, Danahar Automation, Wood Dale, IL) and a 1300 N load cell (Transducer Technique, Temecula, CA) were connected in-line with the quadriceps clamp to produce deep knee flexion to approximately 120 degrees and to measure the resulting quadriceps load. The quadriceps line of action was applied through the combined tendons of the rectus femoris and vastus intermedialis. In addition, a static weight of 89 N was applied to the semimembranosus and biceps femoris hamstring muscles. An Optotrak 3020 motion capture system (accuracy within 0.04 deg.

and 0.03 mm) was used to record tibiofemoral and patellofemoral kinematics (Maletsky et al., 2007).

Each knee specimen cycled through a deep knee bend in the MLR under three conditions: intact, ACL-resected, and both ACL and PCL-resected (referred to subsequently as PCL resected). Dynamic knee flexion tasks were repeated 5 times in intact and cruciate-resected conditions. Following testing, the specimen was removed from the MLR. Anatomical landmarks on the femur, tibia, and patella were digitized to establish bone fixed coordinate systems and track relative kinematics of the bones. In addition, position of soft tissue attachments and MLR components were digitized for constructing a finite element model of the experimental setup (quadriceps and hamstrings muscle line of action, patellar tendon attachment sites, rectus-femoris patellar attachment, biceps femoris and semimembranosus tibial attachments, point clouds of bone and articular geometry).

3.3.2 Computational Modeling

Specimen-specific finite element (FE) models of the MLR experiment were developed in Abaqus/Explicit (Simulia, Providence, RI) to recreate the loading and boundary conditions for the intact and cruciate-resected conditions (Figure 3.1). Given the complex, changing contact conditions and large deformations of soft tissue structures, explicit analyses were chosen for computational efficiency (Abaqus 6.11 Analysis Users Manual 2011). Bone and cartilage geometry were segmented and reconstructed from CT

and MR imaging (1x0.35x0.35mm), respectively, using ScanIP (Simpleware, Exeter, UK). Bones were represented using rigid triangular shell elements (R3D3), and cartilage was represented using hexahedral continuum elements (C3D8R). The cartilage FE mesh was formed using a semi-automated morphing technique to match the surface geometry reconstructed from MRI to a hexahedral template (Baldwin et al., 2010). Patellofemoral soft tissue structures including the rectus femoris tendon, patellar tendon, medial patellofemoral ligament, and lateral patellofemoral ligament were modeled by 2D fiber reinforced membrane (M3D4R) and non-linear spring elements (CONN3D2). Ligament/tendon material properties were established in separate planar analyses to match published experimental uniaxial force-displacement data (Baldwin et al., 2009). A mesh convergence study was performed on the cartilage and PF soft tissue to ensure sufficient accuracy (<5% difference in kinematics and joint loads). Quadriceps and hamstring muscles were represented using point-to-point slot connections (CONN3D2): a single connector element for quadriceps, two connectors for the biceps femoris and semimembranosus.

Bone and cartilage were aligned to MLR test space using a semi-automated procedure that minimized the distance between points digitized on the specimen during testing and reconstructed geometry surfaces. Location and orientation of PF soft tissue structures, quadriceps and hamstring muscle line of actions were defined using digitized points from the experiment. The influence of patellar parameters on PF mechanics was isolated by kinematically prescribing TF motions. TF flexion-extension was driven using

quadriceps tendon excursion measured from the experiment. The resulting reaction load in the quadriceps tendon was then compared to the experimental value as part of the calibration and validation of PF mechanics. All other TF DOFs were kinematically prescribed to match the experiment. TF kinematics were applied using tabular amplitude cards to reproduce the motions in the MLR experiment; motions were discretized at 0.1 second intervals over the 8 second analysis. For computational efficiency, bone and cartilage geometry were defined as rigid bodies, with appropriate mass and rotational inertia properties, in the FE simulation. Penalty-based rigid-body contact was defined between the articular cartilage of the patella and femur using a previously calibrated surface pressure-overclosure relationship (Fitzpatrick et al., 2010), and a hard pressure-overclosure relationship (zero surface penetration) was defined between bone and soft tissue (Halloran et al., 2005). A previous study compared deformable and rigid body contact in eight test specimens, and found similar contact pressures and area with kinematic differences less than 0.5° and 0.2 mm (Fitzpatrick et al., 2010). Model setup was repeated for all intact knees and their corresponding cruciate-resected cases.

In order to calibrate the intact models to the experimental kinematic data, soft tissue attachment locations and orientations were perturbed within measurement error of digitized points. Rectus femoris, patellar tendon, and hamstrings attachment locations were adjusted to calibrate model PF flexion-extension, internal-external rotation, and medial-lateral translation in intact knees to the experimental measurements. Additionally, pre-strain in medial and lateral PF ligaments was calibrated for each

specimen in the intact condition. The pre-tension was manually adjusted for each specimen to minimize differences in initial experimental and model patellar alignment after quadriceps loading and prior to flexion (Baldwin et al., 2009). To validate performance of the model knees, soft tissue attachment sites and ligament pre-strain were not changed in the following ACL and PCL resected simulations. Outputs from specimen-specific models of the intact and resected knees included PF kinematics, joint contact mechanics, quadriceps force, patellar tendon moment arm, patellar tendon angle, and patellar force ratio.

3.4 Results

3.4.1 PF Kinematics

Experimental TF kinematics showed notable increases in internal rotation and posterior translation of the tibia after PCL resections, but presented only small changes in ACL resected specimens (Figure 3.2). There were consistent trends in all other DOF between the three specimens that remained following cruciate ligament resection.

Model predicted PF kinematics showed agreement with experimental data in both trend and magnitude. The model matched experimental data with average root-mean-square (RMS) differences of 3.6° in rotations and 2.5 mm in translations for the intact trials, 3.9° and 3.1 mm in the ACL-deficient trials, and 4.6° and 3.7 mm in the PCL-deficient trials (Figure 3.3a). Specifically, PF flexion-extension and medial-lateral

translation matched experimental kinematics with average RMS differences less than 5° and 3 mm. The model predicted PF tilt to the experiment in deep flexion (> 50°) with average RMS difference less than 2°.

Measurement uncertainty in soft tissue attachments influenced model predicted PF kinematics (Figure 3.3b). Accounting for measurement error, the bounds of uncertainty in PF kinematics captured specimen-specific behavior.

3.4.2 Quadriceps Forces

When comparing model quadriceps forces to experimental load cell data, peak forces in the intact, ACL-deficient, and PCL-deficient trials had average errors of 4.3%, 7.2%, and 5.3% averaged across all specimens, respectively (Figure 3.4, Table 1). The modeled extensor mechanism was able to distinguish peak quadriceps loads between each of the specimens. Specimen 2 demonstrated notable increases in peak quadriceps force with subsequent cruciate resections (~24% from intact to PCL-resected) consistent with trends reported in literature (Ostermeier et al., 2004), however Specimen 1 showed a slight decrease (~8% from intact to PCL-resected) and Specimen 3 showed no difference in quadriceps load.

3.4.3 Patellar Tendon Moment Arm

Patellar tendon moment arm was calculated as the perpendicular distance between the patellar tendon and the helical axis center. The center of rotation in the tibiofemoral

joint was determined using equations described by (Spoor and Veldpaus, 1980). In specimens 1 and 2, cruciate resections presented increases in patellar tendon moment arm in deep flexion, while Specimen 3 remained consistent (Figure 3.5a).

3.4.4 Patellar Tendon Angle

Patellar tendon angle was calculated as the angle between the tendon line of action and the mechanical axis of the tibia. In general, trends showed a positive angle in knee extension, which decreased with knee flexion; a negative angle accompanied wrapping of the patellar tendon around the anterior face of the tibia (Buff et al., 1988; Price et al., 2004; Yamaguchi and Zajac, 1989) (Figure 3.5b). While the magnitude of patellar tendon angle remained consistent from the healthy to the ACL-deficient condition, in the PCL-deficient condition, the patellar tendon angle was significantly larger through the flexion-extension cycle.

3.4.5 Patellar Force Ratio

Patellar force ratio was defined as the patellar tendon force (Fpt) divided by quadriceps force (Fq) (Figure 3.5c). An increase in force ratio following cruciate resection indicated either higher strain in the patellar tendon or redistribution of load from the quadriceps tendon to joint contact. Specimen 1 showed an increase in patellar force ratio following ACL and PCL resections. In Specimen 2, forces were redistributed from the quadriceps to the patellar tendon only in early flexion, but remained consistent with healthy joint loads at later flexion angles. Specimen 3 demonstrated an increase in

patellar force ratio in the ACL deficient knee, but healthy and PCL-deficient trials showed similar magnitudes.

3.4.6 PF Contact

The ratio of PF cartilage contact force to quadriceps force increased with subsequent cruciate resections for all specimens (Figure 3.5d). PF contact distributions travelled superiorly and contact area increased as a function of knee flexion (Besier et al., 2005) (Figure 3.6).

3.5 Discussion

A detailed representation of the patellofemoral joint and quadriceps mechanism was developed to create a computational tool for the evaluation of PF mechanics in healthy and cruciate-deficient conditions. Prior computational studies of the PF joint have modeled healthy mechanics, and simulated injured and repaired knee conditions (Barry et al., 2010; Mesfar and Shirazi-Adl, 2006a; Salehghaffari and Dhaher, 2014). The current work created specimen-specific PF representations of soft tissue attachments and muscle line of actions, and provided a direct validation of cruciate-deficient mechanics. The FE representation of the healthy PF joint was kinematically calibrated to results from in-vitro testing of three intact specimens. The model was then validated through comparisons to experimental kinematics, quadriceps force, and extensor function in the cruciate resected conditions. The validated computational model of the PF joint

effectively captured the overall path and range of motion in the patella (Figure 3.3a, 3.3b). Model results for the intact and cruciate resected trials successfully matched experimental kinematics with average RMS differences (4.0°, 3.1 mm) similar to values reported by others (Baldwin et al., 2009; Blankevoort and Huiskes, 1996; Guess et al., 2010), while effectively replicating individual differences between specimens.

Measurement uncertainties in soft tissue attachments and muscle line of action during the experiment affected model accuracy (Figure 3.3b). AP positions of the rectus femoris and patellar tendon attachments influence the extensor moment arm and quadriceps force. As a result, the orientation and patellar attachment sites of the rectus femoris and patellar tendon had a significant impact on PF flexion range of motion; a 1 mm anterior shift of the rectus femoris attachment site on the patella increased maximum PF flexion by ~3°. Although articulating geometry was the primary determinant of PF medial-lateral translations and internal-external rotations, variation in attachment sites and pre-strain of the PF ligaments influenced initial settling of the patella into the trochlear groove. Medial and lateral PF ligaments provided constraint and improved stability in M-L translations in early flexion.

Across specimens and conditions, peak quadriceps forces matched experimentally measured loads with an average difference of 5.6% (Figure 3.4). Forces were most accurate in mid flexion, where geometric constraint of the patella was the greatest. Magnitudes of quadriceps forces were consistent with loads described in similar knee-

extension experiments (Buff et al., 1988; Grood et al., 1984). Perturbation of parameters with experimental measurement uncertainty (TF kinematics, soft-tissue attachments) demonstrated substantial influence in altering quadriceps load; in particular, uncertainty in the tibial attachment location of the hamstrings altered the flexion angle at which peak quadriceps force occurred, while measurement error in TF anterior-posterior kinematics influenced predicted force at deepest flexion.

Patellar tendon moment arm and angle were consistent with previous findings (Figure 3.5a, 3.5b). Moment arm and patellar tendon angle matched values reported in the literature in both trend and magnitude (Ahmed et al., 1987; Grood et al., 1984; Krevolin et al., 2004). When comparing healthy and cruciate-deficient conditions, patellar tendon moment arm increased in deep flexion consistent with the variations presented in patellar tendon angle. The ACL-deficient experimental kinematics did not produce a substantial change in TF anterior tibial translation, and so, patella tendon angle remained relatively consistent when compared to the healthy knee. Greater changes in patella tendon angle were observed in the PCL-resected condition due to the posterior shift of the tibia during knee flexion.

Cruciate resections demonstrated either increased patellar tendon loads or increased joint reaction forces (Figure 3.5c, 3.5d). Each specimen was unique in balancing load through the PF joint, highlighting the need for specimen-specific analyses of the quadriceps mechanism. While specimen 1 distributed forces from the quadriceps

to both patellar tendon and cartilage surfaces, specimen 2 primarily transferred load to joint contact. Specimen 3 alternated load distribution from the patellar tendon to the joint reaction in subsequent ACL and PCL resections, with an increase in patellar force ratio after removing the ACL and an increase in joint contact force after removing the PCL. PF contact distributions travelled superiorly and contact area increased as a function of knee flexion, consistent with patterns reported by others (Besier et al., 2005; Huberti et al., 1984) (Figure 3.6). Specimens 1 and 3 showed only small changes to PF contact center of pressure following ACL and PCL resections, however, specimen 2 demonstrated a lateral shift in the PCL-deficient trial (shown in Figure 3.6). Even though contact patterns were similar in healthy and pathological conditions, peak contact pressures increased (2-12%) with cruciate resections.

The main limitation of the current study is the relatively small differences in TF and PF kinematics between healthy and ACL-deficient conditions. The inverted position of the experimental setup did not promote anterior translation of the tibia from an ACL resection during knee extension as the weight of the remaining lower limb tended to place a posterior load on the tibia. Also, the application of hamstrings forces in extension may have contributed to reducing the anterior motion of the tibia. Because TF A-P differences were small, the ACL may have been lightly loaded in the fully-intact trials as well. However, the PCL-deficient condition, the inverted experimental setup and hamstrings loads caused large posterior tibial translations. Therefore, PCL-deficient trials presented significant TF and PF kinematic variability when compared to the healthy

specimen. A second limitation was that thigh/calf contact was not modeled and may have influenced quadriceps force in deep flexion. Model predicted quadriceps forces were in reasonable agreement to the experiment, however, the flexion angle at which peak loads occurred was difficult to match computationally with an average error of 14.8%. In PCL-deficient trials, the experiment reported an average 8° reduction in peak flexion angle. As joint stability decreased with PCL resections, each specimen demonstrated increased posterior translation of the tibia in deep flexion. As a results, the knee joint may have partially been supported in deep flexion by the soft-tissue mass (muscle, fat, posterior capsule) posterior to the joint. The FE representations did not include modeling this soft-tissue, and so quadriceps force predictions did not account for off-loading from thigh-calf reaction force.

Additionally, finite element analyses relied on PF ligament material properties from literature (Baldwin et al., 2009). To evaluate the sensitivity of model kinematics on these properties, ligament stiffness parameters were doubled; differences in PF kinematic predictions remained less than 1° and 1 mm.

Furthermore, the experiment and associated computational model produced loads less than in vivo weightbearing conditions. The purpose of this work was to demonstrate that the computational model could appropriately evaluate different normal and pathological states produced by a repeatable experiment. Considering the role of cruciate ligaments in anterior-posterior constraint at the knee and overall joint stability, cruciate

injuries have been identified as a key factor in altered neuromuscular function at the knee (Devita et al., 1997; Patel et al., 2003), which will typically present altered muscle activations thought to compensate for the partial or complete absence of the cruciates. Future application of the validated PF model could be used to simulate in vivo correction of tibial anterior-posterior constraint through changes in muscle force (Mesfar and Shirazi-Adl, 2006b).

Finally, TF motions were kinematically prescribed in the model. A resultant quadriceps line of action was used to describe TF flexion-extension, but may have limited the contribution of individual vastus muscles on PF mechanics, especially PF kinematics in off-axis DOF. Prescribing TF kinematics was necessary to focus on patellar calibration and isolation of the effects of patellar parameters on the extensor mechanism. Future models will include musculoskeletal loads and specimen-specific representations of TF soft tissue structures.

The validated computational model predicts PF joint mechanics in the intact and cruciate-deficient knee. The PF model developed in this study will be used for subject-specific predictions of PF joint kinematics and quadriceps force, integrated into a multi-scale musculoskeletal model of the lower extremity for investigation of normal, pathologic, and repaired function. These models may be used to simulate soft-tissue injury and repair and quantitatively assess the effect of surgical decisions during ACL or PCL reconstruction on PF mechanics and extensor mechanism efficiency and function.

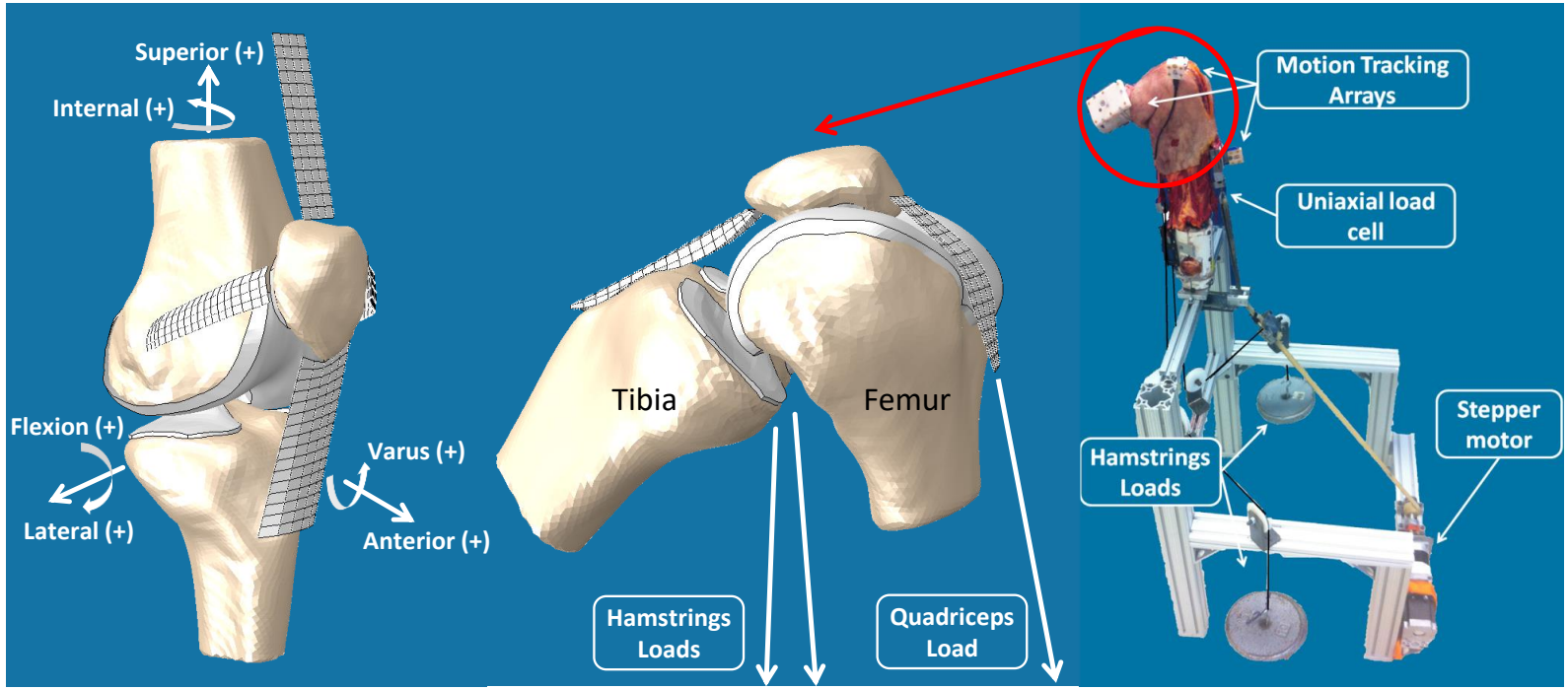

Figure 3.1 Knee cadaver mounted in muscle loading rig (MLR) (right) and its computational representation (left)

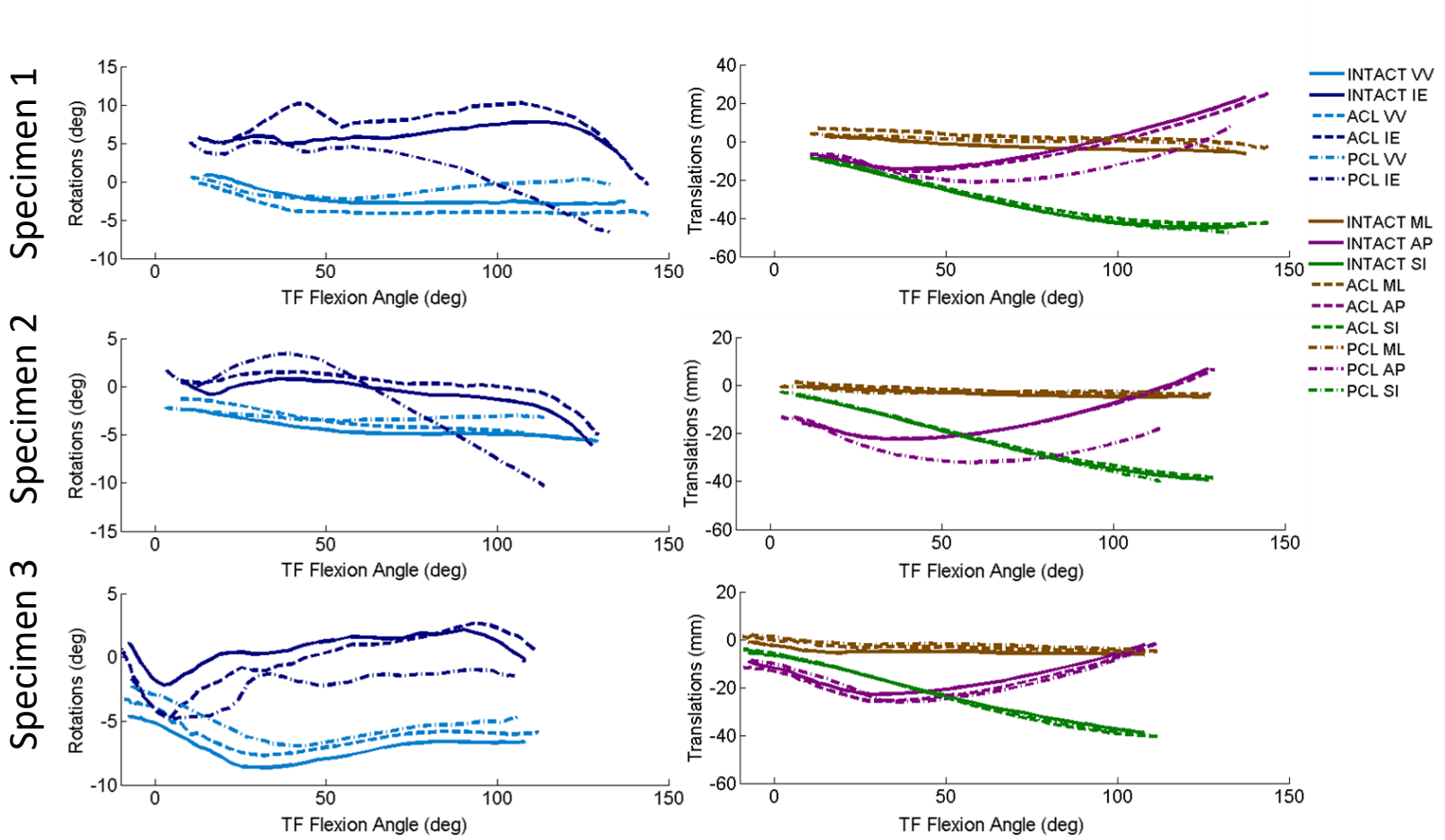

Figure 3.2 Experimental TF kinematics for the intact, ACL-deficient, and PCL deficient conditions (VV: varus(+)/valgus(-), IE: internal(+)/external(-), ML: medial(-)/lateral(+), AP: anterior(+)/posterior(-), SI: superior(+)/inferior(-))

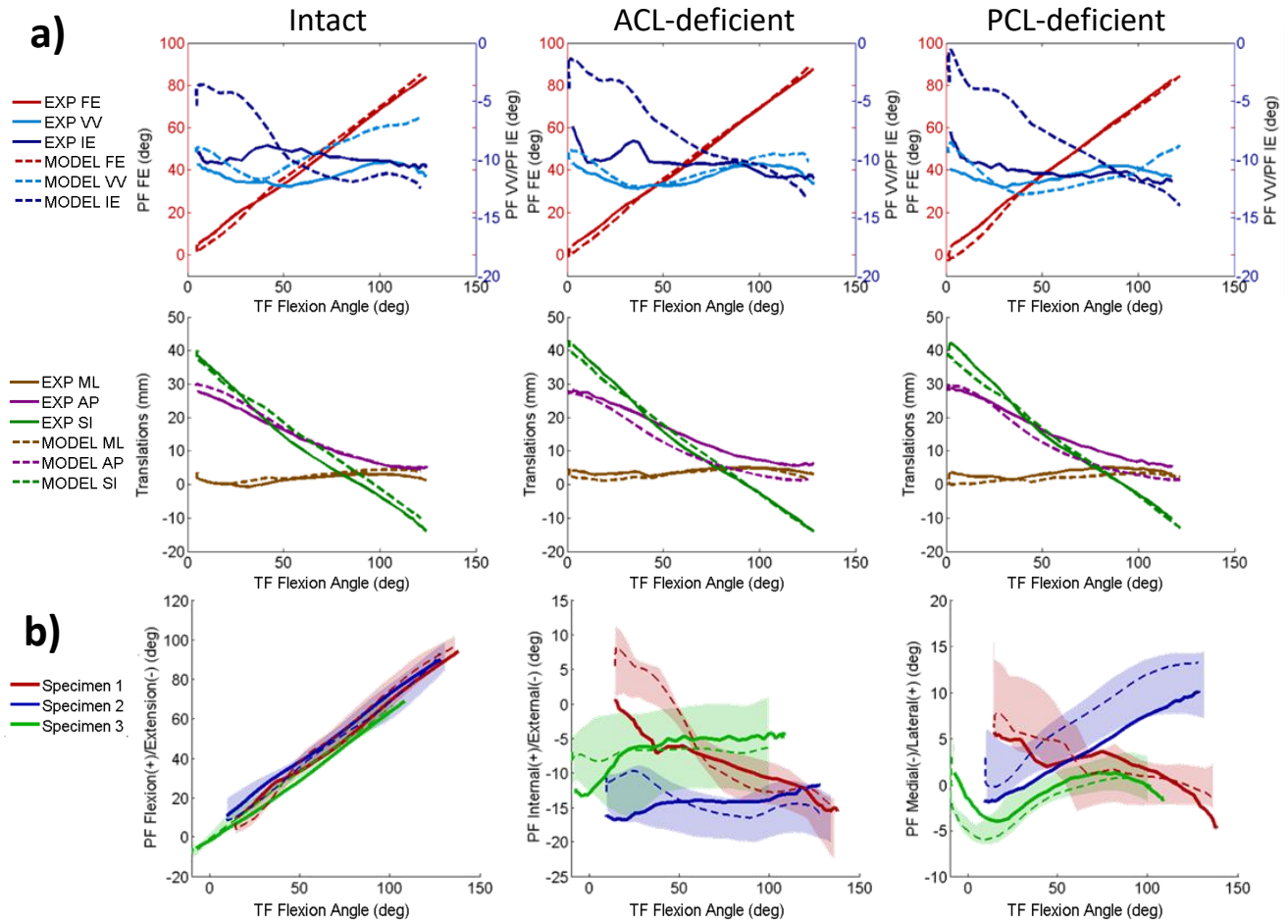

Figure 3.3 a) Comparison of experimental and model predicted PF kinematics in the intact (left), ACL-deficient (middle), and PCL-deficient (right) conditions averaged across specimens. b) Uncertainty in model PF kinematics (F-E, I-E, and M-L) shown for 3 intact specimens with experimental (solid line), model (dashed line), and bounds of uncertainty (shaded region). (FE: flexion(+)/extension(-), VV: varus(+)/valgus(-), IE: internal(+)/external(-), ML: medial(-)/lateral(+), AP: anterior(+)/posterior(-), SI: superior(+)/inferior(-))

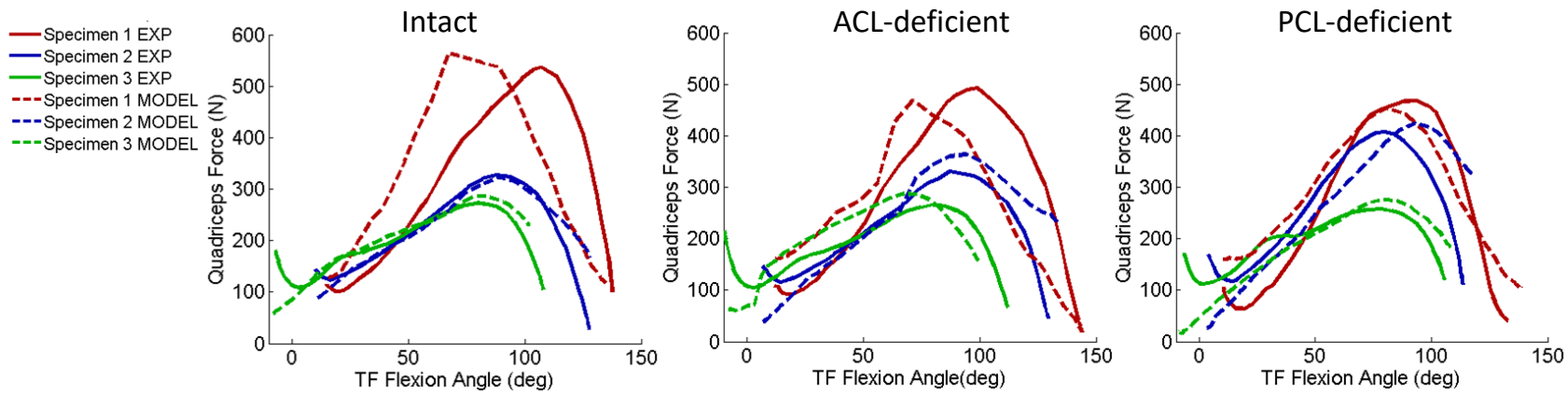

Figure 3.4 Model predicted quadriceps forces in the intact (left), ACL-deficient (middle), PCL-deficient (right) conditions

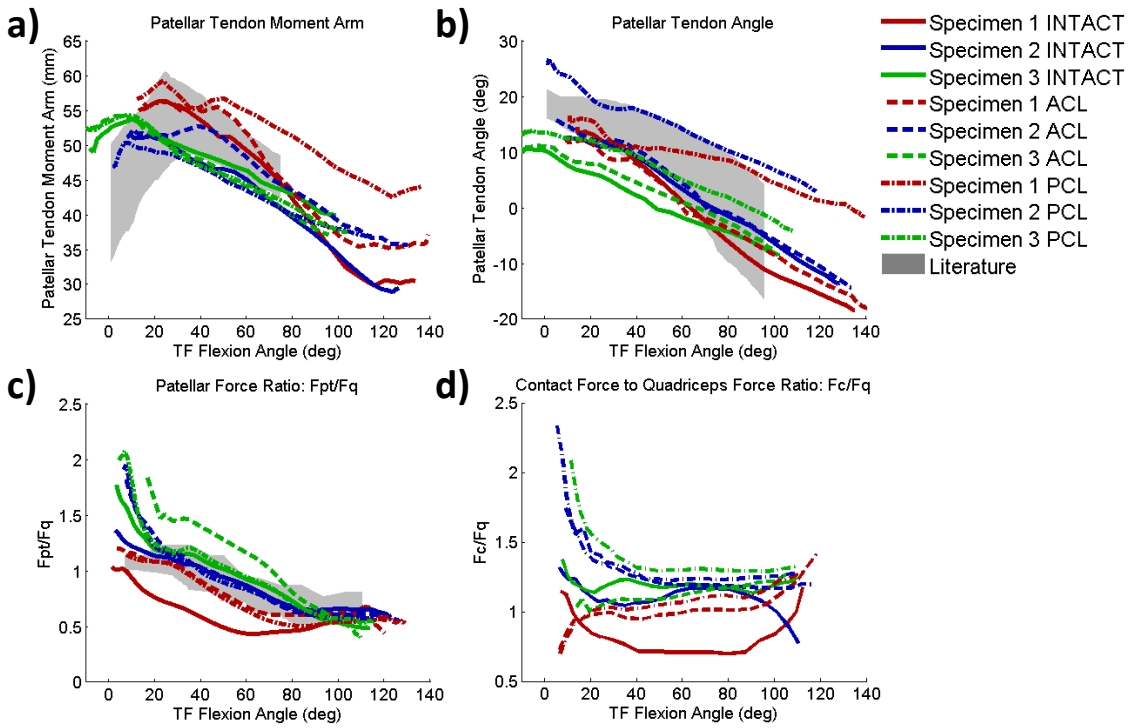

Figure 3.5 a) Patellar tendon moment arm, b) patellar tendon angle, c) patellar force ratio, and d) contact to quadriceps force ratio presented for intact and cruciate-deficient conditions. Shaded regions represent the span of experimental data from literature sources (Ahmed et al., 1987; Buff et al., 1988; Grood et al., 1984; Yamaguchi and Zajac, 1989)

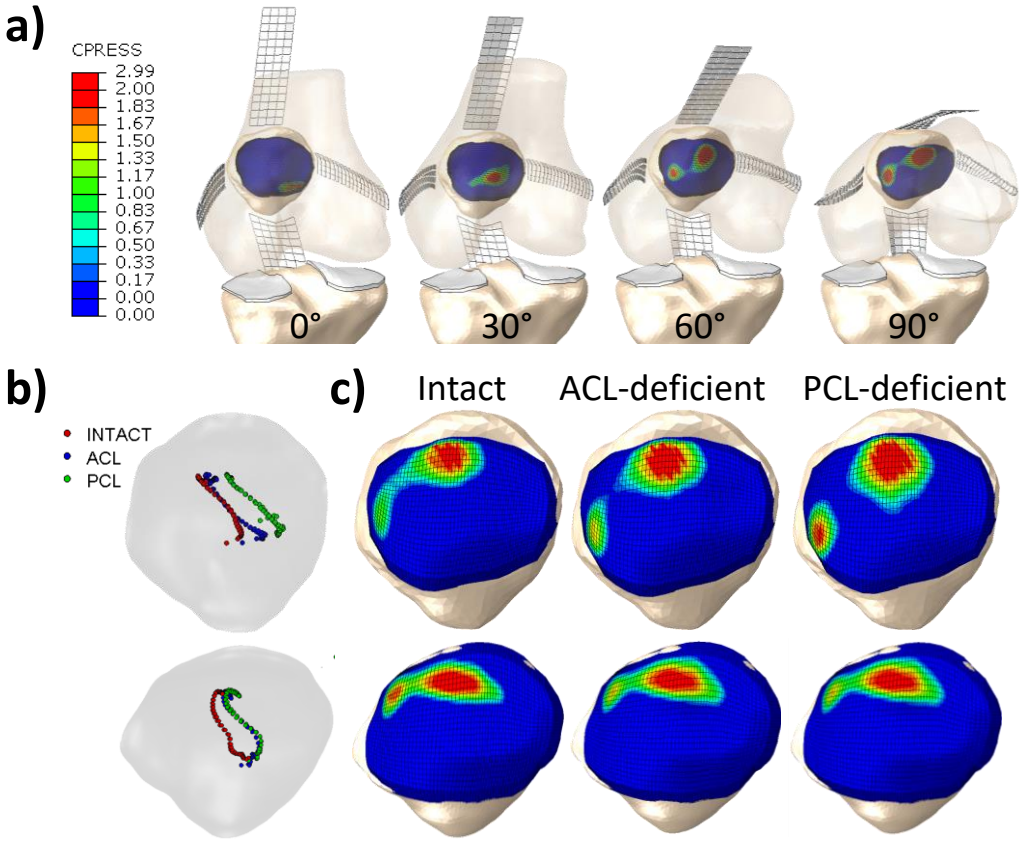

Figure 3.6 a) PF contact pressure distributions shown in a representative specimen at knee flexion angles of 0°, 30°, 60°, and 90°. b) PF contact center of pressure through the flexion activity and c) contact distribution at ~90° is shown for a representative specimen in intact and cruciate-deficient conditions.

Table 3.1 Experiment and model quadriceps forces and corresponding flexion angles shown for intact and cruciate-deficient conditions. Peak forces are averaged over the flexion and extension portions of the activity.

Specimen		Maximum Quad Force											
		Intact				ACL				PCL			
		(N)	% Error	(°)	% Error	(N)	% Error	(°)	% Error	(N)	% Error	(°)	% Error
DU01	Exp	536.0	5.6	103.7	26.8	512.0	0.2	105.0	24.3	559.0	4.2	90.5	18.4
	Model	566.1		76.0		512.9		79.5		582.5		73.9	
DU02	Exp	333.1	1.1	84.8	8.9	332.7	11.7	91.2	0.4	415.0	2.6	76.8	25.6
	Model	329.5		92.4		371.6		90.9		425.7		96.5	
DU03	Exp	272.7	6.3	77.0	11.4	266.5	9.6	80.1	3.7	258.9	9.2	73.7	13.5
	Model	289.9		85.8		292.1		77.2		282.8		83.6	
Average			4.3		15.7		7.2		9.4		5.3		19.1

CHAPTER 4 – COMBINED MEASUREMENT AND MODELING OF SPECIMEN-SPECIFIC KNEE MECHANICS FOR HEALTHY AND ACL-DEFICIENT CONDITIONS

4.1 Abstract

Quantifying the mechanical environment at the knee is crucial for developing successful rehabilitation and surgical protocols. Computational models have been developed to complement in-vitro studies, but are typically created to represent healthy conditions, and may not be useful in modeling pathology and repair. Thus, the objective of this study was to create finite element (FE) models of the natural knee, including specimen-specific tibiofemoral (TF) and patellofemoral (PF) soft tissue structures, and to evaluate joint mechanics in intact and ACL-deficient conditions. Simulated gait in a whole joint knee simulator was performed on two cadaveric specimens in an intact state and subsequently repeated following ACL resection. Simulated gait was performed using motor-actuated quadriceps, and loads at the hip and ankle. Specimen-specific FE models of these experiments were developed in both intact and ACL-deficient states. Model simulations compared kinematics and loading of the experimental TF and PF joints, with average RMS differences [max] of 3.0°[8.2°] and 2.1°[8.4°] in rotations, and 1.7[3.0] and

2.5[5.1] mm in translations, for intact and ACL-deficient states, respectively. The timing of peak quadriceps force during stance and swing phase of gait was accurately replicated within 2° of knee flexion and with an average error of 16.7% across specimens and pathology. Ligament recruitment patterns were unique in each specimen; recruitment variability was likely influenced by variations in ligament attachment locations. ACL resections demonstrated contrasting joint mechanics in the two specimens with altered knee motion shown in one specimen (up to 5 mm anterior tibial translation) while increased TF joint loading was shown in the other (up to 400 N).

4.2 Introduction

When healthy knee mechanics are compromised by injury or disease, the load distribution through the joint is altered, which can lead to pain, additional injury, and long-term disability (Fulkerson, 2002; Nebelung and Wuschech, 2005). In particular, long-term studies of anterior cruciate ligament (ACL) injury have associated increased joint loading and altered knee kinematics with a high prevalence of osteoarthritis, knee pain, and instability (Lohmander et al., 2007; Nebelung and Wuschech, 2005). The ACL acts as the primary restraint to anterior translation of the tibia with respect to the femur, and a secondary restraint to internal-external and varus-valgus rotation (Girgis et al., 1975), and is the most frequently disrupted ligament in the knee (Beynnon et al., 2005).

Quantifying the mechanical environment at the knee is crucial for developing successful rehabilitation and surgical protocols following ACL injury. Since joint contact, soft tissue and muscle forces are difficult to quantify in-vivo, researchers have developed in-vitro cadaveric tests to evaluate natural knee mechanics. By simulating everyday activities, in-vitro measurements can be used to compare joint motions and tissue forces in healthy, pathological, and repaired specimens (Maletsky and Hillberry, 2005). Experimental testing provides a repeatable controlled environment for evaluation of joint mechanics, but can be costly and time-intensive when considering multiple design iterations and large numbers of specimens.

Hence, computational models have been developed to complement in-vitro studies (Bendjaballah et al., 1995; Blankevoort and Huiskes, 1996; Godest et al., 2000; Guess and Stylianou, 2012; Pena et al., 2006), and enable prediction of internal joint and soft tissue stresses/strains for efficient evaluations of knee mechanics. Computational knee models are typically built from digital representations of cadaver specimens from imaging, and tissue properties are calibrated using experimental measurements of tissue and whole-joint mechanics. Decisions on model complexity and the ability to calibrate model estimates are influenced by the available experimental data. For example, experimental joint laxity tests have been performed to develop load-displacement curves for calibration of computational representations of the passive soft-tissues of the knee (Godest et al., 2000; Kiapour et al., 2014; Mootanah et al., 2014). While passive experiments are important for quantifying joint stiffness and identifying ligament

properties, these data do not necessarily represent the performance of the knee in activities. To that end, researchers have developed muscle-loaded experiments to simulate quadriceps (Ahmad et al., 1998; Baldwin et al., 2009) and hamstrings (Kwak et al., 2000) forces during dynamic tasks, and utilized these data in predictive musculoskeletal simulations (Adouni et al., 2012; Piazza and Delp, 2001; Shelburne et al., 2004a) to estimate knee mechanics under conditions challenging to reproduce with in-vitro experiments. Taking a further step, studies have used computational models to simulate injury and degenerated conditions, such as rupture of the ACL and menisectomy (Halonen et al., 2016; Li et al., 2002b; Mesfar and Shirazi-Adl, 2006a; Moglo and Shirazi-Adl, 2003; Shelburne et al., 2004a; Tanska et al., 2015), however, computational models are typically not compared to specimen-specific experimental data under both healthy and pathological conditions.

Our prior work focused on the development of computational models of the implanted knee during dynamic activity (Baldwin et al., 2012). Computational predictions were compared to experimental data from the six-degree-of-freedom electro-hydraulic Kansas knee simulator (KKS). More recently, models have been developed of the natural knee. Calibration of specimen-specific PF mechanics was performed in a muscle-loaded rig (MLR) designed to isolate the quadriceps mechanism during knee flexion (Ali et al. 2016). Joint laxity tests were performed on the same specimens to quantify joint constraint and derive optimized TF ligament material properties (Harris et

al., 2016). However, these models of the PF and TF articulations of the knee were not combined into a dynamic representation of the natural knee.

The objective of this study was to create specimen-specific finite element (FE) models of the natural knee, including specimen-specific TF and PF soft tissue structures supported through kinematic comparisons to cadaveric experiments, and to evaluate joint mechanics for intact and ACL-deficient conditions. A muscle-loaded in-vitro simulation of gait using motor-actuated quadriceps forces, and loads at the hip and ankle was used to measure the dynamic motion of knee specimens. FE modeling replicated experimental loading conditions and model accuracy was evaluated through direct comparisons to the experimental TF and PF kinematics, and quadriceps forces in intact and ACL-deficient conditions. FE models included predictions of joint contact forces and ligament tensile and shear forces with respect to the tibia.

4.3 Methods

4.3.1 Summary

The current work was the third step in a three-step combined measurement and modeling approach to develop FE models of the natural knee for two specimens. In the first step, in-vitro testing replicated a deep knee bend using motor-actuated quadriceps force to calibrate PF mechanics in specimen-specific FE models of the experiment (Ali et al., 2016). In the second step, laxity experiments were performed in the same knees to

capture passive constraint of the TF joint (Harris et al., 2016). FE modeling of the laxity experiments allowed calibration of TF soft tissue material properties and attachment locations for intact and ACL-deficient conditions. In the third and final step, the current study integrated TF and PF soft tissue representations developed in the previous two steps to evaluate subject-specific knee mechanics of the same specimens during dynamic activity replicated using the KKS.

4.3.2 Experimental Setup

Dynamic *in-vitro* tests were conducted on two fresh frozen cadavers (2 male; age: 50, 72 years; height: 175, 183 cm; weight: 127, 77 kg). Knees were thawed at room temperature and computed tomography (CT, 0.39x0.39x0.6mm, resolution:512x512) and magnetic resonance (MR, 0.53x0.53x0.6mm, resolution:320x320, sequence:T2 trufi3d_we_SAG) images were captured. Next, the femur and tibia bones were sectioned approximately 20 cm from the joint line, cemented into aluminum fixtures, and all soft tissue beyond 10 cm of the joint was removed except quadriceps muscles. Each knee was subjected to three experiments in intact and ACL-deficient conditions. First, passive TF laxity was measured by manually applying ± 8 Nm internal-external (I-E) torques, ± 10 Nm varus-valgus (V-V) torques, and ± 80 N anterior-posterior (A-P) loads ~300 mm below the joint line at 0-60° knee flexion (Harris et al., 2016). A load cell attached to the proximal end of the tibia recorded 6 DOF loads from each laxity test and provided real-time user feedback via a LabView interface (National Instruments, Austin, TX). Second, PF mechanics were measured by placing the specimens in a test fixture that applied

quadriceps force to extend the knee (Ali et al., 2016). Finally, specimens were mounted in the KKS to simulate the stance and swing phase of gait using load-controlled actuators (Figure 4.1). The KKS is a five-axis simulator designed to replicate knee joint loading during dynamic activity (Maletsky and Hillberry, 2005). Loads applied to the KKS actuators included a vertical hip load, quadriceps load, ankle flexion and I-E torque, and ankle medial-lateral (M-L) load. Quadriceps force was applied through the combined tendons of the rectus femoris and vastus intermedius using a proportional-integral-derivative (PID) controlled actuator tuned to match hip and ankle motions. Three-dimensional kinematic data were collected with an Optotrak motion capture system (Northern Digital Inc., Waterloo, CA). Simulated gait in the KKS was repeated following ACL resection. Anatomical landmarks on the femur, tibia, and patella, cruciate and collateral ligament attachment, articulating geometry (bone and cartilage surfaces), and KKS assembly components were digitized for constructing FE models of the experimental setup.

4.3.3 Computational Modeling

Specimen-specific FE models were developed in Abaqus/Explicit (Simulia, Providence, RI) to recreate the loading and boundary conditions for the intact and ACL-resected conditions (Figure 4.1). Bone and cartilage geometry were manually reconstructed from CT and MR imaging, respectively, using ScanIP (Simpleware, Exeter, UK). Post-processing of geometric reconstructions and mesh refinement was performed in Hypermesh (v11.0, Altair, Troy, MI). Bones were represented using rigid triangular

shell elements (R3D3), and cartilage was represented using hexahedral continuum elements (C3D8). The cartilage FE mesh was formed using a semi-automated morphing technique to match the surface geometry reconstructed from MRI to a hexahedral template (Baldwin et al., 2010). Although articular cartilage consists of several fibrous layers and viscoelastic properties (Halonen et al., 2013), cartilage was modeled using rigid pressure-overclosure behavior to minimize computational cost. Penalty-based contact (weight =0.5, friction =0.01) was defined between articulating cartilage using a calibrated surface pressure-overclosure relationship (Fitzpatrick et al., 2010); bone and soft tissue contact was defined using a zero surface penetration constraint (Halloran et al., 2005).

Tibiofemoral ligament structures were represented using non-linear tension-only springs (CONN3D2) and included the anteromedial-ACL bundle (ACLam), posterolateral-ACL bundle (ACLpl), anterolateral-PCL bundle (PCLal), posteromedial-PCL bundle (PCLpm), the lateral collateral ligament (LCL), popliteofibular ligament (PFL), medial collateral ligament (MCL), deep medial collateral ligament (dMCL), posterior oblique ligament (POL), anterolateral structure (ALS), and medial and lateral posterior capsule (PCAPm, PCAPl). As described by Harris et al. (2016), TF ligament attachment sites, stiffness, and reference strain were optimized using an adaptive simulated annealing algorithm in Isight (Simulia, Providence, RI) to match specimen-specific laxity measurements. In brief, specimen-specific optimizations were performed

across multiple flexion states, multiple laxity tests, and multiple resection levels to provide a wide-ranging representation of joint constraint (Harris et al. 2016).

Menisci geometry were developed from MR reconstructions and modeled using hexahedral continuum elements (C3D8) with 1D linear springs (CONN3D2) attaching the horns (N=37) and periphery of the geometry (medial N=16; lateral N=8) to the tibia bone. Menisci geometry were manually meshed and morphed based on the reconstruction in Hypermesh (v11.0, Altair, Troy, MI). Material properties for the menisci utilized a Fung orthotropic hyperelastic material model (Erdemir, 2016; Sibole et al., 2010; Yao et al., 2006); material constants for Young's moduli (E, MPa), poisson's ratio (v), and shear moduli (G, MPa) were $E_x=E_y=27.5$, $E_z=125$, $v_{xy}=0.33$, $v_{xz}=v_{yz}=0.1$, $G_{xy}=12.5$, $G_{xz}=G_{yz}=2$ (Figure 4.1). Spring stiffness of the horn attachments was computed as a function of literature-reported Young's modulus (E=600MPa) (Hauch et al., 2009), cross-sectional area of digitized attachment locations (A=~30mm^2), number of springs (N=37), and length of the spring (L=~10-15mm); k=EA/NL. Rigid-deformable frictionless contact was defined between the meniscus and articulating cartilage.

Patellofemoral soft tissue structures were represented by 2D fiber-enforced membrane elements and included the rectus-femoris tendon, patellar tendon, and medial and lateral patellofemoral ligaments. Ligament and tendon material properties and soft-tissue attachments of the patellar mechanism were adopted from our prior computational studies (Ali et al., 2016; Baldwin et al., 2009).

KKS actuator loads at the hip and ankle joint were applied to the computational model to simulate dynamic activity performed in the experiment (Figure 4.1). KKS actuator components were represented using point-to-point connectors (CONN3D2) for computational efficiency. KKS assembly components were aligned using digitized points from the motion tracking system. Experimental actuator loads were applied to the modeled KKS components (vertical hip load, ankle flexion torque, ankle I-E torque, and ankle medial-lateral load) using connector load definitions. Quadriceps excursion drove knee flexion and matched the experimentally prescribed hip flexion profile. By prescribing quadriceps excursion, the resulting connector load was used to predict model quadriceps force. Model setup and dynamic simulation was repeated for all specimens and their ACL-resected conditions.

In summary, experimental measurements consisted of TF and PF kinematics, and quadriceps forces from the KKS for intact and ACL-deficient conditions. Model accuracy was assessed using root-mean-square (RMS) differences between model and experimental TF and PF kinematics computed over the entire range of the gait cycle. Also, peak quadriceps forces during stance and swing phase of gait were compared in the model and experiment for intact and ACL-deficient conditions. Additionally, outputs from FE simulations included TF and PF contact forces, ligament tensile forces, and ligament A-P shear forces with respect to the tibia to describe changes in knee mechanics associated with ACL removal.

4.4 Results

4.4.1 TF Kinematics

Experimental TF kinematics were similar in both specimens (Figure 4.2) with two flexion peaks for the stance and swing phases of gait. TF kinematics were characterized by internal tibial rotation and posterior femoral rollback as a function of knee flexion. Following ACL resection, Specimen 1 showed notable increases in anterior tibial translation during swing phase of gait (+4.0 mm); Specimen 2 showed an overall shift in anterior position of the tibia (avg. +3.5 mm) and an average 4° increase in tibial external rotation.

Model-predicted TF kinematics agreed with the experiment in trend and magnitude. In Specimen 1, RMS and range [max,min] of differences between model and experiment were 3.1°[6.5,-2.7] and 3.5°[7.4,1.9] in flexion-extension (F-E), 1.0°[0.5,-2.2] and 1.6°[0.1,-3.3] in V-V, 5.4°[8.2,0.1] and 6.1°[8.4,0.2] in I-E rotation, and 0.9[2.1,-1.2] mm and 2.4[3.7,-5.1] mm in A-P translation, in the intact and ACL-resected condition respectively. In Specimen 2, RMS and range [max,min] of differences were 2.2°[4.9,-6.1] and 2.9°[4.1,-6.1] in F-E, 0.9°[2.1,-1.1] and 2.4°[1.5,-4.3] in V-V, 2.0°[3.8,-4.1] and 3.9°[5.8,-3.9] in I-E, and 1.6[3.0,-2.5] mm and 2.7[3.5,-5.0] mm in A-P, in the intact and ACL-resected condition respectively.

4.4.2 PF Kinematics

Experimental PF kinematics followed similar trends in both specimens, except in PF tilt, where Specimen 1 rotated internally and Specimen 2 rotated externally through the gait cycle (Figure 4.3). ACL resection produced minor changes in PF kinematics. Specimen 2 presented a 2-4 mm medial shift in patellar alignment.

Model-predicted PF kinematics agreed with the experiment. In Specimen 1, RMS and range [max,min] of differences between model and experiment were 2.2°[3.3,-4.2] and 1.9°[5.0,-2.6] in F-E, 2.2°[4.5,-3.0] and 2.9°[5.5,-3.9] in I-E, and 1.6[4.5,-4.0] mm and 2.5[5.0,-3.1] mm in M-L, for the intact and ACL-resected condition, respectively. In Specimen 2, RMS and range [max,min] of differences between model and experiment in the intact and ACL-resected condition were 4.2°[0.5,-7.0] and 1.8°[2.5,-4.9] in F-E, 1.0°[2.3,-1.8] and 3.2°[4.4,0.0] in I-E, and 2.2[0.2,-3.5] mm and 1.5[1.6,-3.9] mm in M-L, respectively.

4.4.3 Quadriceps Force

Comparing model quadriceps force to PID-controlled actuator load in the KKS, peak quadriceps forces (during stance and swing phase of gait) in the intact and ACL-deficient trials had differences of 21.1% and 22.1% for Specimen 1, and 9.7% and 7.6% for Specimen 2 (Figure 4.4). Differences in quadriceps force from intact to the ACL-deficient condition were small with negligible change in Specimen 1 (experimental RMS

< 50 N) and a small decrease in peak quadriceps force during swing (328 N) in Specimen 2.

4.4.4 Contact Force

Total TF contact forces demonstrated decreasing trends from 0-45° in both specimens, but diverging trends from mid-to-deep flexion with decreasing forces as a function of knee flexion in Specimen 1 and increasing forces in Specimen 2 (Figure 4.5). In contrast, total PF contact forces were consistently increasing as a function of knee flexion in both specimens. TF center of pressure travelled posteriorly on the tibia and rotated internally, consistent with experimental TF kinematics; PF center of pressure and contact force travelled distal to proximal and increased in magnitude as knee flexion increased (Besier et al., 2005).

4.4.5 Ligament Forces

Ligament recruitment patterns were unique in each subject (Figure 4.6). In both specimens, ligament forces decreased as the knee flexed up until approximately 30°, after which ligament forces in Specimen 1 continued to decrease as a function of flexion, while ligament forces in Specimen 2 increased (Figure 4.6). In Specimen 1, primary contributors to joint constraint were the MCL, LCL, and the ACLam. In Specimen 2, the MCL, POL, DMCL, ACLam, and PCL were primarily active. Following ACL resection, Specimen 1 demonstrated an increase in total ligament force, with the MCL accounting for a majority of the constraint lost by ACL resection. In Specimen 2, POL force

increased to compensate for the loss of the ACL. Following ACL resection, Specimen 1 showed little to no changes in ligament A-P shear force, but Specimen 2 demonstrated significantly lower anterior shear force, approximately equal to load carried by the ACL in the intact condition.

4.5 Discussion

FE modeling predicted TF kinematics, PF kinematics, and quadriceps force in intact and ACL-deficient specimens for an in-vitro simulation of gait. While prior computational studies have evaluated healthy and ACL-deficient knee mechanics, they have not verified predictions in both states during dynamic activity (Guess and Stylianou, 2012; Li et al., 2002b; Mesfar and Shirazi-Adl, 2006a; Moglo and Shirazi-Adl, 2003; Shelburne et al., 2004a). The current study provided a specimen-specific representation of the TF and PF joints by incorporating material properties and geometric alignment from previous modeling of the same specimens (Ali et al., 2016; Harris et al., 2016).

Model simulations captured experimental kinematics and loading of the TF and PF joints. In the intact condition, RMS differences between model and experiment TF kinematics were F-E<3.1°, V-V<1.0°, I-E<5.4°, and A-P<2mm. Removing the ACL in the model produced modest increases in RMS of <2° across all rotations and <1.5 mm in A-P. RMS differences in PF rotations were similarly low across all rotations (<4.2°). Even so, portions of the gait cycle were difficult to match to the experiment. For

example, TF I-E rotations were the most challenging DOF to match computationally with differences of up to 8° during swing (50- 90% in Figure 4.2) when compared to the experiment. While TF and PF kinematic predictions were similar to differences reported in the literature (Baldwin et al., 2009; Blankevoort and Huiskes, 1996; Guess et al., 2010), large differences highlight challenges in replicating specimen-specific passive constraint during dynamic activity. The largest RMS differences between model and experiment occurred at flexion angles beyond which laxity calibration was performed (>60°). Dynamic modeling suggests the need for additional evaluations of knee laxity, and potentially more sophisticated geometric and material representations.

The computational model was also compared to experimentally-measured quadriceps force. Peak quadriceps force during stance and swing phase of gait had an average error of 16.7% across specimens and pathology. Force predictions in both specimens followed the experimental trend in quadriceps force and matched the F-E angle at which peak quadriceps force occurred within 2°. Since the experimental setup was an in-vitro representation of gait, quadriceps forces changed little following ACL resection.

TF and PF contact forces and center of pressure were consistent with previous reports. Total PF contact forces increased as a function of flexion, similar to the findings of (Besier et al., 2005; Fernandez et al., 2008). While Specimen 1 presented decreasing TF contact forces as the knee flexed, Specimen 2 demonstrated increased TF contact

forces in swing phase at deeper flexion angles. This was likely influenced by contrasting ligament recruitment patterns in each specimen (Figure 4.6).

The modeling and comparison of two specimens revealed important individual differences that can be lost in generic models of the knee calibrated to average behavior (Mesfar and Shirazi-Adl, 2006a; Mootanah et al., 2014; Pandy and Shelburne, 1997). Our previous work, evaluating the joint laxity response of the two specimens, demonstrated significant intersubject variability in both ligament attachment locations and TF load response (Harris et al., 2016). Additionally, PF joint modeling demonstrated specimen-specific load transfer with either increased PF contact forces or increased patellar tendon loads following cruciate resection (Ali et al., 2016). Our recent and current studies successfully capture unique differences in joint mechanics between specimens, and emphasize the need for specimen-specific evaluations in computational modeling.

Although increasing joint contact forces corresponded to increasing ligament loads, each specimen displayed unique patterns of recruitment, especially at higher knee flexion angles (Figure 4.6). Contrasting ligament recruitment patterns and TF contact trends could stem from variability in knee anatomy (size, tibial slope), alignment (TF position, ligament attachments), and material properties (reference strain, stiffness) (Harris et al., 2016). The current specimens shared a similar size and shape (tibial slope=~7°), but there were important differences in ligament attachment locations.

Ligament engagement was particularly sensitive to the location of soft tissue attachments on the femur. In Specimen 2, the MCL and DMCL femoral attachments were located anterior to the TF center of rotation, causing the anterior bundles to generate substantial force in deep flexion; as a result, total ligament force increased as a function of flexion. Unique ligament engagement highlights the importance of specimen-specific representations of soft tissue structures.

ACL resections resulted in contrasting joint mechanics in the two specimens. Specimen 1 showed small changes in A-P position of the tibia, but displayed an increase in total joint forces, specifically in stance. However, TF contact and ligament forces were small during the peak of swing phase and resulted in a 4 mm anterior shift of the tibia. Specimen 2 demonstrated contrasting joint mechanics with increasing TF contact and ligament loads as a function of flexion. Specimen 2 showed a 4-6 mm shift in initial A-P alignment of the tibia. At deeper flexion angles during swing phase, TF contact forces and ligament loads were more active in preventing excessive TF motion. Measurements of ligament and contact forces were not available from the KKS to corroborate these results, but ACL forces were similar in magnitude to forces measured in situ by (Gabriel et al., 2004). The prediction of specimen-specific response to ACL-deficiency warrants further investigation into the structural characteristics of the knee that allow some individuals to cope with ACL-deficiency (Moksnes et al., 2008).

The main limitation of the current study was the in-vitro representation of gait, which did not fully reproduce in vivo conditions. Quadriceps forces in the experiment and simulations were higher during swing phase than forces reported in vivo. Larger quadriceps forces may have resulted in overestimation of contact and ligament forces at deep flexion angles. The current study modeled the resulting load response in the knee joint following ACL resection, but did not account for adaptive behavior that may be present in vivo, such as neuromuscular adaptation to excessive anterior-posterior motion through increased muscle recruitment. Nonetheless, the computational framework may be used to simulate soft-tissue injury and in-vivo correction by altering the tibial constraint through changes in muscle force (Mesfar and Shirazi-Adl, 2006b).

A second limitation was that the study was limited to two specimens due to challenges in cost and labor of collecting data for passive and dynamic tests, and calibrating specimen-specific FE models. The current work demonstrated the variability of ligament recruitment across two specimens and its impact on knee mechanics. However, additional specimens could better characterize ligament variability across the population to better inform engineers and clinicians on the mechanisms surrounding injury.

Furthermore, passive laxity tests and ligament calibrations were performed without the meniscus, thus the experiment and model may have overestimated the role of the ligaments in passive constraint (Harris et al., 2016). The meniscus is important to

load distribution in the TF joint, which protects tibial cartilage from excessive loading and wear (Englund et al., 2009). Also, the meniscus may provide secondary constraint and stability of the ligament-deficient knee under joint load (Allen et al., 2000; Levy et al., 1982; Petrigliano et al., 2011). In prior work, knee laxity experiments were performed on specimens in this study using intact and meniscus-resected conditions to isolate the impact of the meniscus on joint constraint, however, likely due to absence of TF compressive load in the experiment, no significant differences were measured (Shoemaker and Markolf, 1986). TF compressive loads in the KKS were much greater and inclusion of the meniscus more accurately modeled joint constraint to reproduce experimental kinematics. Future work may be strengthened through specimen-specific calibration of meniscus material properties.

Finally, FE models of the knee and the KKS included 1D representations that were necessary for efficient model calibration. Ligament 1D elements effectively captured joint stiffness, but were not capable of modeling stress/strain distributions or wrapping contact. Simplified 1D representations enabled reasonable computational run times in analyses of the dynamic activity, and also the optimizations used to tune ligament properties in our previous study (Harris et al., 2016). Previous modeling of the natural knee has included depth-dependent, collagen fiber cartilage (Halonen et al., 2013; Shirazi et al., 2008), and subject-specific modeling of the menisci (Guess et al., 2010) that might strengthen the accuracy and realism of our model predictions.

In conclusion, the current work expanded an existing FE framework of the KKS to include evaluations of healthy and ACL-deficient knee mechanics. FE models may be used for investigations that inform researchers and clinicians on the mechanisms surrounding injury, and support of surgical and conservative treatments. Recognizing the challenges in cost and labor to produce in-vitro biomechanical data, and develop specimen-specific computational models, the experimental motion and load data, and knee geometry are available for download at www.du.edu/biomechanics.

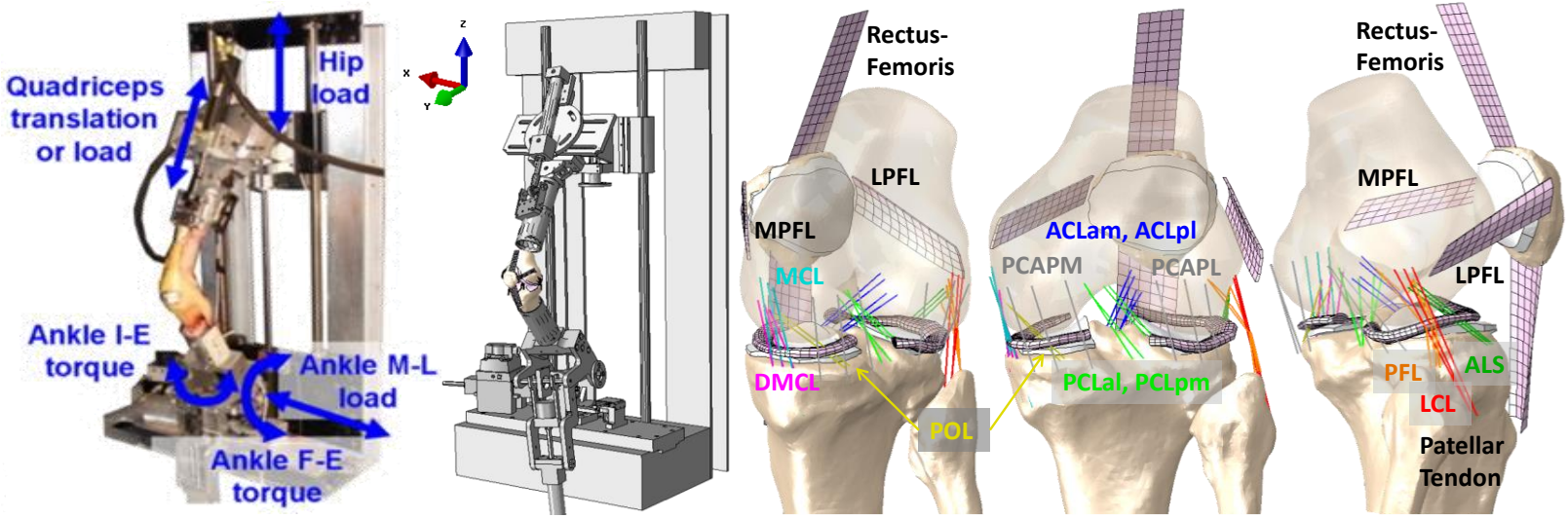

Figure 4.1 Knee cadaver mounted in the Kansas Knee Simulator (KKS) (left), and its computational representation (middle) with specimen-specific TF and PF soft tissue structures (right): anterior cruciate ligament (**ACLam**, **ACLpl**), posterior cruciate ligament (**PCLal**, **PCLpm**), lateral collateral ligament (**LCL**), popliteofibular ligament (**PFL**), medial collateral ligament (**MCL**), superficial medial collateral ligament (**DMCL**), posterior oblique ligament (**POL**), anterolateral structure (**ALS**), posterior capsule (**PCAPM**, **PCAPL**)

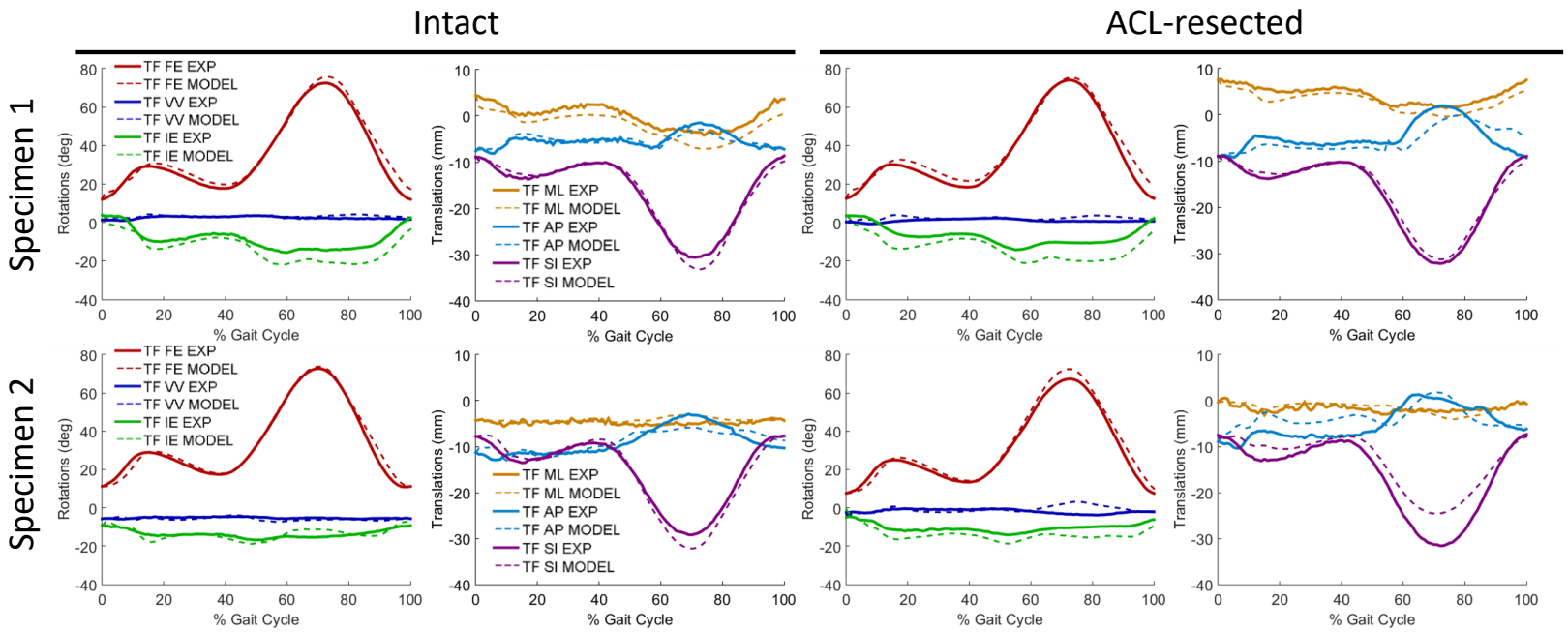

Figure 4.2 Comparison of model (dashed) and experimental (solid) TF kinematics in the KKS simulator for intact and ACL-resected conditions in two specimens

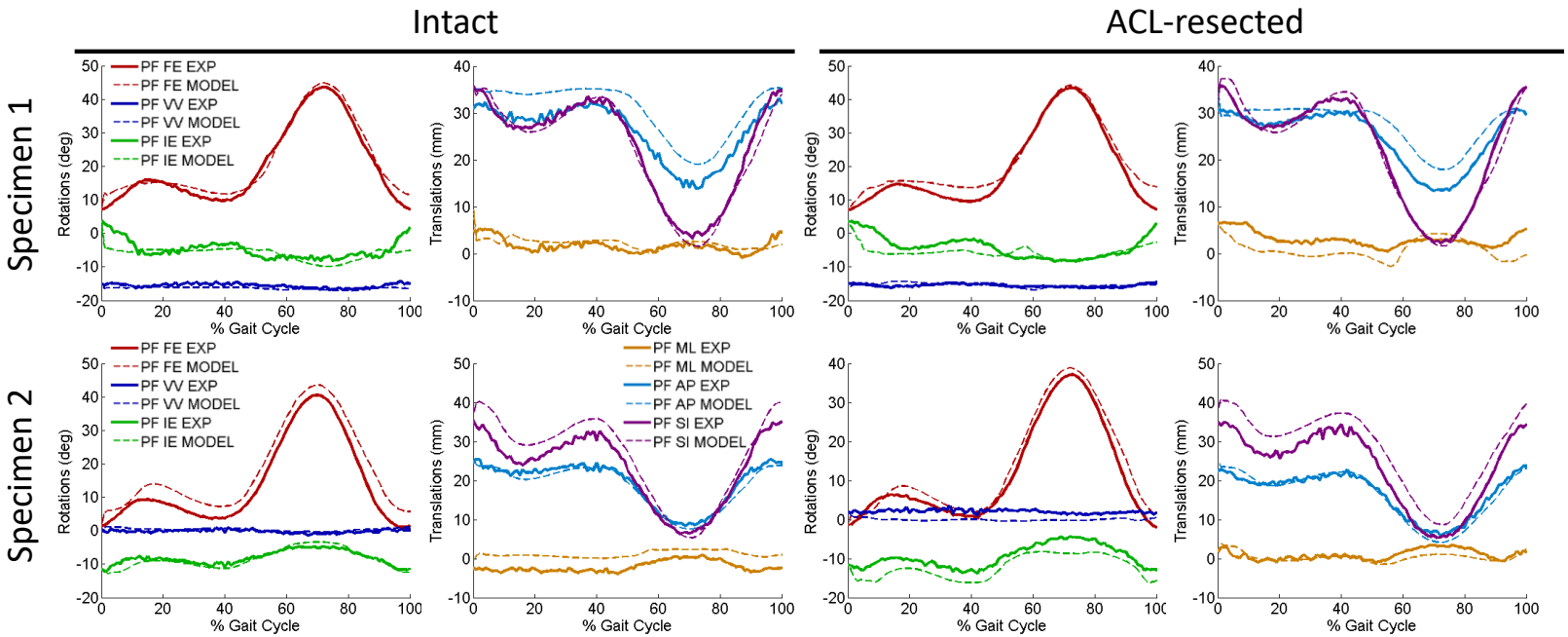

Figure 4.3 Comparison of model (dashed) and experimental (solid) PF kinematics in the KKS simulator for intact and ACL-resected conditions in two specimens

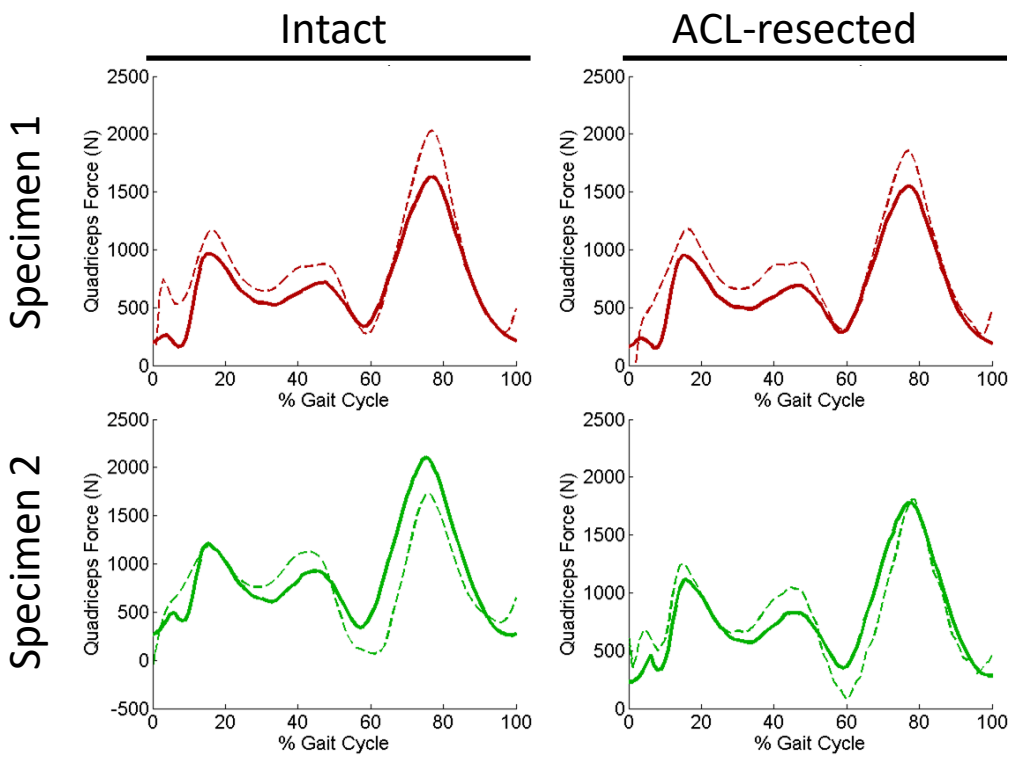

Figure 4.4 Comparison of model (dashed) and experimental (solid) quadriceps force in the KKS simulator for intact and ACL-resected conditions in two specimens

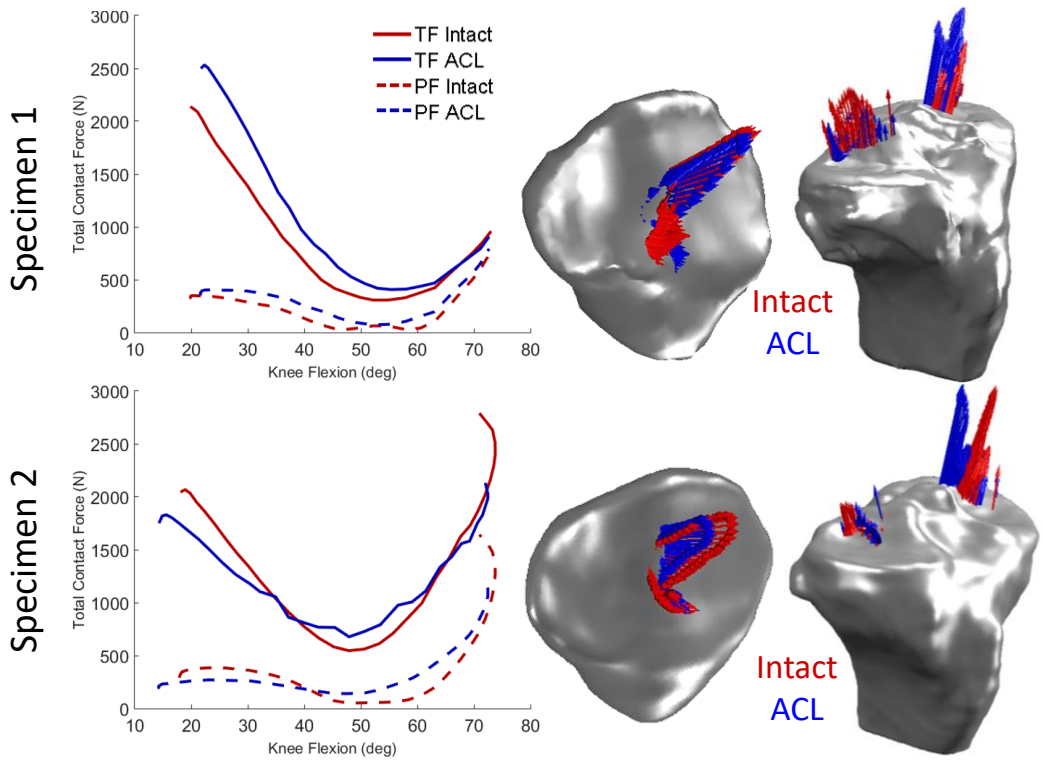

Figure 4.5 Total TF and PF contact force (left) and contact center of pressure with force vectors (right) shown for two specimens in intact and ACL-deficient conditions

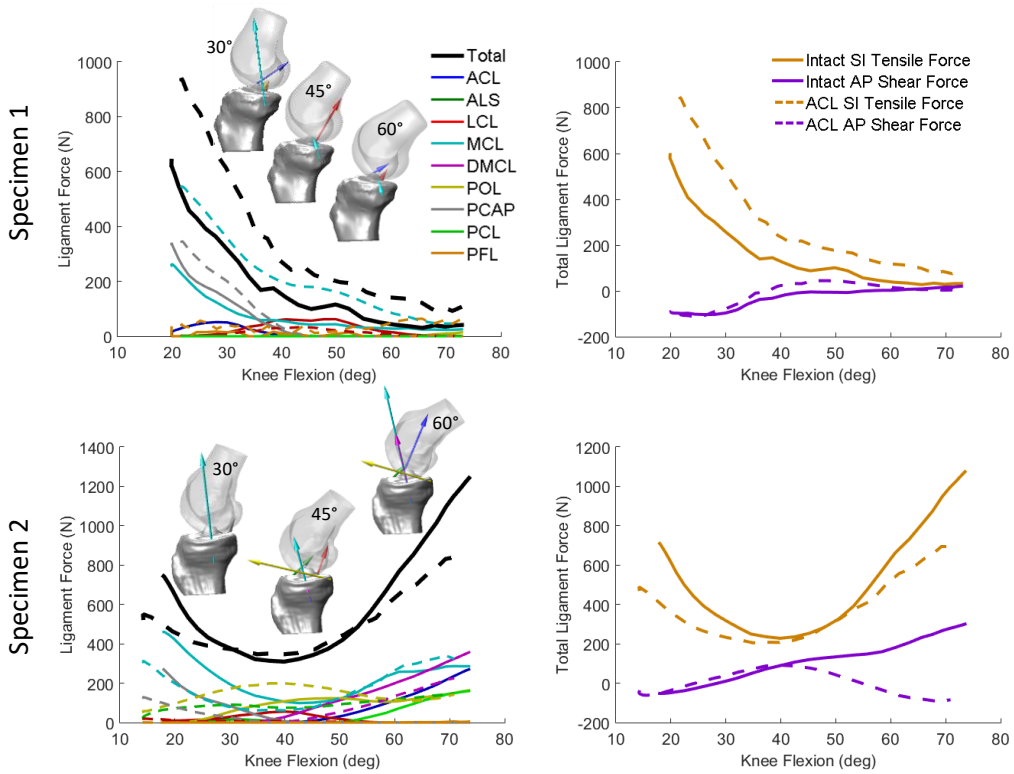

Figure 4.6 Ligament recruitment as a function of knee flexion (left), and total ligament shear and tensile forces (right) for intact (solid) and ACL-deficient (dashed) conditions in two specimens

CHAPTER 5 – EVALUATION OF IN-VIVO MECHANICS FOR MEDIALIZED DOME AND ANATOMIC PATELLOFEMORAL GEOMETRIES DURING KNEE EXTENSION AND LUNGE

5.1 Abstract

Successful function and outcome following total knee arthroplasty (TKA) with patella resurfacing is partly determined by the restoration of patellofemoral (PF) function and recovery of the quadriceps mechanism of the knee. Patellar resurfacing affects the geometry of the articular surface and alters the kinematics and loading of the PF joint. The current study compared the performance of two patellar TKA geometries (medialized dome and anatomic) to determine their impact on PF mechanics and quadriceps function. In-vivo, subject-specific patellar mechanics were evaluated using a sequential experimental and modeling approach. First, stereo radiography, marker-based motion capture, and force plate data were collected for TKA patients (10 dome, 10 anatomic) performing a knee extension and lunge. Second, subject-specific, whole-body, musculoskeletal models, including 6 degrees-of-freedom (DOF) knee joint kinematics, were created for each subject and activity to predict quadriceps forces. Lastly, finite element models of each subject and activity were created to predict PF kinematics,

patellar loading, moment arm, and patellar tendon angle. Differences in mechanics between dome and anatomic subjects were highlighted during load-bearing (lunge) activity. Anatomic subjects demonstrated larger PF flexion-extension angles compared to dome subjects during lunge with an average 11±3° difference ranging from 40-100° knee flexion. Contact locations migrated distal to proximal as the knee flexed in anatomic subjects, but remained relatively proximal in dome subjects. Differences in kinematics and contact location likely contributed to altered mechanics with anatomic subjects presenting increased load transfer from the quadriceps to the patellar tendon in deep flexion (>75°), and dome subjects demonstrating larger contact forces during lunge. Although there is significant patient variability, evaluations of PF mechanics suggested improved quadriceps function and more natural kinematics in the anatomic design.

5.2 Introduction

Successful function and outcome following total knee arthroplasty (TKA) with patella resurfacing is partly determined by the restoration of patellofemoral (PF) function and recovery of the quadriceps mechanism of the knee. While TKA has successful surgical outcomes with 8% or fewer requiring revision (Kurtz et al., 2005), variations in movement patterns and functional limitations during everyday activities such as kneeling and squatting are still present long after knee repair (Noble et al., 2005; Stevens-Lapsley et al., 2012). TKA patients have demonstrated asymmetric movement in contralateral limbs, reduced range of motion, and reduced quadriceps strength and extensor efficiency

(Mizner and Snyder-Mackler, 2005; Silva et al., 2003). Quadriceps efficiency is a measure of the effective moment arm of the quadriceps, where greater efficiency allows the quadriceps to extend the knee with less force. TKA has reduced knee pain and restored greater knee range of motion in patients with severe knee osteoarthritis, however, patients still exhibit significant decreases in functional performance and quadriceps strength due to failure of voluntary muscle activation and muscle atrophy (Mizner et al., 2005; Mizner and Snyder-Mackler, 2005).

Patellar resurfacing alters the geometry of the patella, which can affect the kinematics and loading of the PF joint. For TKA in the U.S., resurfacing of the patella involves removing the articular surface and replacing it with a polyethylene implant. Common patellar TKA designs have included a dome or rounded shape, while more recently, anatomic geometries that retain a shape closer to the natural anatomy have been developed. In both the dome and anatomic designs described in this study, the articulating surface includes a medialized peak that mimics the native patellar ridge. Previous comparisons of PF kinematics between dome and anatomic resurfacing geometries have revealed larger patellofemoral flexion angles with the anatomic geometry, more like the native patella (Stiehl et al., 2001), suggesting improved quadriceps efficiency and patient satisfaction. Important differences in kinematics and contact mechanics between TKA-implanted patellar designs are typically evaluated using in vitro testing, which applies an idealized set of loading conditions and may not replicate in vivo conditions (Amis et al., 2006; Browne et al., 2005; Lee et al., 1997). These

studies recorded reduced patellar flexion that may compromise quadriceps efficiency by decreasing the effective moment arm of the extensor mechanism. In addition, changes in PF kinematics may also alter the distribution of joint loading observed in joint contact loads, patellar tendon forces, and angle of the patellar tendon. Large patellar tendon forces may lead to PF pain (Fulkerson, 2002), while large contact forces may lead to accelerated implant wear (Churchill et al., 2001).

Accurate in vivo measurement of six degree-of-freedom (DOF) tibiofemoral (TF) and PF kinematics is critical for quantifying differences in function between TKA designs but can be challenging to obtain using conventional motion capture methods. Previous studies have used in-vivo imaging techniques to quantify patellar motion in TKA-implanted subjects (Carpenter et al., 2009; Katchburian et al., 2003; Price et al., 2004; Stiehl et al., 2001), but rarely include six DOF PF kinematics. Furthermore, these evaluations are typically limited to sagittal plane measurements and may not capture knee kinematics with the accuracy needed for comparative evaluations of knee function. Recently, Mannen et al. used stereo radiography to compare the 6 DOF PF kinematics between medialized dome and anatomic patellar designs (Mannen et al. 2017). Although accurate and precise measurement of knee motion revealed subtle differences in joint kinematics, the impact that the kinematic differences may have on PF joint forces and implant performance may require further investigation.

PF mechanics, consisting of quadriceps, patellar tendon, and joint contact forces, are impractical to measure in vivo and are thus estimated using computer models of the knee and extensor mechanism. Multiple computational models have been developed to investigate PF kinematics and contact mechanics in simulations of TKA-implanted cadaver specimens (Baldwin et al., 2009; Besier et al., 2005; Elias et al., 2004; Fitzpatrick et al., 2011; Mesfar and Shirazi-Adl, 2005). Notably, (Rullkoetter et al., 2014) found greater PF flexion and lower contact pressures in subjects with anatomic implants compared with dome implants, consistent with findings from in-vitro studies. However, these cadaver-based simulations may not capture the loading conditions and kinematic variability present in vivo. Alternatively, researchers have estimated in vivo PF contact mechanics using dynamic-MRI and fluoroscopy imaging (Borotikar and Sheehan, 2013; Komistek et al., 2000; Pal et al., 2013a; Salsich et al., 2003; Sharma et al., 2008), but these models generally lack bone and soft tissue characteristics specific to the patient. More recently, finite element modeling of the knee combined with precise kinematic measurements from stereo radiography and predicted muscle forces from musculoskeletal simulations was used to evaluate contact mechanics, ligament strain, and the distribution of joint loading in TKA (Navacchia et al., 2016c). Integrating simultaneous, whole body measurements (motion capture and force plate data) with stereo radiography can provide insight to the relationship between joint-level and whole-body function, and enable the creation of subject-specific computational models of the knee and lower extremity.

The purpose of this study was to compare PF mechanics between medialized dome and medialized anatomic implants during knee extension and lunge activities using subject-specific computational models. Knee kinematics measured from stereo radiography and quadriceps muscle forces obtained from subject-specific musculoskeletal simulations were used as inputs to finite element models of the implanted knee to predict PF kinematics, contact mechanics, load transfer surrounding the patella, and patellar tendon moment arm and angle.

5.3 Methods

Subject-specific patellar mechanics were simulated with a three step process (Figure 5.1). First, stereo radiography, marker-based motion capture, and force plate data were collected for patients with TKA performing a seated knee extension and lunge. Second, subject-specific, whole-body, musculoskeletal models, including 6 DOF knee joint kinematics, were created for each subject and activity. Using motion capture and ground reaction forces as inputs to inverse kinematics and inverse dynamics, a static optimization analysis of the musculoskeletal model derived subject-specific quadriceps forces. Lastly, finite element models of each subject and activity were created to predict PF joint kinematics, contact mechanics, patellar tendon moment arm, and patellar tendon angle.

5.3.1 Data Collection

High-speed stereo radiography (HSSR) was used to capture 3D sub-mm measurement of bone and implant motion (Ivester et al., 2015). The HSSR system is composed of two 40 cm diameter image intensifiers with high-speed, high-definition (1080x1080) digital cameras positioned at a relative 70° angle (Ivester et al., 2015; Kefala et al., 2017; Mannen et al., 2017). This study was approved by the University of Denver Institutional Review Board and all participants provided informed consent. HSSR images were collected for 16 patients (bilateral) implanted with Attune® (DePuy Synthes, Warsaw, IN) posterior-stabilized, rotating-platform components, 10 knees with medialized dome and 10 with medialized anatomic patellar geometries (7M/9F, 63.4±6.3 years, 2.3±0.7 years post-surgery, BMI: 27.0±3.7 kg/m^2). The subjects performed two activities of daily living: an unloaded, seated knee extension ranging from high flexion to full extension, and a single-leg weight-bearing lunge (Figure 5.1a). Collection frequency was 50 Hz for both activities.

Relative motions of the femoral and tibial tray components were tracked using Autoscoper by optimizing the alignment of the 3D implant components to the 2D HSSR images (Brown University, Providence, RI). Since plastic patellar components are not visible in the imaging data, the patella bone was tracked to describe the relative patellar motions. A statistical shape model (SSM) of the knee was used to predict the anterior surface of the patella bone (Smoger et al. 2017). In summary, the SSM of the knee described by Smoger et al. was constructed using a 50 subject training set (25M/25F)

with a size distribution representative of the population (Mahfouz et al., 2012). The shape and alignment of the mean SSM patellar geometry was optimized to match 2D projections of the imaged patella. Furthermore, the resection plane of the patella was determined using static radiographic images from the HSSR and pre-operative x-rays. The alignment of the TKA patellar component on the resection plane was optimized to maximize coverage and reduce overhang. Local coordinate systems were defined for each implant component as described by the manufacturer: the origin of the femoral coordinate system was located along the flexion-extension axis of femoral condylar geometry between the most medial and lateral points. The origin of the patellar construct was located at the center of the resection plane. TF and PF joint kinematics were calculated based on (Grood and Suntay, 1983). In addition to HSSR measurements, marker-based motion capture data were collected using an eight-camera, passive-marker, video photogrammetric system (Vicon Motion Analysis Corp., Centennial, CO), and simultaneous ground reaction forces were collected using four six-component, strain-gauged force plates (Bertec Corp., Columbus, OH).

5.3.2 Musculoskeletal Modeling

Subject-specific musculoskeletal models were used to estimate muscle forces for each activity using stereo radiography kinematics, marker-based video motion capture, and ground reaction force data as inputs. For each subject and activity, a subject-specific, whole body, musculoskeletal model was created in OpenSim (Delp et al., 2007; Navacchia et al., 2016b; Navacchia et al., 2016c) (Figure 5.1b). The anthropometry of

the model was scaled based on the ratio of relative marker distances from motion capture and the virtual markers in the template model. Each model consisted of 12 segments (torso, pelvis, femurs, tibiae, tali, calcanei, toes) and 92 Hill-type, musculotendon units. The lower limb included a ball-and-socket hip joint, a revolute ankle joint and a knee joint with prescribed TF and PF relative motion measured from stereo radiography. Specifically, TF and PF joint kinematics from the HSSR system were incorporated into the musculoskeletal model by decomposing motions into intrinsic Euler angles and a translation vector, and defining spline functions described with respect to knee flexion. All TF DOF and PF flexion-extension, superior-inferior translation and anterior-posterior translation DOFs were prescribed. The patellar tendon was modeled as a point-to-point muscle unit connecting the distal end of the patella to the tibial tuberosity. Wrapping surfaces were included to simulate contact between muscle and bone.

For the knee extension simulation, pelvis and lumbar motion were fixed to a seated position, and a vertical, body weight load was applied to the pelvis to simulate the support from a chair. Static optimization in OpenSim was performed to compute quadriceps forces during the lunge and seated knee extension from the rectus femoris, vastus intermedius, vastus lateralis, and vastus medialis for input into FE analyses.

5.3.3 Finite Element Modeling

Subject-specific finite element models of the experiments were developed for all subjects and activities. Each model included TKA implant components, SSM-predicted

patella bone, rectus femoris, vastus intermedius, vastus lateralis, vastus medialis, patellar tendon, and medial and lateral PF ligaments (Figure 5.1c). Implant components, obtained from the manufacturer, were modeled using rigid triangular shell elements (R3D3) with corresponding mass and rotational inertia properties. Rigid-body contact was defined between the patellar and femoral implant components using a previously-calibrated, tabular, pressure-overclosure relationship based on femoral and insert contact interactions (Halloran et al., 2005). Quadriceps and patellar tendons were modeled using 2D fiber-enforced membrane elements (M3D4R) and embedded 1D non-linear springs (CONN3D2). Medial and lateral PF ligaments were modeled using 1D non-linear springs. Quadriceps muscle paths were defined along the centroid of the muscle cross-sectional area described in imaging from the Visible Human Project (Ackerman, 1991). A series of rigid connectors followed the muscle centroid path to provide a more realistic quadriceps line of action. Ligament/tendon material properties were calibrated in previous analyses to match uniaxial test data from literature (Baldwin et al., 2009). While TF kinematics were prescribed based from HSSR data, the PF joint was unconstrained. Quadriceps force, derived from subject-specific musculoskeletal modeling in OpenSim, was applied to the FE simulation. Soft tissue attachment location and pre-strain in PF ligaments were calibrated to match experimental PF kinematics. Relative position of the quadriceps and patellar tendon were significant in calibrating model PF kinematics, but model calibration was not unique to a single solution and could predict multiple loading profiles on the patella. To compare PF mechanics across subjects, the position of the quadriceps tendon relative to the patella was fixed for every

subject; soft-tissue calibration included perturbations of patellar tendon and PF ligament attachment sites only.

Model outputs included PF kinematics, patellar tendon angle and moment arm, and patellar and contact force ratios. PF kinematics were computed from the FE model using equations described by (Grood and Suntay, 1983). Patellar tendon moment arm was measured as the perpendicular distance between the center of rotation of the knee and the line of action of the patellar tendon (Figure 5.6a). Patellar tendon angle was measured between the mechanical axis of the tibia and the line of action formed by the patellar tendon, where positive angles represent inclination anterior to the tibia (Figure 5.6b) (Buff et al., 1988; Yamaguchi and Zajac, 1989). In addition, to compare how quadriceps force impacted patellar tendon force and patellar contact force, two ratios were calculated. Contact force ratio was described as the total force due to patellar contact (Fc) divided by the total quadriceps force (Fq) (Figure 5.5a). Patellar force ratio was defined as the ratio of patellar tendon force (Fpt) divided by the total quadriceps force (Fq) (Figure 5.5b). The force ratios were important in comparing load transfer from the quadriceps between dome and anatomic designs.

5.4 Results

5.4.1 PF Kinematics

Experimental PF kinematics showed similar trends across subjects, activity, and implant geometry. Patellar components shifted medially and rotated internally with increasing knee flexion (Figure 5.2). Patellar flexion was an average 60-80% of the TF flexion angle. Kinematic differences between knee extension and lunge activities were small evidenced by the overlapping bounds in variability across patients; however, differences between medialized dome and medialized anatomic subjects were most apparent during the lunge. For example, anatomic subjects demonstrated larger PF flexion-extension angles compared to the dome subjects during lunge with an average 11±3° difference ranging from 40-100° knee flexion. Additionally, dome subjects experienced greater patellar tilt than anatomic subjects by an average 6±5° (Figure 5.2).

Model PF kinematics closely replicated the experiment with average root-mean-square differences of 4.2° in flexion-extension, 3.1° in internal-external, and 1.9 mm in medial-lateral for knee extension (Figure 5.2). For lunge, average root-mean-square differences were 2.7° in flexion-extension and 2.7° in internal-external rotations, and 1.8 mm in medial-lateral translation.

5.4.2 Quadriceps Force

Quadriceps force was described as the vector sum of forces from the rectus femoris, vastus intermedius, vastus lateralis, and vastus medialis. Quadriceps force predictions from musculoskeletal modeling were significantly larger in lunge than knee extension (e.g. average peak force of 2425 N and 1950 N in anatomic and dome subjects respectively, Figure 5.4). Also, trends in quadriceps force decreased as a function of flexion in knee extension, but increased in lunge. Differences in quadriceps forces between dome and anatomic subjects were small during knee extension; however, during lunge, forces were larger in dome subjects at mid-flexion (eg. 567 N difference at 60°), and larger in anatomic subjects at deep flexion (eg. 524 N difference at 90°).

5.4.3 Contact Force and Force Ratio

PF contact forces were consistent with trends in quadriceps force such that loads decreased as a function of flexion during knee extension and increased during lunge. Contact forces ranged from approximately 100-500 N during knee extension, and 300-2400 N during lunge. Also, contact forces moved superiorly along the patellar component as the knee flexed, consistent with trends reported in the literature (Besier et al., 2005) (Figure 5.5c). Near full extension, the center of contact pressure appeared more distal on the patella in anatomic subjects than dome subjects by an average of 2.2 mm in the knee extension activity and 1.3 mm in the lunge. The total superior-inferior excursion of contact center of pressure was larger in anatomic subjects than dome subjects (9mm for anatomic and 4 mm for dome during knee extension; 5mm for

anatomic and 2mm for dome during lunge). Contact force ratios increased as a function of flexion in both the knee extension and lunge activity. Dome subjects demonstrated larger contact force ratios than anatomic subjects during lunge ($p<0.05$), approximately equal to 250 N of PF contact force averaged across subjects and knee flexion.

5.4.4 Patellar Force Ratio

Patellar force ratios were approximately one near full extension and decreased as knee flexion increased, similar to patterns reported in the literature for natural subjects (Ahmed et al., 1987). Dome and anatomic subjects presented similar patellar force ratio magnitudes as a function of flexion during knee extension, but anatomic subjects demonstrated larger patellar force ratios in deep flexion (>75°, $p=0.06$) during lunge.

5.4.5 Patellar Tendon Moment Arm

Patellar tendon moment arm showed no significant difference when compared across knee extension and lunge activities. Therefore, given the greater range of motion captured in the knee extension activity, results were presented for knee extension only in Figure 5.6a. Anatomic subjects presented significantly larger moment arms than dome subjects in early flexion (<30°, 5-9 mm, $p<0.05$). Following a peak value ranging from 30-45° of knee flexion, moment arm decreased as knee flexion increased. When comparing to natural data (Buff et al., 1988; Yamaguchi and Zajac, 1989), implanted subjects demonstrated an average 6 mm decrease in moment arm at full extension.

5.4.6 Patellar Tendon Angle

Similar to moment arm, patellar tendon angle was consistent across activities so results were presented for the knee extension task only. Patellar tendon angle decreased as knee flexion increased (Figure 5.6b). Differences in patellar tendon angle between anatomic and dome subjects were not significant. However, there was substantial variation across subjects, particularly in anatomic subjects (average standard deviation of 6.2° in anatomic subjects and 2.9° in dome subjects).

5.5 Discussion

The current study examined the impact of patellar component geometry on PF mechanics and quadriceps efficiency. While measuring patellar kinematics is a crucial step towards understanding the in vivo performance of TKA, our novel subject-specific computer modeling techniques provided the means to evaluate the effect of PF motion on the mechanics of the knee following TKA. Through sequential subject-specific, whole-body and joint-level simulations, computational models produced a more complete picture of quadriceps forces and the distribution of forces to the patellar tendon and joint contact.

Patellar resurfacing geometry influenced PF kinematics, contact mechanics, and loading of the patellar mechanism. Anatomic subjects achieved greater PF flexion than dome subjects, which was consistent with previous experiment (Stiehl et al., 2001) and

modeling (Rullkoetter et al., 2014). These differences in PF kinematics resulted in altered PF joint loading; anatomic subjects demonstrated decreased contact forces and higher patellar tendon loads at deeper flexion angles relative to their peers with dome implants, suggesting quadriceps mechanics in TKA with the anatomic geometry was more like the natural knee.

Large variation in model-predicted quadriceps forces characterized variability in the performance of the task, which in some subjects may suggest compensation for quadriceps weakness. Generally, quadriceps forces calculated from musculoskeletal modeling were consistent with forces described in similar knee extension and lunge simulations (Shelburne and Pandy, 1997b; Zheng et al., 1998). However, as subject-specific models were scaled by mass and marker-based segment lengths, patient size significantly influenced quadriceps force. Also, patients were asked to perform the lunge activity as naturally as possible while keeping their knee within the imaging volume, which led to unique movement strategies, specifically in the position of the contralateral limb. For example, some subjects slid the contralateral foot or adjusted its position to maintain balance through the activity. In addition, subjects with the dome geometry tended to utilize less quadriceps force in the deepest part of the lunge compared to anatomic subjects, perhaps indicative of dome subjects off-loading their weight onto the contralateral limb during the most difficult part of the task (Figure 5.4, from 75 to 100 degrees).

Patella kinematics calculated with subject-specific finite element models closely resembled the subject-specific kinematics measured with HSSR, providing confidence models and loading conditions used in the simulations of PF mechanics were effective. Average RMS differences between calibrated model and experiment were 3.5° in flexion-extension and 2.8° in internal-external rotations, and 1.7 mm in medial-lateral translations. While the articulating geometry of the patella strongly predicted PF motion, calibration of soft tissue attachments on the patella also affected model kinematics. For example, PF flexion-extension was sensitive to the anterior-posterior position of the quadriceps and patellar tendon on the patella; an anterior shift in the patellar tendon resulted in an increase in PF flexion (3° increase in PF flexion per 1 mm of anterior shift in patellar tendon attachment). Also, the pre-strain in PF ligaments was adjusted to settle the patellar component in the trochlear groove and provide stability in patellar tilt and medial-lateral translations near full extension (<30°); forces in the PF ligaments decreased as the knee flexed as described by Nomura et al. (Nomura et al., 2000).

Stereo radiography revealed differences between dome and anatomic patellar kinematics that were accompanied by differences in the kinematics and loading of the quadriceps mechanism. Patients with anatomic geometry achieved greater PF flexion than those with the dome during lunge. The load-bearing lunge revealed greater differences than the seated knee extension in PF kinematics, likely due to larger quadriceps forces in the lunge. Differences in patellar flexion accompanied differences in patellar contact on the femoral component. Center-of-pressure in the dome subjects

generally remained on the proximal half of the patellar component as the knee flexed, while contact locations in the anatomic subjects shifted from a more distal to proximal position as knee flexion increased (3 mm more distal at 30° and 4 mm larger excursion in anatomic subjects, Figure 5.5c). Since the patella behaves like a class 1 lever, where the PF contact location is the fulcrum, more distal PF contact locations, as shown in anatomic subjects, may increase the effective moment arm of the knee near full extension (Yamaguchi and Zajac, 1989). Effective moment arm is a measure of the mechanical advantage of the extensor mechanism; larger moment arm allows the quadriceps to extend the knee with less force. The influence of patellar flexion on patellar tendon moment arm was not as great as PF contact location, with model calculations of patellar tendon moment arm for both dome and anatomic subjects consistent with values reported in the literature (Buff et al., 1988; Krevolin et al., 2004; Price et al., 2004; Yamaguchi and Zajac, 1989). Anatomic subjects demonstrated larger moment arms than dome subjects in early flexion, likely due to the differences in patellar flexion and PF contact. However, some differences in moment arm might be attributed to sizing variation between the two cohorts. For example, the anterior-posterior dimension of the femoral component and thickness of the patellar construct have a significant impact on moment arm (D'Lima et al., 2001). A larger construct may place the patella more anterior to the femoral component, thus creating greater distance between the patellar tendon line-of-action and the femoral flexion axis. Although anatomic subjects had larger combined femoral implant size and patellar thickness by an average of 3mm, sizing and surgical variability did not account for the significant difference in moment arm between implant

designs. Notably, patellar tendon angles relative to the tibial axis remained consistent for dome and anatomic subjects, but were significantly smaller in magnitude near full extension (<30°) when compared to natural data (Buff et al., 1988; Yamaguchi and Zajac, 1989) (Figure 5.6b). The patellar tendon angle is one determinant of the anterior-posterior shear forces applied to the tibiofemoral joint (Yamaguchi and Zajac, 1989), and PF contact forces. Patellar tendon angles may be lower in implanted subjects due to anterior subluxation of the tibia common in TKA (Price et al., 2004).

Differences in PF flexion angle and contact location were associated with differences in the distribution of quadriceps force to the patellar tendon and PF joint contact. The anatomic design supported higher load transfer to the patellar tendon and smaller implant forces due greater patellar flexion more distal PF contact. Even so, when comparing to natural data, dome and anatomic implants demonstrated substantially lower patellar force ratios than natural subjects in early flexion (<40°) (Ahmed et al., 1987). That is, the amount of quadriceps force transmitted to the patellar tendon was less. Lower implanted patellar force ratios may indicate quadriceps deficiency. In the lunge, dome subjects presented smaller patellar force ratios in deep flexion. Likewise, dome contact force ratios were larger than anatomic. The more extended angle of the dome implants likely influenced the increase in contact force ratio, which may increase implant forces and decrease quadriceps efficiency (Figure 5.3). In contrast, the flexed angle of the anatomic design distributed load to the patellar tendon at deeper flexion angles, which may provide better extensor efficiency.

There are some limitations associated with the FE models presented in this study. FE models may have been limited by the use of generic soft tissue geometry for the patellar ligaments and quadriceps muscles. Quadriceps forces were applied to an estimated line of action based on the Visible Human Project as described by (Fitzpatrick et al., 2016). Subject-specific q-angle might improve calibration of model patella tilt and lateral translation near full extension and, consequently, prediction of PF mechanics (Huberti and Hayes, 1984; Mesfar and Shirazi-Adl, 2005), but may not have a significant effect on predictions of patellar flexion. Quadriceps forces were created in separate musculoskeletal simulations, which lacked detailed, deformable representations of PF soft tissue. A goal of our future work is to develop analyses in which muscle forces are calculated within the FE framework. Also, PF ligaments were based on literature descriptions. Patient-specific models of the PF ligaments may improve the prediction of load distribution across the patellar mechanism. To test PF ligament sensitivity, similar to (Ali et al., 2016), PF ligament stiffnesses were doubled and found to have no significant impact on model kinematics. And finally, experimental TF kinematics were prescribed in the model to isolate the PF mechanism. Future analyses could investigate the interaction of the TF and PF joints and its impact on patellar mechanics.

The current study compared PF mechanics between medialized dome and medialized anatomic PF geometries using subject-specific, stereo radiography-driven, FE models. The experimental and modeling framework combined accurate in vivo kinematics with musculoskeletal and finite element modeling to evaluate the effect of

patella implant geometry on loading and kinematics of the quadriceps mechanism. The anatomic geometry demonstrated kinematics closer to that of natural knees allowing greater load transfer from the quadriceps to the patellar tendon, but patient variability and compensation strategies potentially masked the effect of implant geometry on functional performance. Although average behavior suggests improved quadriceps function with the anatomic implant, knee function and strength should be evaluated on a patient-specific basis. The sequential modeling approach, developed in this study, integrated whole-body and joint-level measurement and simulation to provide a comprehensive evaluation of in vivo joint mechanics.

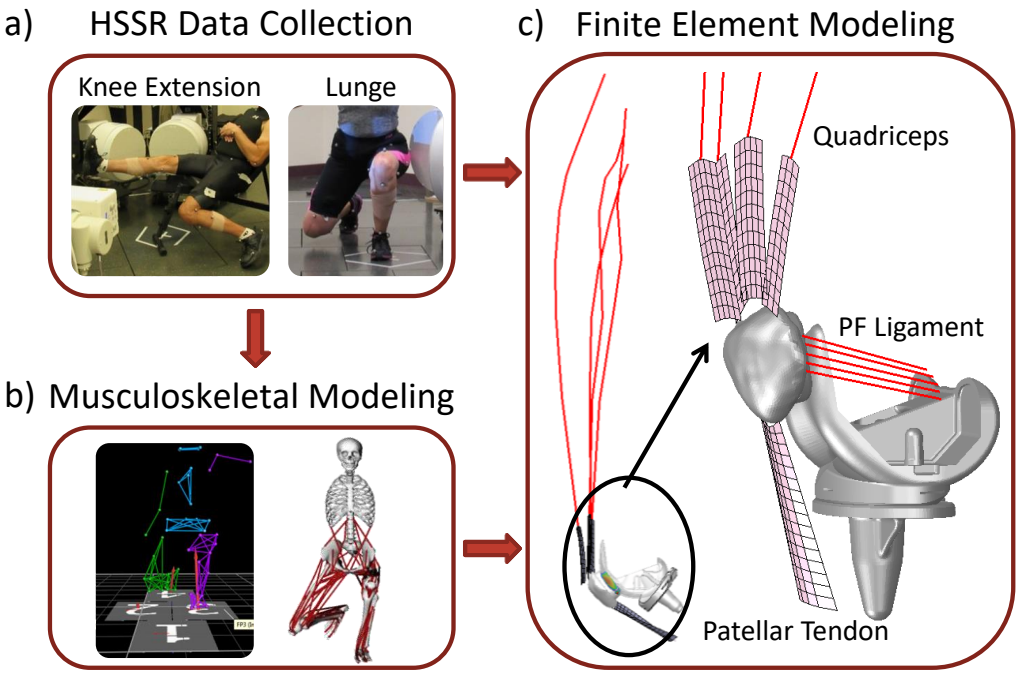

Figure 5.1 Workflow for the current study describing a) HSSR measurements of the knee extension and lunge activities, b) motion capture and force plate data used to drive musculoskeletal simulations, and c) subject-specific finite element modeling for the evaluation of PF mechanics

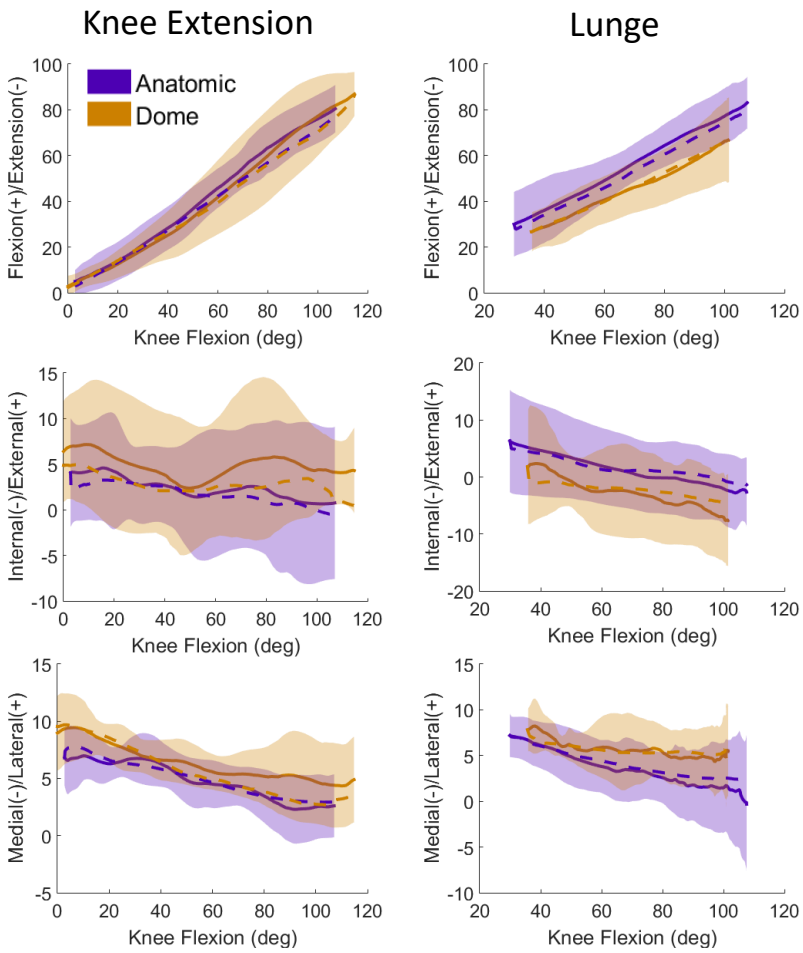

Figure 5.2 Comparison of average +/- 1 standard deviation experimental (-) and model (--) PF kinematics for medialized anatomic and medialized dome implants

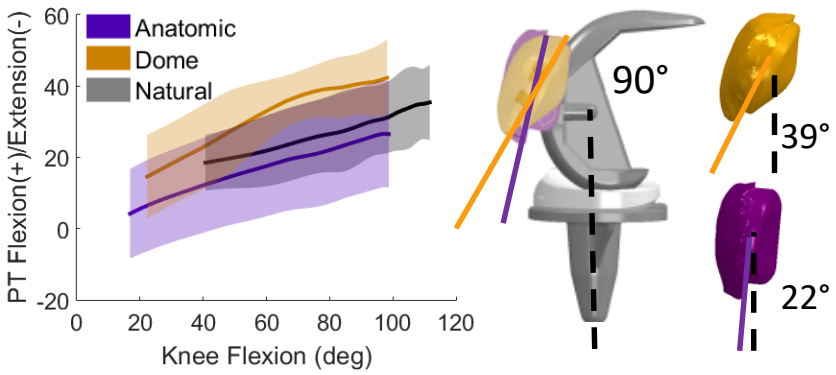

Figure 5.3 Average (line) ± 1 standard deviation (shaded) of patellotibial flexion-extension for natural knees, and medialized dome and medialized anatomic implants during lunge

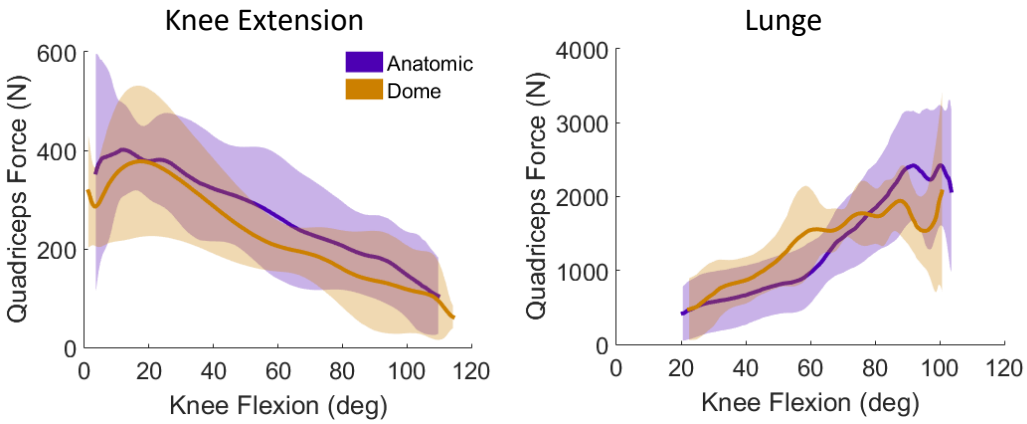

Figure 5.4 Average +/- 1 standard deviation of quadriceps force predictions from musculoskeletal modeling for knee extension and lunge

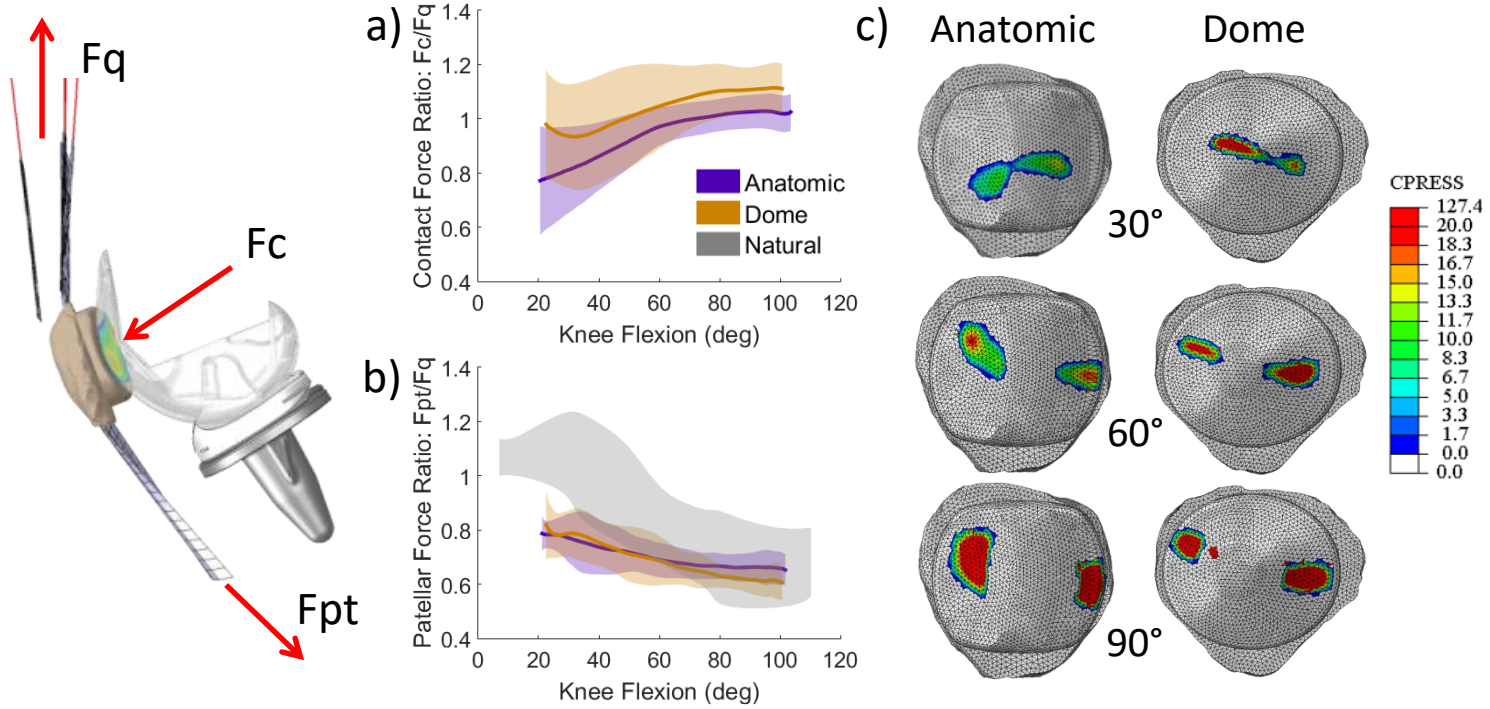

Figure 5.5 Comparison of mean (line) and ± 1 standard deviation (shaded) of a) contact force ratio and b) patellar force ratio between medialized dome, medialized anatomic, and natural subjects (Ahmed et al., 1987). Force ratios (right) shown for the lunge activity: Fc = contact force, Fq = quadriceps force, Fpt = patellar tendon force.

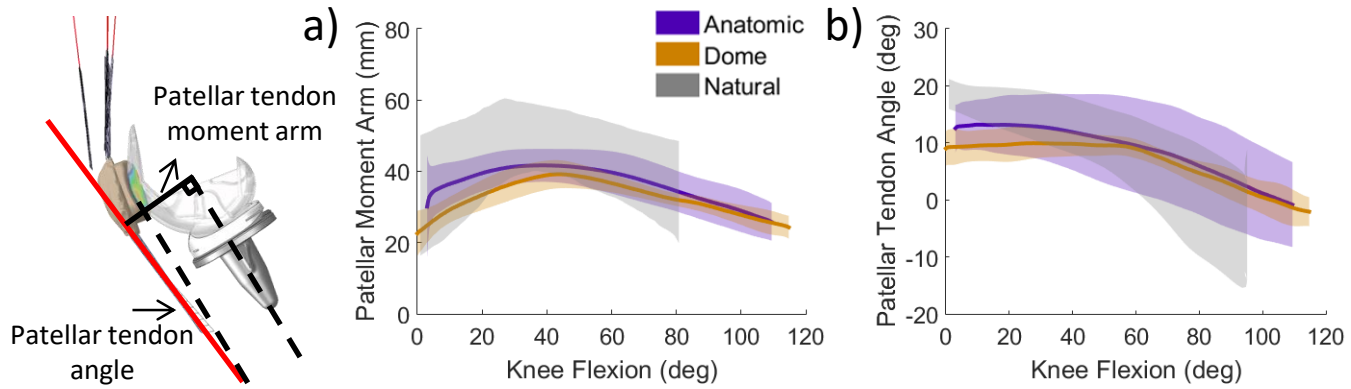

Figure 5.6 Comparison of mean (line) and ± 1 standard deviation (shaded) of a) patellar tendon angle, and b) moment arm between natural, medialized dome and medialized anatomic subjects. Natural subject results are described from (Buff et al., 1988; Yamaguchi and Zajac, 1989)

CHAPTER 6 – AN EXPERIMENTAL AND COMPUTATIONAL MODELING FRAMEWORK FOR EVALUATION OF IN-VIVO KNEE MECHANICS DURING KNEE EXTENSION AND LUNGE

6.1 Introduction

Due to the high prevalence of knee pain and injury, and demand for higher functionality in total knee replacements, researchers are interested in quantifying knee function during dynamic activity (Kurtz et al., 2007; Nguyen et al., 2011). Dynamic evaluations of knee mechanics are important for developing successful treatments of pathological conditions. For example, cruciate injury is one of the most common pathologies in the U.S. with over 100,000 anterior cruciate ligament (ACL) reconstructions per year, and an estimated incidence rate of one injury per 3500 people (Beynnon et al., 2005). While the ACL and PCL play an important role in anterior-posterior constraint, the ACL also contains proprioceptive mechanoreceptors that influence muscle activation, which is important for perception of healthy knee stability and function (Barrack et al., 1989; Georgoulis et al., 2001). As a result, implant manufacturers are interested in developing bi-cruciate-retaining total knee replacement designs to preserve the proprioceptive characteristics in the knee, allowing greater "feel"

of natural stability and, thus, potentially improving patient satisfaction. Understanding knee injury and repair requires subject-specific analysis of dynamic activity under physiological loading. By quantifying healthy joint mechanics, clinicians and implant designers can develop targeted rehabilitation and surgical therapies to restore healthy knee function. Experimental and computational methodologies have been employed to improve our understanding of knee mechanics, but previous efforts typically lack measurements of joint forces under dynamic, in-vivo loading.

Computational models enable the testing of new treatments in ways that are impractical with in vivo and in vitro experiments. Video photogrammetric, marker-based motion analysis is the most common method for measuring in-vivo, lower limb motion, but the accuracy of this technique can be limited by skin motion artifacts (Stagni et al., 2005). Dynamic MRI has been used to overcome some of the challenges with marker-based kinematic measurements (Besier et al., 2005; Carpenter et al., 2009), however, MRI is an expensive imaging modality and the technique requires substantial labor from manual segmentation of bone and soft tissue. Recent advances in dynamic, single- and dual- plane radiography allow direct measurement of bone and implant motion by superimposing the 3D geometric representations onto the captured images (Banks and Hodge, 1996; Dennis et al., 2003; Ivester et al., 2015). The main limitation of stereo radiography is the relatively small field of view for capturing dynamic activity. Since, internal joint and soft tissue forces are impractical to measure using non-invasive methods, researchers have developed in-vitro cadaveric tests to directly measure cartilage

and ligament forces (Draganich and Vahey, 1990; Elias et al., 2004; Li et al., 2004b; Markolf et al., 2004). In-vitro tests are useful for quantifying joint loading, deriving soft tissue material characteristics, and developing computational representations (Harris et al., 2016), but may not represent in vivo conditions.

Predictive computational models have been used with in-vivo and in-vitro experiments to quantify joint mechanics. Musculoskeletal models can combine motion and ground reaction force data from in-vivo experiments to estimate muscle and ligament forces using optimization techniques (Delp et al., 2007). For example, whole-body musculoskeletal models have been used to predict patterns of quadriceps, ACL and PCL loading, and compare changes in knee kinematics and joint loads for healthy and cruciate-deficient conditions (Moissenet et al., 2014; Shelburne et al., 2004b). While these models provide estimates of whole-body function, the detail and complexity within the joint remains overly simplistic: bone and soft tissue geometry is typically generic; joint definition is often estimated as a simple hinge (Neptune et al., 2004); and, contact interactions are modeled using rigid body constraints. With some compromise to computational efficiency, finite element analysis provides detailed solutions of internal joint stress/strain and soft tissue loading that may be necessary for studying pathology and developing cruciate-retaining TKR designs.

Finite element (FE) models have been used to reproduce in-vitro loading and boundary conditions from dynamic, experimental knee simulators (Ali et al., 2016;

Baldwin et al., 2012; Godest et al., 2000; Halloran et al., 2010), but have rarely been utilized for simulation of in vivo knee mechanics. There are exceptions though, as (Beillas et al., 2004) have incorporated radiography-based kinematics into a FE model to study in-vivo knee mechanics of a single-leg hop, and (Fernandez et al., 2008) included kinematics from x-ray fluoroscopy and quadriceps force predictions from musculoskeletal modeling into a FE framework for prediction of PF kinematics and contact mechanics during a step-up task. Similar to (Fernandez et al., 2008), the current study applies a sequential approach integrating in-vivo stereo radiography kinematics, and predicted joint motions and muscle forces from musculoskeletal modeling into detailed, subject-specific FE models of the knee. The goal of the current work was to develop a computational tool for implant evaluations through three primary objectives: 1) developing load-controlled models of in-vivo natural knee motion, 2) performing subject-specific calibration of cruciate properties, and 3) simulating two activities spanning the entire range of motion of the subject (knee extension and lunge). While the overall goal is to develop a computational tool for implant evaluations, the first step is to reproduce healthy knee motion to quantify the contribution of ligament structures, and to develop a baseline for healthy knee function. Model calibration was performed using comparison to experimental, in-vivo tibiofemoral (TF) and PF kinematics during a knee extension task, and the predictive capability of the model was assessed through comparisons of experimental and model kinematics in the lunge activity.

6.2 Methods

6.2.1 Data Collection

High-speed stereo radiography (HSSR) images were collected for one healthy, older adult male (age=52years, height=172cm, weight=126lbs, BMI=19.3) performing two activities of daily living: an unloaded, seated knee extension ranging from high knee flexion to full extension, and a single-leg lunge (Figure 6.1a). This study was approved by the University of Denver Institutional Review Board and informed consent was provided by the subject. HSSR was used to capture 3D sub-mm measurement of bone motion for each activity (Ivester et al., 2015). The HSSR system is composed of two 40 cm diameter image intensifiers with high-speed, high-definition (1080x1080) digital cameras positioned at a relative 70° angle for collection of two images at a frequency of 50 Hz for the knee extension activity, and 100 Hz for the lunge activity. Computed tomography (CT, 0.39x0.39x0.6mm, resolution: 512x512) and magnetic resonance (MR, 0.53x0.53x0.6mm, resolution: 320x320) images were captured for the subject. Bone and cartilage geometry was reconstructed from CT and MR imaging, respectively, using ScanIP (Simpleware, Exeter, UK). A femoral local coordinate system was defined by fitting a cylinder through the center of the medial and lateral femoral condyles; the medial-lateral (M-L) axis was defined by the most posterior points on each condyle; the superior-inferior (S-I) axis was parallel to the posterior edge of the femoral shaft; the anterior-posterior (A-P) axis was defined by the cross product between the S-I and M-L axes. The relative position of femur, tibia, and patella bones was tracked using

Autoscoper by manually aligning 3D reconstructed geometry to the 2D images from radiography (Brown University, Providence, RI). TF and PF joint kinematics were described relative to a pose near full extension using a joint coordinate system defined by (Grood and Suntay, 1983).

In addition to HSSR, simultaneous marker-based motion capture and ground reaction forces were collected for knee extension and lunge. The motion capture system consisted of an eight-camera, passive marker, video photogrammetric system (Vicon Motion Analysis Corp., Centennial, CO) for measurement of whole-body motion. Ground reaction forces were recorded using four six-component, strain gauged force plates (Bertec Corp., Columbus, OH).

6.2.2 Musculoskeletal Modeling

A subject-specific, whole-body, musculoskeletal model was developed in OpenSim (Figure 6.1b). The model was based on that developed by (Navacchia et al., 2016b) and consisted of 12 body segments (torso, pelvis, femurs, tibiae, tali, calcanei, toes), and 92 Hill-type musculotendon units. Model segments were scaled based on the ratio of relative marker distances from motion capture and the virtual markers in the template model. Lower limb joint definition included a ball-and-socket hip joint, a revolute ankle joint, and a knee joint with prescribed TF and PF motion from the HSSR system. TF and PF kinematics were prescribed to a femoral coordinate system located at the midpoint of the femoral condyles using splines as a function of knee flexion

(Navacchia et al., 2016a). Separate musculoskeletal models were created for each activity to allow description of knee joint kinematics specific to the knee extension and lunge. All TF DOF were prescribed, whereas the DOF prescribed to the PF joint were flexion-extension, superior-inferior translation and anterior-posterior translation. The patellar tendon was represented by a musculotendon unit attaching the distal end of the patella to the tibial tuberosity.

Motion capture and ground reaction forces were input into the musculoskeletal model for prediction of joint kinematics and muscle forces. For simulation of the knee extension activity, pelvis and lumbar motion were fixed to a seated position, and a body weight load was applied to the pelvis to simulate the support from a chair. Inverse kinematics of the marker-based motion was used to predict hip and ankle kinematics. Static optimization in OpenSim was used for efficient evaluation of muscle forces.

6.2.3 Finite Element Modeling

Subject-specific finite element models were developed in Abaqus (Simulia, Providence, RI) for the knee extension and lunge activity (Figures 6.1c, 6.2, 6.3). Bone and cartilage reconstructions from imaging were post-processed in Hypermesh (v11.0, Altair, Troy, MI) using rigid, triangular, shell elements (R3D3) for bone, and hexahedral, continuum (C3D8R) elements for cartilage. Scaled mass and rotational inertial properties of the bones were obtained from musculoskeletal modeling and applied to the FE representations. Although cartilage contains time- and depth-dependent characteristics

(Halonen et al., 2015), frictional contact (0.01) between bone and cartilage was defined using a computationally-efficient, pressure-overclosure relationship, which is representative of deformable contact (Fitzpatrick et al., 2010).

Tibiofemoral ligament structures were represented using non-linear tension-only springs (CONN3D2) and included the anteromedial-ACL bundle (ACLam), posterolateral-ACL bundle (ACLpl), anterolateral-PCL bundle (PCLal), posteromedial-PCL bundle (PCLpm), the lateral collateral ligament (LCL), popliteofibular ligament (PFL), medial collateral ligament (MCL), deep medial collateral ligament (dMCL), posterior oblique ligament (POL), anterolateral structure (ALS), and medial and lateral posterior capsule (PCAPm, PCAPl). Initial estimates of ligament stiffness and reference strain were obtained from combined cadaveric experiment and modeling of four specimens by (Harris et al., 2016). TF ligament attachment locations were determined from MR imaging (cruciate and collateral ligaments), and anatomical bony landmarks.

Patellofemoral soft tissue structures were modeled using 2D fiber-reinforced membrane elements (M3D4R) and 1D, non-linear, embedded springs (CONN3D2). Quadriceps tendon and patellar ligament properties were defined using a Van der Waals, hyperelastic model, calibrated to match uniaxial test data from the literature (Baldwin et al., 2009; Staubli et al., 1999). Zero surface-penetration contact was defined between the PF soft tissue geometry, bone and articulating surfaces.

Quadriceps, hamstrings, and gastrocnemius muscles included the rectus-femoris (RF), vastus-medialis (VM), vastus-lateralis (VL), vastus-intermedius (VI), semimembranosus (SM), biceps femoris (BF), and gastrocnemius medial ($G_{med)}$ and lateral (G_{lat}) bundles. Quadriceps lines of action were estimated from reconstructions of the muscle centroid path in the Visible Human Project (Ackerman, 1991). A series of slipring connectors (CONN3D2) directed forces along the centroid of the muscle cross-sectional area. Hamstrings and gastrocnemius muscles were represented using a combination of point-to-point connectors (CONN3D2) and truss elements (T3D2). Truss elements allowed wrapping contact around analytical surfaces representing the femoral condyles, and the posterior aspect of the tibia bone.

FE model loading and boundary conditions replicated the experimental motion for knee extension and lunge activities. Models included hip (3 DOF), ankle (1 DOF), and knee joints (12 DOF), consistent with the joint definition described in the musculoskeletal models. For knee extension, the hip joint was constrained in all translational DOF to reproduce the support from the chair; the ankle/foot was unconstrained. Hip rotations were applied based on inverse kinematics from musculoskeletal modeling. TF flexion-extension and internal-external rotations, and medial-lateral translation were prescribed from HSSR measurements; all other TF DOF and all DOF in the PF joint were unconstrained. The vector sum of quadriceps forces from musculoskeletal modeling were applied to the FE model, and the distribution of quadriceps force among the individual muscle groups was determined from (Amis and

Farahmand, 1996). A static analysis, in the deep flexion pose of the knee extension activity, was used to determine the peak magnitude of hamstrings and gastrocnemius forces. The static analysis utilized a proportional-integral-derivative (PID) controller to simultaneously solve for the combination of hamstrings and gastrocnemius loads required to maintain the deep flexion angle (~135°). PID-controlled muscle forces were applied to the FE analysis using a user-defined VUAMP subroutine. The dynamic simulation of the knee extension activity applied a ramped load from 15 N to the peak hamstrings and gastrocnemius loads (SM=25N, BF=35N, G_{med}=G_{lat}=200N) as the knee flexed from 90° to deep flexion.

In the simulation of the lunge activity, constraint of the open-chain dynamic, FE model was reversed, such that, the foot was constrained in all DOF and the hip was free to move. The TF and PF joints were load-driven, as the motions at the knee were driven by a combination of hip and ankle joint kinematics and loads, and quadriceps and hamstrings muscles. The foot was attached to an ankle revolute joint, which prescribed ankle flexion-extension based on inverse kinematics from musculoskeletal modeling. TF flexion-extension was driven using PID-controlled quadriceps force, designed to match the experimental knee flexion profile. The model included an internal-external torque, which was derived from PID-control of the experimental TF internal-external rotation. Hip rotations were enforced based on inverse kinematics from musculoskeletal modeling, and a ramped, medial-lateral load (<40N) was applied to the hip joint to stabilize the TF

varus-valgus kinematics. Forces in the hamstrings and gastrocnemius were estimated from static optimization analyses within the musculoskeletal modeling framework.

Calibration of TF and PF soft tissue alignment and material properties was performed in simulations of the knee extension activity to match experimental joint kinematics using a design-of-experiments approach. Properties of the PF soft tissue remained consistent with literature definition (Baldwin et al., 2009); a sensitivity analysis doubled the stiffness of the quadriceps and patellar tendons, and found no significant differences in PF kinematics (<1° and 1 mm) (Ali et al., 2016). Quadriceps and patellar tendon attachment locations were perturbed to match experimental PF kinematics; perturbations primarily consisted of anterior-posterior translation of the patellar ligament attachment on the patella, but also included medial-lateral tilt and translation of the quadriceps tendons and patellar ligament. For calibration of TF anterior-posterior kinematics, the alignment and properties of the ACL and PCL were modified. Cruciate reference strain (EREF) (Harris et al., 2016), ACL stiffness (K) (Woo et al., 1991), and PCL stiffness (Race and Amis, 1994) were perturbed within the bounds described in the literature (Table 6.1). ACL and PCL attachment locations were varied according to MRI reconstructed origin and insertion areas, and bony landmarks described in the literature.

Outputs from FE simulations included predictions of TF and PF kinematics, contact mechanics, and ligament forces for the knee extension and lunge activities. Root-mean-square (RMS) differences between the model and experiment were calculated to

describe model accuracy. The calibration space was identified by simulating the knee extension activity with and without the ACL and PCL ligaments to establish the bounds of TF anterior-posterior kinematics. Calibration was achieved through adjustment of ligament stiffness and references strain properties for two bundles of the ACL and PCL. Also, sensitivity analyses were performed in simulations of the lunge activity to evaluate the impact of cruciate stiffness and reference strain on TF anterior-posterior kinematics. Cruciate ligament parameters were perturbed for mean +/- 1 standard deviation of ligament stiffness and reference strain. Mean and standard deviations for reference strain (Harris et al., 2016), ACL stiffness (Woo et al., 1991), and PCL stiffness (Race and Amis, 1994) were determined from cadaveric joint laxity experiments and mechanical testing described in the literature (Table 6.1); Table 6.1 describes the range of values, mean and standard deviations from literature, initial set of parameters, and calibrated values applied to the FE representations of the cruciate ligaments. Total contact forces in the medial and lateral TF cartilage, and PF cartilage were computed from simulation of the lunge activity. Also, the contribution of individual ligaments and total ligament tensile and anterior-posterior shear forces were described with respect to the tibial local coordinate system.

6.3 Results

6.3.1 Experimental kinematics

The subject achieved knee flexion angles as large as 135° in the knee extension activity and 132° in the lunge activity (Figures 6.2 and 6.3). Differences in TF and PF kinematics between knee extension and lunge were small (RMS<5° in rotations; RMS<4mm in translations). Similar to trends in kinematics reported in the literature (Kefala et al., 2017), the tibia rotated internally (~27°) and translated anteriorly (~16 mm) with respect to the femur as the knee flexed. The patella flexed at approximately 60% of the knee flexion angle. Also, the patella rotated internally (~7°) as the knee flexed, and had relatively small medial-lateral excursion (<3mm).

6.3.2 Quadriceps and Hamstrings Forces

Quadriceps force predictions from musculoskeletal and FE modeling were consistent with magnitudes and trends reported in the literature (Shelburne and Pandy, 1997a; Zheng et al., 1998). Peak quadriceps force occurred near full extension (473N at 15° TF flexion) in the knee extension activity, and forces decreased as the knee flexed. In the lunge activity, quadriceps forces increased as the knee flexed with the peak magnitude of load equal to 2972 N at 100°. The hamstrings muscles co-contracted with the quadriceps during the lunge activity, and peak hamstrings forces in the semimembranosus and biceps femoris were equal to ~750 N. Gastrocnemius forces also increased as a function of flexion and reached a combined load of ~300 N.

6.3.3 Knee Extension Model Kinematics

Experimental TF kinematics were compared to simulations of ACL-deficient and PCL-deficient behavior (Figure 6.2). In the ACL-deficient condition, the model predicted an anterior shift of the tibia with respect to the femur through the entire range of motion, particularly in early flexion as differences between the model and experiment reached up to ~13 mm at 30° knee flexion. In the PCL-deficient condition, the model predicted an increase in posterior tibial translation, primarily in deep flexion (~6 mm maximum difference between model and experiment at 120° knee flexion).

Model TF and PF kinematics were calibrated to the experimental motion for the knee extension activity (Figure 6.2). Initial estimates of soft tissue properties and alignment from (Harris et al., 2016) significantly under-predicted anterior translation of the tibia with respect to the femur (RMS=7.3 mm). The calibrated model matched experimental TF anterior-posterior kinematics with a RMS difference of 0.92 mm. Calibrated model PF kinematics predicted experimental motion with RMS differences of 5.2° in flexion-extension and 4.2° in patellar tilt, and 2.6 mm in medial-lateral translation (Figure 6.2).

6.3.4 Lunge Model Kinematics

In the simulation of the lunge activity, PID-controlled, TF flexion-extension kinematics were accurate to within 1.5° of the experimental knee flexion angle. The lunge model also showed good agreement to experimental TF kinematics in varus-valgus

(RMS=2.1°), internal-external (RMS=2.4°), medial-lateral (RMS=3.0 mm), anterior-posterior (RMS=1.2 mm), and superior-inferior (RMS=2.1 mm) motions (Figure 6.3a). Lunge model PF kinematics had similar accuracy to the knee extension model with RMS differences between model and experiment equal to 2.5° in flexion-extension, 2.3° in internal-external, and 4.3 mm in medial-lateral.

6.3.5 Joint Contact Forces

In the knee extension activity, peak TF contact force (1001 N) occurred at full extension (~2°) and decreased up until ~90° knee flexion, where TF contact forces then increased until deep flexion. TF contact forces were small near 90° (197 N) due to small quadriceps and hamstrings loads. PF contact forces were consistent with trends in quadriceps force such that the peak load (595 N) occurred at 15° knee flexion and decreased as the knee flexed. In the lunge activity, TF and PF contact forces increased as the knee flexed, consistent with increasing muscle and joint loads (Figure 6.4). Peak TF contact force was 2367 N and occurred at 132° knee flexion, and peak PF contact force was 2505 N at 90° knee flexion.

6.3.6 Ligament Forces

The cruciate ligaments were the primary contributors to total ligament force in the knee extension and lunge activity. Trends in ligament force recruitment were consistent in both activities; ligament forces are shown for lunge only (Figure 6.5). The ACL was active in early to mid-flexion (0-60°), and the PCL was active in mid to deep

flexion (60-130°). In general, the posterolateral bundle of the ACL was more active in early flexion than the anteromedial bundle, which engaged in mid flexion. The anterolateral bundle of the PCL was the primary contributor to posterior constraint of the tibia in deep flexion. The posterior capsule was active near full extension and quickly became inactive as the knee flexed. In deep flexion, increased TF internal rotation of the subject resulted in constraint forces from the ALS and ACL. Ligament forces were highest near full extension and decreased as the knee flexed. Ligament shear forces dominated total ligament force in early-to-mid flexion, but tensile forces were greater in deep flexion.

6.3.7 Sensitivity Analysis

Sensitivity analyses evaluated the impact of cruciate ligament stiffness and reference strain properties on joint kinematics and loading during simulation of the lunge activity (Figure 6.3b, Table 6.1). Perturbations of ligament stiffness had sub-mm and sub-degree differences in TF kinematics. Ligament reference strain had a greater impact on TF kinematics than ligament stiffness; 1 standard deviation in cruciate reference strain resulted in differences of up to 9 mm in TF anterior-posterior motion and 12° in TF internal-external rotation. Average RMS difference in TF anterior-posterior translation and internal-external rotation between mean and ± 1 standard deviation of ligament reference strain was 6.2 mm and 6.4°, respectively.

Cruciate ligament stiffness had only minor effects on total TF contact force (~50N difference from the mean in deep flexion) in the lunge activity (Figure 6.4c). In contrast, reference strains of +1 and -1 standard deviation increased TF contact force by an average 258 N from the mean across the lunge activity. The calibrated model had the lowest TF contact force with ~216 N less force than the mean model at 132° knee flexion.

Similar to the sensitivity described in TF kinematics and contact forces, cruciate ligament stiffness had negligible effects on total ligament force (Figure 6.5c). Perturbations of reference strain increased total ligament forces; reference strain values greater than 1 represented pre-tensioning of the ligament, so ligament forces were the largest in simulation of +1 standard deviation of reference strain. While ACL and PCL ligament forces were small in the simulation of -1 standard deviation of reference strain, forces from the ALS and MCL increased due to posterior translation and internal rotation of the tibia with respect to the femur.

6.4 Discussion

The current study presents a novel integrated approach with stereo radiography, musculoskeletal modeling and finite element modeling for evaluation of subject-specific, in-vivo joint mechanics during a knee extension and lunge task. Detailed FE models of the knee are typically developed using in-vitro cadaveric tests, but rarely simulate in-vivo

motion. Few studies have combined in-vivo kinematic measurement and FE modeling for evaluation of joint and soft tissue forces (Beillas et al., 2004; Fernandez et al., 2008). The current work advances previous in-vivo knee modeling through simulation of dynamic activities across the entire range of motion of the knee, modeling of subject-specific knee behavior, and development of a load-controlled knee model allowing potential investigations of pathology, implant design, surgical technique, and rehabilitation therapies. The current study applied the computational modeling framework to investigations of cruciate ligament function and its impact on joint kinematics and contact mechanics.

Subject-specific characteristics were implemented into the FE framework using CT and MR reconstructions of geometry and soft tissue landmarks, and calibration of ligament properties and alignment to match experimental knee motion. Model calibration was performed in the knee extension activity, which was well-suited for evaluations of ligament function due to the relatively small muscle forces. Calibrated model kinematics demonstrated good agreement to the experimental HSSR kinematics with similar RMS differences between model and experimental TF and PF kinematics shown in the literature (Baldwin et al., 2012; Godest et al., 2000; Guess et al., 2010).

Application of soft tissue properties from an in vitro experiment resulted in poor representation of subject kinematics. In an effort to explore the calibration space, the knee extension activity was simulated with and without the ACL and PCL ligaments.

The initial estimate of cruciate properties from (Harris et al., 2016) predicted TF anterior-posterior kinematics beyond the bounds of the calibration space, but the initial analysis required some adjustments to the soft tissue attachment locations in addition to the ligament properties. While soft tissue attachment locations were informed by CT and MRI, the anterior-posterior position of the MCL, ACL, and PCL insertions and origins were modified; for example, a posterior shift in the femoral attachment of the ACL decreased its contribution in deep flexion, and an inferior shift in the femoral attachment of the PCL increased its contribution in deep flexion. The femoral, anterior-posterior attachment of the MCL relative to the knee joint center affected distribution of loading from the anterior to posterior bundles.

Ligament reference strain was the most critical material property in the calibration process, evidenced by the substantial differences in TF anterior-posterior kinematics, and TF contact and ligament forces (Figure 6.3b, 6.4c, 6.5c). While ligament stiffness affected the magnitude of contact and ligament forces, reference strain altered the trend and timing of ligament recruitment. Ligament strains were relatively small during the knee extension and lunge activity. As a result, perturbations of ligament stiffness had only minor effects on TF kinematics and contact mechanics during knee extension and lunge. Greater influence from ligament stiffness may occur in activities with extreme motions and loading, such as pivot or kneeling, because these activities may induce higher ligament strains.

The experimental and computational workflow can be applied to alternative in-vivo activities including chair rise, stepping up and down from stairs, and pivoting. A combination of hip and ankle joint loading, muscle force predictions from musculoskeletal modeling, and PID-control within the FE framework were used to develop external loads surrounding the knee for load-controlled simulation of the lunge activity. The FE model accurately predicted knee kinematics in the lunge activity with RMS differences between model and experiment less than 5° and 4 mm in both TF and PF joints. In order for the model to be used reliably as a clinical and research tool, direct validation of predicted contact and ligament mechanics is necessary, but difficult to obtain using in-vivo data. Model validation of joint mechanics is an on-going challenge within the biomechanics community due to the difficulty in measuring internal joint and soft tissue forces in-vivo (Fleming and Beynnon, 2004). Instead, joint and contact forces were qualitatively compared to predictions from the Orthoload database; model-predicted TF contact force compared well in trend and magnitude to average TF contact forces (700-2000 N from 0-100° knee flexion) for 8 subjects performing a deep knee bend (Bergmann et al., 2014). Although, there is limited direct validation of joint and ligament mechanics, subject-specific calibration of soft tissue properties to experimental kinematics provides confidence in model predictions.

There are some limitations to the proposed modeling framework. FE models could be improved through subject-specific, continuum representations of muscle and soft tissue. For efficient evaluation of dynamic activity, the current study utilized 1D

ligaments, which effectively capture overall joint stiffness, but do not model stress/strain distributions and wrapping contact around bone and soft tissue. Also, FE models did not incorporate a meniscus, which is important for distribution of joint loading to the TF cartilage (Englund et al., 2009). Subject-specific muscle geometry could be reconstructed from MRI to provide more accurate direction of loading, and continuum representations could be used to model thigh-calf contact in simulations of deep flexion.

While simulations of the knee extension and lunge activities included representations of the hip and ankle joints, these models are not useful for describing hip and ankle loading. Hip and ankle joints were modeled in the FE framework to provide a physiological reference for applied kinematics and loads from musculoskeletal models. While the current study successfully developed a set of hip and ankle loads for load-controlled simulation at the knee, there are infinite combinations of hip and ankle external loads to reproduce subject-specific knee motion; the loads described in this study represent a possible solution. The current knee model could be used for prediction of hip and ankle joint mechanics by calibrating the external loads to match model and experimental ground reaction forces at the ankle. To achieve more physiological hip and ankle loading, the FE model could apply experimental ground reaction forces at the hip and a corresponding hip moment to account for load transfer from the foot to the hip joint. By altering the input loads at the hip, the net knee torque would also be affected, which would require additional calibration of the hamstrings and gastrocnemius forces to maintain subject-specific knee loading; quadriceps forces would automatically adjust for

the altered loading at the hip using PID-control. The current study developed a model for subject-specific evaluation of in-vivo knee mechanics, but future work could advance the capabilities of the FE model for prediction of hip and ankle mechanics.

A load-controlled model of the knee can be a powerful tool for researchers, clinicians, and implant manufacturers by allowing investigations of knee mechanics following simulated pathology or total knee arthroplasty. The model can be used to 1) evaluate implant design features under dynamic, in-vivo loading (eg. cruciate-retaining design iterations), 2) investigate surgical techniques (eg. mechanical vs. anatomic alignment), and 3) identify and diagnose patients at-risk of knee pathologies (eg. osteoarthritis and PF pain).

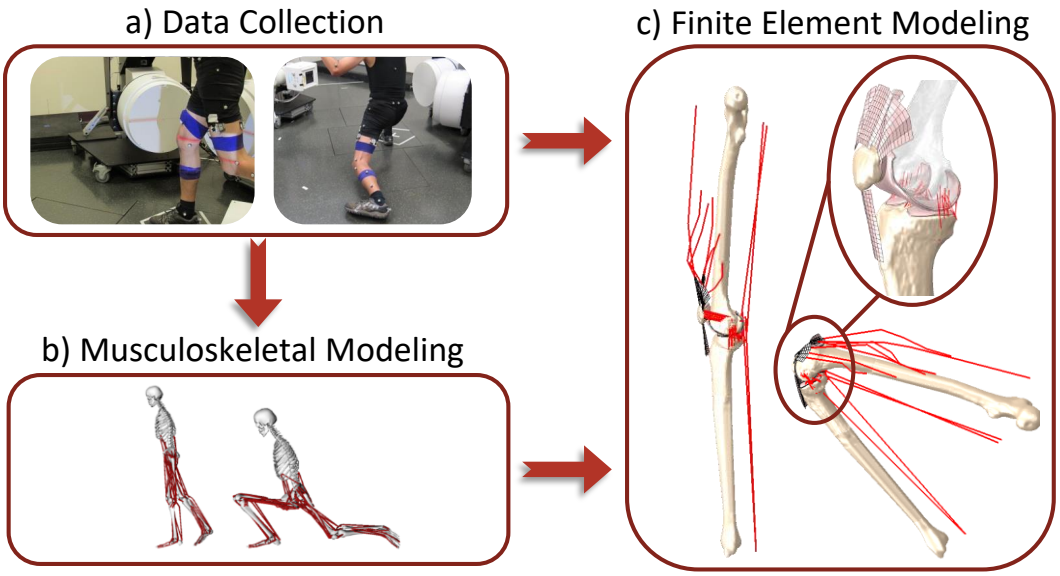

Figure 6.1 Experiment and computational modeling workflow including a) data collection of HSSR images, motion capture, and ground reaction forces, b) whole-body musculoskeletal modeling, and c) detailed, subject-specific finite element modeling for knee extension and lunge activities

Table 6.1 Cruciate ligament stiffness (K) and reference strain (EREF) properties applied to FE simulations. Bounds, and mean ± 1 standard deviation for ACL stiffness (Woo et al., 1991), PCL stiffness (Race and Amis, 1994), and reference strain (Harris et al., 2016) were obtained from the literature. Calibrated values describe the final set of parameters used for subject-specific simulation.

	ACLam		ACLpl		PCLal		PCLpm	
	Stiffness (K, MPa)	Reference Strain (EREF)	Stiffness (K, MPa)	Reference Strain (EREF)	Stiffness (K, MPa)	Reference Strain (EREF)	Stiffness (K, MPa)	Reference Strain (EREF)
Bounds	50-240	0.85-1.15	45-240	0.85-1.15	30-300	0.85-1.15	30-100	0.85-1.15
Mean ± Standard Deviation	180 ± 25	0.99 ± 0.11	180 ± 29	0.98 ± 0.10	176 ± 57	0.95 ± 0.08	77 ± 32	0.97± 0.09
Initial Estimate	100	1.04	47	1.01	35	0.93	60	1.00
Calibrated Values	70	1.03	120	1.08	80	0.97	60	1.06

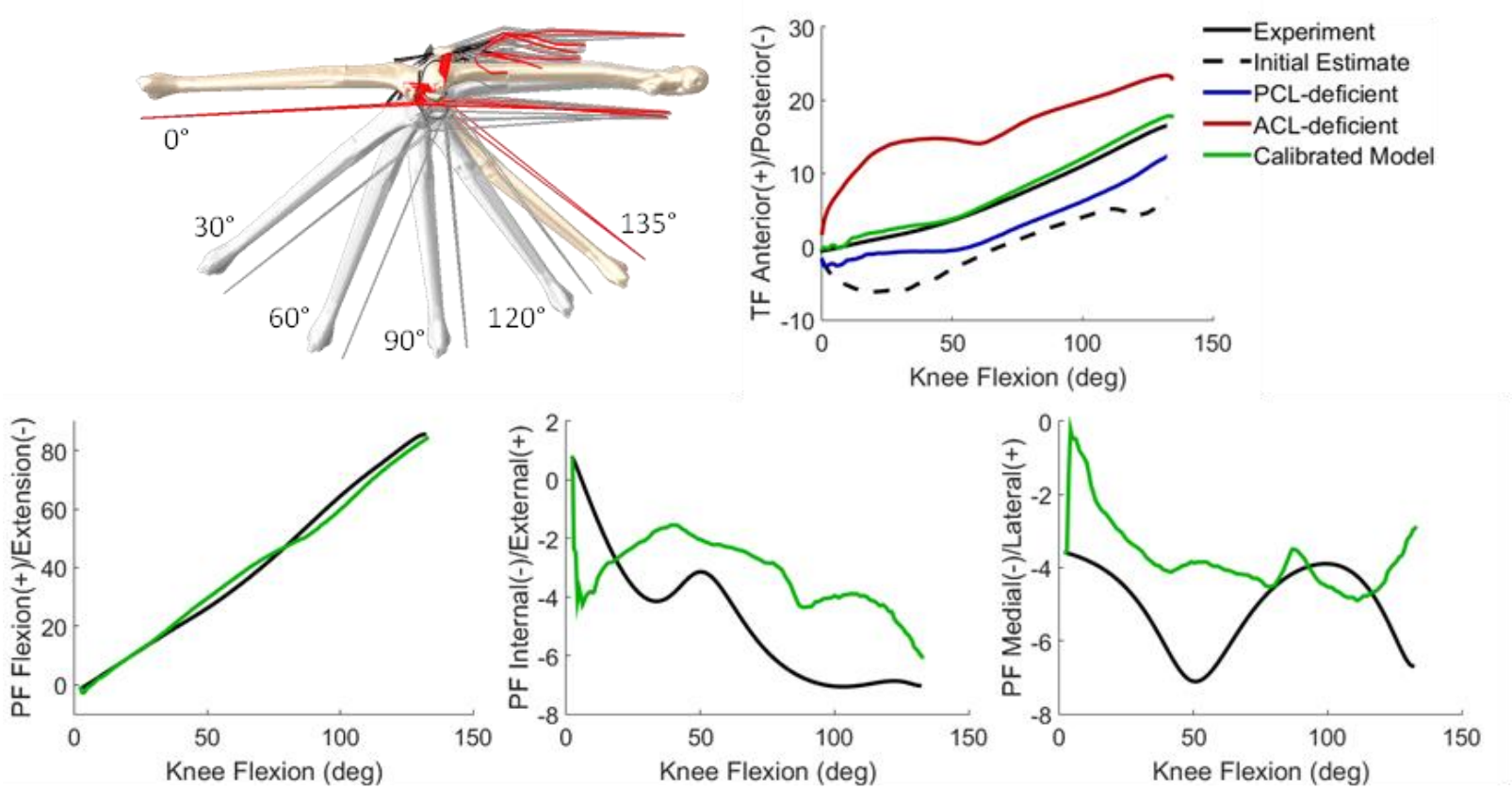

Figure 6.2 Comparison of model and experimental TF and PF kinematics for the knee extension activity: experiment (-), initial estimate of soft tissue properties from (Harris et al., 2016) (--), ACL-deficient, PCL-deficient, and calibrated model predictions

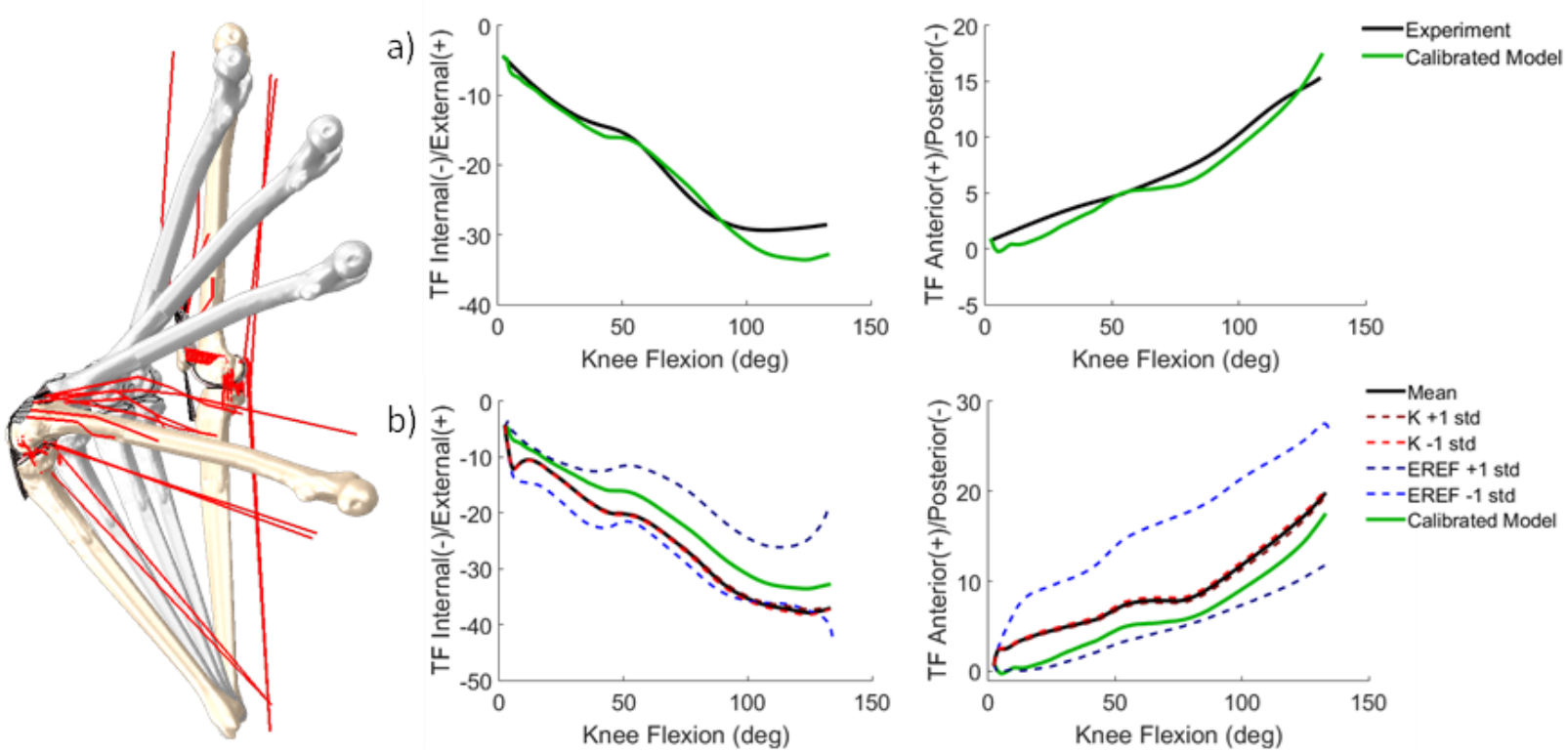

Figure 6.3 a) Comparison of model and experimental TF kinematics for the lunge activity: a) experiment and calibrated model predictions, b) sensitivity analysis comparing the impact of mean ± 1 standard deviation of ligament stiffness (K) and reference strain (EREF) on TF internal-external and anterior-posterior kinematics. Mean and standard deviations obtained from the literature (see Table 1).

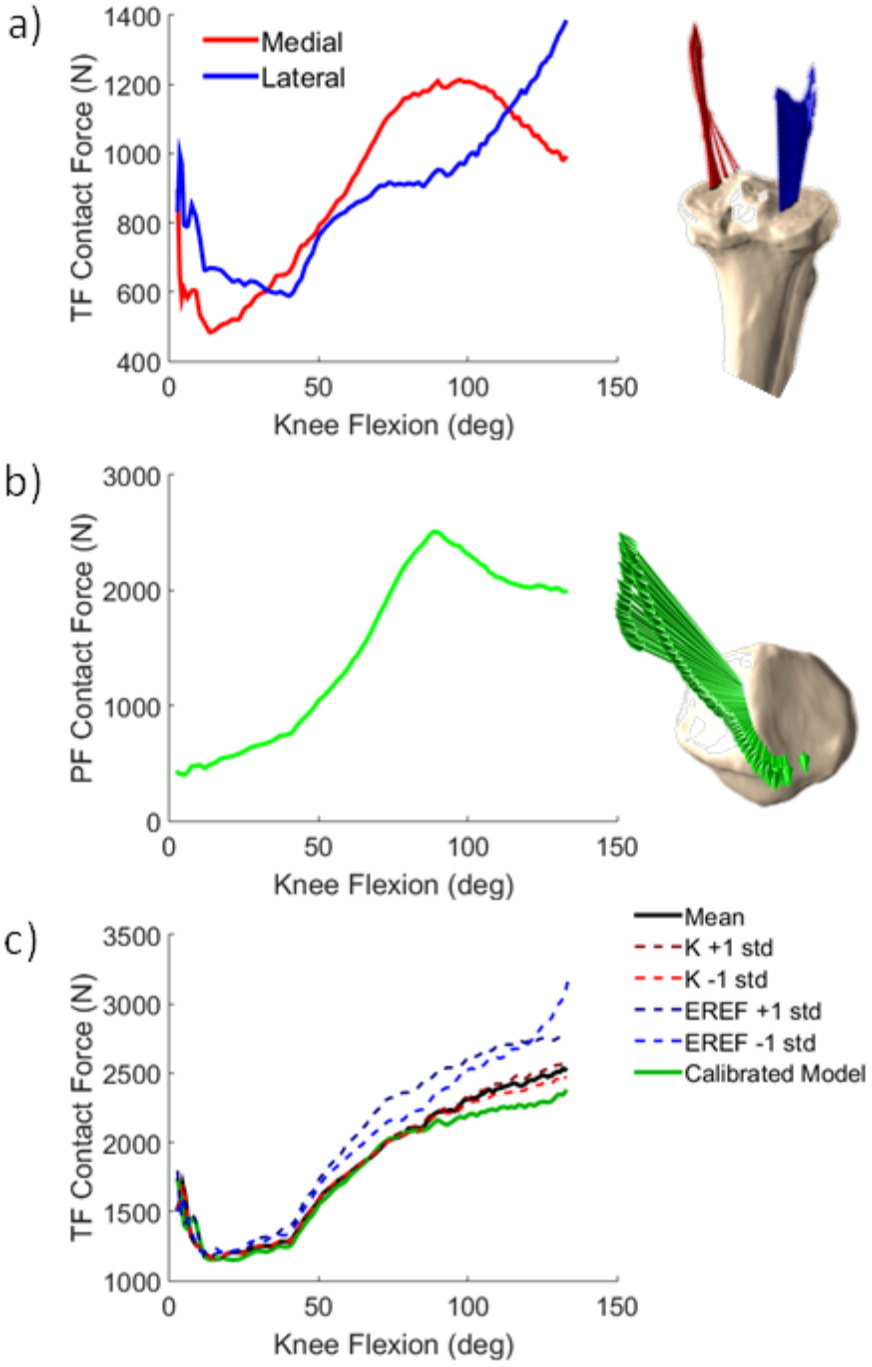

Figure 6.4 a) Total TF contact force, b) PF contact force (middle), and c) comparison of TF contact forces between calibrated, mean, and ±1 standard deviation of ligament stiffness and reference strain analyses during the lunge activity.

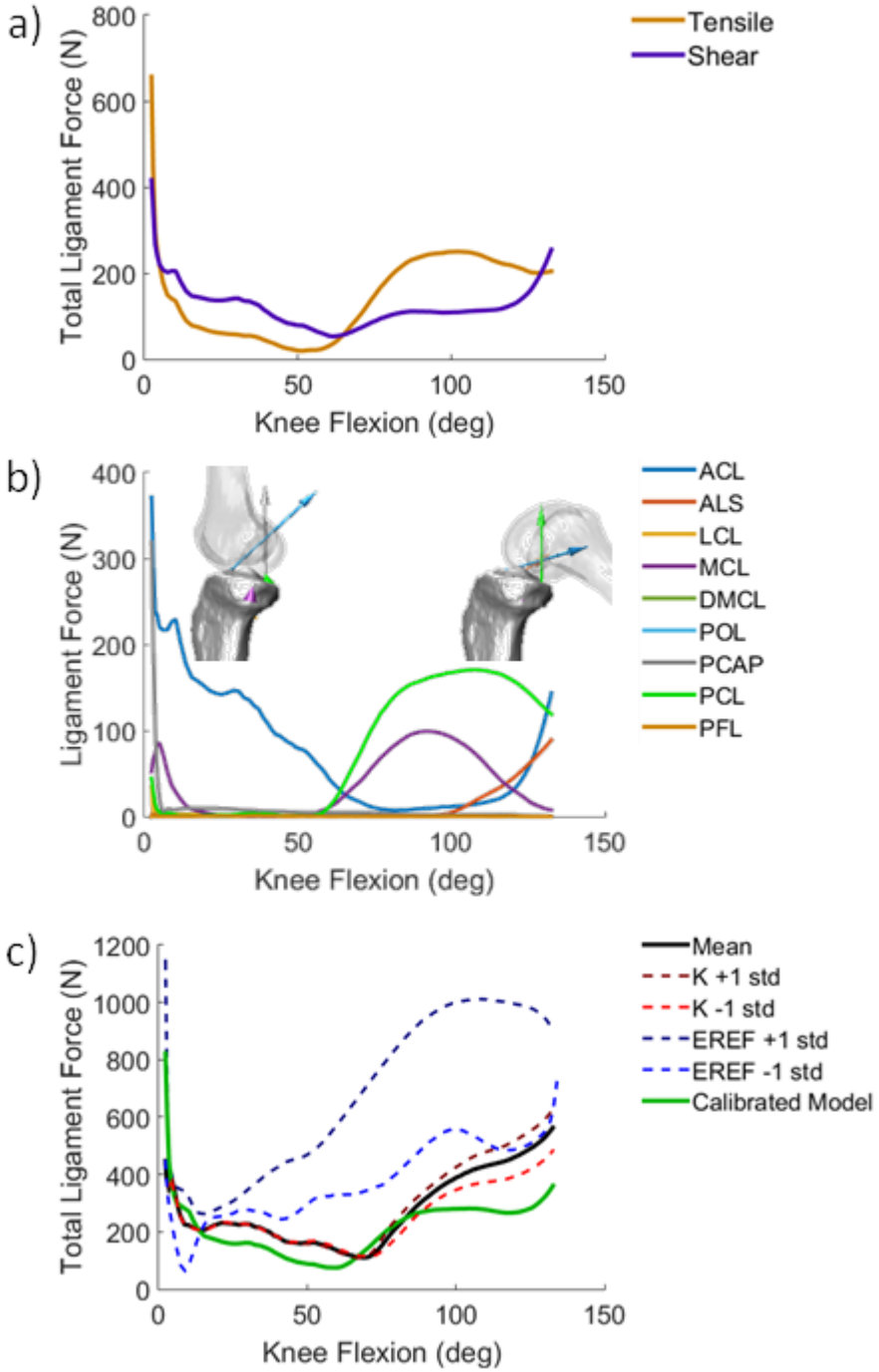

Figure 6.5 a) Total tensile and shear ligament forces, b) individual ligament forces, and c) comparison of total ligament force between calibrated, mean, and standard deviation of ligament stiffness and reference strain analyses during the lunge activity.

CHAPTER 7 – CONCLUSIONS & RECOMMENDATIONS

7.1 Conclusion

The experimental and computational modeling framework, developed in this dissertation, was an effort to expand the current state-of-the-art in modeling knee biomechanics. The main objective was to develop detailed, subject-specific finite element (FE) models of the knee for investigation of healthy, pathological and implanted knee conditions. In-vitro tests were performed to characterize soft tissue constraint in the tibiofemoral (TF) and patellofemoral (PF) joints, and to evaluate knee function following cruciate injury. Additionally, in-vitro experiments supported the development of subject-specific FE representations for prediction of joint mechanics. The final chapters (5 and 6) of the dissertation transitioned FE representations developed from modeling of in-vitro experiments into in-vivo evaluations of healthy and implanted subjects. A computational modeling framework was developed that integrated state-of-the-art, in-vivo kinematic measurement, musculoskeletal modeling, and FE modeling for comparison of implant performance between two patellar designs (anatomic and dome). And finally, the in-vivo modeling workflow was expanded through development of load-controlled, subject-specific simulations of TF and PF mechanics in a healthy subject.

The clinical significance of these models is multi-fold: 1) investigate dynamic knee function across pathologies such as osteoarthritis, cruciate injury, and PF pain, 2) explore the impact of patient variability on knee mechanics to better diagnose and support patients more susceptible to injury or surgical revision, and 3) perform design iterations to optimize implant performance.

A significant contribution of this research was the extensive model calibrations and validations, which were separately performed for all subjects, activities, experimental tests, and knee conditions. Typically, computational models are extrapolated beyond their intended use, such as using models validated for healthy behavior to predict pathological conditions; the current study made an effort to compare model results to experimental data across varying knee conditions. In Chapters 3 and 4, in-vitro experiment allowed direct measurement of internal joint and soft tissue forces, which facilitated investigations of joint mechanics during dynamic activity and supported the development of computational representations of knee structures. Dynamic simulations of knee flexion and gait activities were repeated following resection of the cruciate ligaments, which isolated their contribution to joint constraint and knee function. Computational models reproduced experimental motion for healthy and cruciate-deficient conditions, providing confidence in predictions of contact and ligament mechanics. Typically, models are validated under healthy conditions, but the research presented in this dissertation advanced the standard for validation of predictive computational models by comparing model outputs to experimental knee kinematics for healthy and cruciate-

deficient conditions. Additionally, in Chapter 5, in-vivo simulations of healthy and implanted subjects were calibrated to experimental radiographic measurement for all subjects and activities. Through comprehensive comparisons to all available experimental measures, researchers and modelers can eliminate skepticism surrounding computational models and provide confidence to clinicians that models can be used as pre-clinical tools for diagnosis and evaluation of patient care (Oreskes et al., 1994). For simulation of all subjects, activities (e.g. knee extension, lunge, gait), experimental tests (e.g. MLR, laxity tests, KKS), and knee conditions (e.g. healthy, ACL-deficient, PCL-deficient, implanted), model loading and boundary conditions were altered, which required separate calibration and/or validation to experimental data. Care must be taken when extrapolating model outputs/capability to exploring new research questions. For example, can a validated model of a healthy subject be used to predict implanted knee mechanics following virtual implantation? Virtually implanting a natural knee model may be interesting for evaluating how well the implant restores natural function, but description of model outputs should be tempered as the resulting simulation may not represent implanted knee motion (possible changes in motion associated with compensation strategies).

A consistent theme throughout the dissertation was the significant variability in subject-specific knee mechanics. In Chapter 3, cadaveric specimens were subjected to a deep knee bend in the muscle loaded rig (MLR) to quantify the impact of cruciate-deficiency on PF mechanics. Cruciate resections demonstrated altered joint mechanics

through either increased patellar tendon loads or PF contact forces. Even in a sample size of 3 specimens, the distribution of patellar loading was highly variable with a specimen carrying nearly twice the ratio of load in the patellar tendon or PF contact force as another specimen. Similarly, in Chapter 5, in-vivo PF mechanics were evaluated for 20 implanted knees (10 anatomic and 10 dome patellar components), and the ratio of PF contact force to quadriceps force was influenced by patient factors such as bone and soft tissue alignment, and subject-specific TF kinematics, in addition to surgical factors such as implant sizing, alignment, and geometry. In Chapter 4, computational modeling of passive laxity tests allowed optimization of TF soft tissue properties. During dynamic simulation of gait in the Kansas Knee Simulator (KKS), ligament and contact mechanics were evaluated for cadaveric specimens in healthy and ACL-deficient conditions. Patterns of ligament recruitment and joint loading were dependent on the attachment sites and reference strain of the soft tissue. For example, relatively small differences in the femoral attachment of the MCL had a significant impact on joint loading. Subject-specific modeling of two cadaver specimens demonstrated contrasting patterns of ligament recruitment and joint loading in mid-to-deep flexion. Subject-specific calibration of soft tissue properties and alignment were important in distinguishing patient differences in joint mechanics. To further explore how patient variability can affect knee function, Chapter 6 quantified the influence of ligament stiffness and reference strain on TF kinematics, contact forces, and ligament loading in a healthy subject. Knee function was sensitive to soft tissue properties and alignment. Quantifying subject-specific behavior is the first step towards characterizing variability in knee

function across the population, which is important for developing successful surgical and rehabilitation treatments. For example, characterizing subject-specific ligament function could better inform implant placement and ligament balancing pre-operatively.

While subject-specific modeling distinguished important differences in knee function across specimens and patient cohorts, load-bearing activity also highlighted differences in knee kinematics and joint loading. In Chapter 5, PF mechanics were evaluated for patients with anatomic and dome patellar designs during weight-bearing (lunge) and non-weight-bearing (knee extension) activity. Weight-bearing activity highlighted differences in kinematics between the two patellar designs, and consequently demonstrated improved quadriceps function in the anatomic subjects. Similarly, when modeling a healthy subject, perturbations of ligament properties were shown to have a greater effect on TF kinematics and contact mechanics during the lunge activity.

7.2 Recommendations

The research presented in this dissertation advanced FE modeling of the knee using subject-specific representations calibrated and validated across healthy, pathological, and implanted knee conditions, however there will always be opportunities to improve the detail and complexity of models for more accurate predictions of knee function.

For example, a main limitation of the experimental testing, performed in Chapter 4, was the lack of sufficient joint loads in passive laxity tests. As a result, knee laxity evaluations presented insignificant differences in kinematics following resection of the meniscus, and the contribution of ligament structures to joint stiffness may have been overestimated (Shoemaker and Markolf, 1986). Future evaluations of knee laxity should consider load-bearing tests to support more realistic analysis of ligament and meniscus function. In comparative evaluations of knee pathology or implant design, weight-bearing activities should be considered to highlight subtle differences in knee mechanics.

Additionally, knee laxity experiments described in this dissertation were performed across multiple flexion angles (0-60°), multiple tests (I-E, V-V, A-P), and multiple resection levels (healthy, ACL-deficient), but further research is required to understand soft tissue mechanics during deep flexion. Given the increasing demand for improved knee function during high-demand tasks such as squatting and kneeling, researchers and implant manufacturers are interested in developing total knee replacement designs that support deep flexion activities. While previous studies have quantified joint and ligament forces at high flexion angles (Li et al., 2004b; Nagura et al., 2006; Sharma et al., 2008), the variability in ligament properties and function across the population is not well understood. Similar to the methodology presented in Chapter 4, in-vitro experiments can be performed to quantify passive constraint in knee flexion angles greater than 60°. However, it is important to include physiological joint forces during evaluation of joint laxity; compressive loads derived from previous experiment (eg.

TekScan sensors, Orthoload database) and/or modeling could be applied in future laxity experiments. Weight-bearing, knee laxity experiment and modeling at higher flexion angles (>60°) could improve our understanding of passive constraint in deep flexion. Developing computational models of deep knee flexion activities, such as squatting and kneeling, becomes increasingly complex due to modeling of contact interactions between the thigh and calf, and the passive components of the musculature. As a result, it is important to incorporate measurements of soft tissue contact and strain during the experimental setup.

Evaluations of soft tissue function and the development of their corresponding computational representations can be supported through experimental measurement of ligament strains. For example, pressure transducers can be embedded in the ligament fibers to quantify ligament strain and forces (Cyr et al., 2015; Fleming and Beynnon, 2004). While the accuracy and repeatability of these measurements are limited, transducer outputs can be useful for identifying when ligaments are active and inactive; these data can be useful in calibrating ligament slack length, which has been shown, in this dissertation, to have a significant impact on joint mechanics.

A second experimental technique for quantifying ligament strains involves experimental measurements using a digital image correlation (DIC) camera system. This technique is recommended for measurement of surface ligament strains due to the recent acquisition of this technology at the University of Denver. The DIC camera system,

complemented by GOM© software, is capable of recording high-precision, 3D measurements of coordinates, displacements, and surface strains with sub-micrometer resolution (http://www.gom.com/metrology-systems/aramis.html). DIC measurements can be recorded simultaneously with traditional motion capture methods (eg. Optotrak) to quantify ligament strains during passive laxity experiments and/or dynamic activities. The DIC system is limited to structures that are easily accessible/visible on the exterior surface of the cadaver knee, but controlled in-vitro experiments can be performed to sequentially resect and remove components of the knee to allow greater visibility of the underlying soft tissue. Initially, measurement of MCL and LCL strains could be a significant addition to our understanding of ligament recruitment and the balance of joint loading in the medial and lateral compartments of the knee. Additional sectioning of the knee could involve cutting away the medial half of the femur to expose the internal ACL and PCL structures. Through consistent, kinematically-driven loads, the strain in ACL and PCL ligaments could be evaluated under physiological or clinically relevant loading.

As described in Chapters 5 and 6, robust evaluations of in-vitro knee laxity can be used to support computational models of in-vivo motion. However, models of in-vivo motion require some assumptions on ligament properties and alignment since detailed information regarding internal joint forces and ligament properties is currently impractical to obtain non-invasively.

In-vivo simulations of knee joint motion could be strengthened through FE-based muscle control, and/or the development of motor-actuated or guided in-vivo experiments. Even in non-weight bearing tasks such as knee extension, quadriceps and hamstrings muscles are significant contributors to the total shear and compressive forces at the knee. As a result, quantifying passive constraint in-vivo becomes challenging. Motor-actuated movement or guided in-vivo experiments could be used to enforce passive motion using knee dynamometers (van der Esch et al., 2006), but the range of laxity loads and the accuracy of the force outputs can be limited. Patients could be instructed to relax their muscles and allow a device to flex/extend their knee while the experimentalist recorded stereo radiographic measurement and external loading from the device. A mechanically-guided experiment could be used to enforce knee motion, and isolate passive constraint in the knee. The challenges with guided in-vivo experiments are: 1) development of a device to guide knee motion with accurate measurement of external forces can be expensive and time-consuming, 2) range of motion must be limited to ensure patients are not harmed (eg. 15-90° knee flexion), 3) training patients to relax their muscles throughout the experiment may not be reliable. While performing activities with minimal muscle function is helpful for isolating the passive components in the knee, quantifying muscle forces remains critical for reproducing in-vivo knee mechanics. Musculoskeletal modeling has provided an effective solution for solving indeterminate systems and, through static optimizations, is capable of reasonably estimating muscle forces, but these models generally lack the necessary level of detail and complexity at the joint to distinguish important patient-specific characteristics.

While research in this dissertation was focused on developing subject-specific soft tissue representations in the knee (such as cruciates, collaterals, meniscus, etc.), implementing simultaneous muscle force prediction within the FE framework can greatly improve evaluations of joint mechanics. A single computational framework for estimation of muscle forces and evaluation of joint mechanics would improve the continuity of model inputs and outputs. In Chapter 6, FE simulations of knee extension and lunge in a healthy subject applied PID-controlled quadriceps forces to match experimental knee flexion. PID-control is useful for estimating muscle forces that are directly influencing a known kinematic degree of freedom (DOF), but the control system can become complex for bi-articulate muscles or muscles that are designed to control multiple DOF. In these indeterminate systems, advanced muscle optimizations are required in the FE framework such as solving for muscle activations by minimizing metabolic energy. Combining advanced muscle control with calibration of subject-specific behavior described in this dissertation could improve the realism and fidelity of FE models for more accurate prediction of joint mechanics.

Future work could expand the existing suite of computational tools by developing subject-specific in-vivo models of pathological and implanted cohorts. In Chapter 6, a load-controlled, subject-specific model of in-vivo motion was developed for a healthy subject. In-vivo evaluations of the healthy subject included calibration of ligament attachments and properties during passive (knee extension) and weight-bearing (lunge) activity. The development of this model was possible through collection of in-vivo

kinematic measurement and subject-specific musculoskeletal modeling. This process could be repeated for patients experiencing osteoarthritis or maltracking/malalignment. Detailed, subject-specific models of pathological cohorts could improve our understanding of changes in knee mechanics associated with injury. Also, in-vivo modeling of pathological behavior could help to identify coping mechanisms that may be adversely affecting long-term health. Similarly, models could be developed for total knee replacement patients with various implant design and surgical alignment features such as rotating platform vs. fixed bearing trays, mechanical- vs. anatomically-aligned implants, and posterior-stabilized vs. cruciate-retaining components. Specific models, capturing the unique behavior of pathologies, implant design characteristics, and surgical techniques, could be useful for comparative evaluations of joint function, and to eventually characterize variation in knee mechanics across the population.

7.3 Closing

Detailed, subject-specific FE models of healthy, pathological, and implanted knee conditions, developed in this dissertation, represent a broad set of computational tools for investigation of knee biomechanics. The current work combined in-vitro experiment and modeling to compare changes in joint loading and function between healthy and cruciate-deficient conditions. These models have been validated under healthy and pathological conditions, and can be used to investigate soft tissue injury and repair. In-vitro experiments also supported the development of subject-specific FE representations of TF

and PF soft tissue, which were then incorporated into FE modeling of healthy and implanted subjects in-vivo. A sequential modeling approach was developed to integrate in-vivo stereo radiographic measurement, musculoskeletal modeling and FE modeling for subject-specific evaluation of in-vivo knee mechanics. This computational framework was used to compare the performance of two patellar implant designs, and quantify the impact of cruciate ligament variability on joint kinematics and loading. The computational tools developed in this research advance our understanding of knee function and injury, and provide a strong platform to address biomechanical concerns surrounding rehabilitation and surgical treatment.

LIST OF REFERENCES

Abo-Alhol, T.R., Fitzpatrick, C.K., Clary, C.W., Cyr, A.J., Maletsky, L.P., Laz, P.J., Rullkoetter, P.J., 2014. Patellar mechanics during simulated kneeling in the natural and implanted knee. J Biomech 47, 1045-1051.

Ackerman, M.J., 1991. The Visible Human Project. The Journal of biocommunication 18, 14.

Adouni, M., Shirazi-Adl, A., Shirazi, R., 2012. Computational biodynamics of human knee joint in gait: from muscle forces to cartilage stresses. J Biomech 45, 2149-2156.

Ahmad, C.S., Kwak, S.D., Ateshian, G.A., Warden, W.H., Steadman, J.R., Mow, V.C., 1998. Effects of patellar tendon adhesion to the anterior tibia on knee mechanics. American journal sports medicine 26, 715-724.

Ahmed, A.M., Burke, D.L., Hyder, A., 1987. Force analysis of the patellar mechanism. Journal of orthopaedic research 5, 69-85.

Ali, A.A., Shalhoub, S.S., Cyr, A.J., Fitzpatrick, C.K., Maletsky, L.P., Rullkoetter, P.J., Shelburne, K.B., 2016. Validation of predicted patellofemoral mechanics in a finite element model of the healthy and cruciate-deficient knee. Journal of biomechanics 49, 302-309.

Allen, C.R., Wong, E.K., Livesay, G.A., Sakane, M., Fu, F.H., Woo, S.L., 2000. Importance of the medial meniscus in the anterior cruciate ligament-deficient knee. J Orthop Res 18, 109-115.

Amis, A.A., Farahmand, F., 1996. Recent advances in surgery pf the patello-femoral joint and extensor appartus'. The Knee 3, 73-105.

Amis, A.A., Senavongse, W., Bull, A.M.J., 2006. Patellofemoral Kinematics during Knee Flexion-Extension : An In Vitro Study. Journal of orthopaedic research, 2201-2211.

Arendt, E., Dick, R., 1995. Knee injury patterns among men and women in collegiate basketball and soccer. NCAA data and review of literature. Am J Sports Med 23, 694-701.

Baldwin, M.A., Clary, C., Maletsky, L.P., Rullkoetter, P.J., 2009. Verification of predicted specimen-specific natural and implanted patellofemoral kinematics during simulated deep knee bend. Journal of biomechanics 42, 2341-2348.

Baldwin, M.A., Clary, C.W., Fitzpatrick, C.K., Deacy, J.S., Maletsky, L.P., Rullkoetter, P.J., 2012. Dynamic finite element knee simulation for evaluation of knee replacement mechanics. Journal of biomechanics 45, 474-483.

Baldwin, M.A., Langenderfer, J.E., Rullkoetter, P.J., Laz, P.J., 2010. Development of subject-specific and statistical shape models of the knee using an efficient segmentation and mesh-morphing approach. Computer methods and programs in biomedicine 97, 232-240.

Banks, S.A., Hodge, W.A., 1996. Accurate measurement of three-dimensional knee replacement kinematics using single-plane fluoroscopy. IEEE Trans Biomed Eng 43, 638-649.

Barrack, R.L., Skinner, H.B., Buckley, S.L., 1989. Proprioception in the anterior cruciate deficient knee. Am J Sports Med 17, 1-6.

Barry, M.J., Kwon, T.H., Dhaher, Y.Y., 2010. Probabilistic Musculoskeletal Modeling of the Knee: A Preliminary Examination of an ACL-Reconstruction, 32nd Annual International Conference of the IEEE EMBS, Buenos Aires, Argentina, pp. 5440-5443.

Beillas, P., Papaioannou, G., Tashman, S., Yang, K.H., 2004. A new method to investigate in vivo knee behavior using a finite element model of the lower limb. Journal of biomechanics 37, 1019-1030.

Bendjaballah, M.Z., Shirazi-Adl, A., Zukor, D.J., 1995. Biomechanics of the human joint in compression: reconstruction, mesh generation and finite element analysis. The Knee 2, 69-79.

Bergmann, G., Bender, A., Graichen, F., Dymke, J., Rohlmann, A., Trepczynski, A., Heller, M.O., Kutzner, I., 2014. Standardized loads acting in knee implants. PloS one 9, e86035.

Bergmann, G., Graichen, F., Rohlmann, A., 1993. Hip joint loading during walking and running, measured in two patients. J Biomech 26, 969-990.

Besier, T.F., Draper, C.E., Gold, G.E., Beaupre, G.S., Delp, S.L., Division, B.E., 2005. Patellofemoral joint contact area increases with knee flexion and weight-bearing. Journal of orthopaedic research 23, 345-350.

Beynnon, B.D., Johnson, R.J., Abate, J.A., Fleming, B.C., Nichols, C.E., 2005. Treatment of anterior cruciate ligament injuries, part I. American journal sports medicine 33, 1579-1602.

Blankevoort, L., Huiskes, R., 1996. Validation of a three-dimensional model of the knee. Journal of biomechanics 29, 955-961.

Borotikar, B.S., Sheehan, F.T., 2013. In vivo patellofemoral contact mechanics during active extension using a novel dynamic MRI-based methodology. Osteoarthritis and cartilage / OARS, Osteoarthritis Research Society 21, 1886-1894.

Boynton, M.D., Tietjens, B.R., 1996. Long-term followup of the untreated isolated posterior cruciate ligament-deficient knee. Am J Sports Med 24, 306-310.

Browne, C., Hermida, J.C., Bergula, A., Colwell, C.W., Jr., D'Lima, D.D., 2005. Patellofemoral forces after total knee arthroplasty: effect of extensor moment arm. The Knee 12, 81-88.

Buff, H.U., Jones, L.C., Hungerford, D.S., 1988. Experimental determination of forces transmitted through the patello-femoral joint. Journal of biomechanics 21, 17-23.

Carpenter, R.D., Brilhault, J., Majumdar, S., Ries, M.D., 2009. Magnetic resonance imaging of in vivo patellofemoral kinematics after total knee arthroplasty. The Knee 16, 332-336.

Churchill, D.L., Incavo, S.J., Johnson, C.C., Beynnon, B.D., 2001. The influence of femoral rollback on patellofemoral contact loads in total knee arthroplasty. J Arthroplasty 16, 909-918.

Clary, C.W., Fitzpatrick, C.K., Maletsky, L.P., Rullkoetter, P.J., 2013. The influence of total knee arthroplasty geometry on mid-flexion stability: an experimental and finite element study. Journal of biomechanics 46, 1351-1357.

Cohen, Z.A., Henry, J.H., McCarthy, D.M., Mow, V.C., Ateshian, G.A., 2003a. Computer simulations of patellofemoral joint surgery. Patient-specific models for tuberosity transfer. American journal of sports medicine 31, 87-98.

Cohen, Z.A., Mow, V.C., Henry, J.H., Levine, W.N., Ateshian, G.A., 2003b. Templates of the cartilage layers of the patellofemoral joint and their use in the assessment of

osteoarthritic cartilage damage. Osteoarthritis and cartilage / OARS, Osteoarthritis Research Society 11, 569-579.

Cyr, A.J., Shalhoub, S.S., Fitzwater, F.G., Ferris, L.A., Maletsky, L.P., 2015. Mapping of contributions from collateral ligaments to overall knee joint constraint: an experimental cadaveric study. J Biomech Eng 137, 061006.

D'Lima, D.D., Poole, C., Chadha, H., Hermida, J.C., Mahar, A., Colwell, C.W., Jr., 2001. Quadriceps moment arm and quadriceps forces after total knee arthroplasty. Clin Orthop Relat Res, 213-220.

Delp, S.L., Anderson, F.C., Arnold, A.S., Loan, P., Habib, A., John, C.T., Guendelman, E., Thelen, D.G., 2007. OpenSim: open-source software to create and analyze dynamic simulations of movement. IEEE transactions on bio-medical engineering 54, 1940-1950.

Delp, S.L., Arnold, A.S., Piazza, S.J., 1998. Graphics-based modeling and analysis of gait abnormalities. Bio-Med Mater Eng 8, 227-240.

Dennis, D.A., Komistek, R.D., Mahfouz, M.R., 2003. In vivo fluoroscopic analysis of fixed-bearing total knee replacements. Clin Orthop Relat Res, 114-130.

DesJardins, J.D., Walker, P.S., Haider, H., Perry, J., 2000. The use of a force-controlled dynamic knee simulator to quantify the mechanical performance of total knee replacement designs during functional activity. J Biomech 33, 1231-1242.

Devita, P., Hortobagyi, T., Barrier, J., Torry, M., Glover, K.L., Speroni, D.L., Money, J., Mahar, M.T., 1997. Gait adaptations before and after anterior cruciate ligament reconstruction surgery. Medical science sports exercise 29, 853-859.

Dhaher, Y.Y., Kwon, T.H., Barry, M., 2010. The effect of connective tissue material uncertainties on knee joint mechanics under isolated loading conditions. Journal of biomechanics 43, 3118-3125.

Draganich, L.F., Vahey, J.W., 1990. An in vitro study of anterior cruciate ligament strain induced by quadriceps and hamstrings forces. J Orthop Res 8, 57-63.

Elias, J.J., Wilson, D.R., Adamson, R., Cosgarea, A.J., 2004. Evaluation of a computational model used to predict the patellofemoral contact pressure distribution. Journal of biomechanics 37, 295-302.

Englund, M., Guermazi, A., Lohmander, L.S., 2009. The Meniscus in Knee Osteoarthritis. Rheum Dis Clin N Am 35, 579-+.

Erdemir, A., 2016. Open Knee: Open Source Modeling and Simulation in Knee Biomechanics. Journal of Knee Surgery 29, 107-116.

Fernandez, J.W., Akbarshahi, M., Kim, H.J., Pandy, M.G., 2008. Integrating modelling, motion capture and x-ray fluoroscopy to investigate patellofemoral function during dynamic activity. Computer methods biomechanical biomedical engineering 11, 41-53.

Fitzpatrick, C.K., Baldwin, M.A., Ali, A.A., Laz, P.J., Rullkoetter, P.J., 2011. Comparison of patellar bone strain in the natural and implanted knee during simulated deep flexion. J Orthop Res 29, 232-239.

Fitzpatrick, C.K., Baldwin, M.A., Clary, C.W., Maletsky, L.P., Rullkoetter, P.J., 2014. Evaluating knee replacement mechanics during ADL with PID-controlled dynamic finite element analysis. Computer methods in biomechanics and biomedical engineering 17, 360-369.

Fitzpatrick, C.K., Baldwin, M.A., Rullkoetter, P.J., 2010. Computationally efficient finite element evaluation of natural patellofemoral mechanics. Journal of biomechanical engineering 132, 121013.

Fitzpatrick, C.K., Clary, C.W., Laz, P.J., Rullkoetter, P.J., 2012a. Relative contributions of design, alignment, and loading variability in knee replacement mechanics. Journal of Orthopaedic Research 30, 2015-2024.

Fitzpatrick, C.K., Clary, C.W., Rullkoetter, P.J., 2012b. The role of patient, surgical, and implant design variation in total knee replacement performance. Journal of biomechanics 45, 2092-2102.

Fitzpatrick, C.K., Steensen, R.N., Tumuluri, A., Trinh, T., Bentley, J., Rullkoetter, P.J., 2016. Computational analysis of factors contributing to patellar dislocation. J Orthop Res 34, 444-453.

Fleming, B.C., Beynnon, B.D., 2004. In vivo measurement of ligament/tendon strains and forces: a review. Ann Biomed Eng 32, 318-328.

Fregly, B.J., Bei, Y., Sylvester, M.E., 2003. Experimental evaluation of an elastic foundation model to predict contact pressures in knee replacements. J Biomech 36, 1659-1668.

Fulkerson, J.P., 2002. Current Concepts Diagnosis and Treatment of Patients with Patellofemoral Pain. American journal of sports medicine 30, 447-456.

Fulkerson, J.P., Shea, K.P., 1990. Disorders of patellofemoral alignment. Journal of bone and joint surgery. American volume 72, 1424-1429.

Gabriel, M.T., Wong, E.K., Woo, S.L., Yagi, M., Debski, R.E., 2004. Distribution of in situ forces in the anterior cruciate ligament in response to rotatory loads. Journal of orthopaedic research 22, 85-89.

Gardiner, J.C., Weiss, J.A., 2003. Subject-specific finite element analysis of the human medial collateral ligament during valgus knee loading. Journal of orthopaedic research 21, 1098-1106.

Gardiner, J.C., Weiss, J.A., Rosenberg, T.D., 2001. Strain in the human medial collateral ligament during valgus loading of the knee. Clinical orthopaedics and related research, 266-274.

Georgoulis, A.D., Pappa, L., Moebius, U., Malamou-Mitsi, V., Pappa, S., Papageorgiou, C.O., Agnantis, N.J., Soucacos, P.N., 2001. The presence of proprioceptive mechanoreceptors in the remnants of the ruptured ACL as a possible source of re-innervation of the ACL autograft. Knee Surg Sports Traumatol Arthrosc 9, 364-368.

Gianotti, S.M., Marshall, S.W., Hume, P.A., Bunt, L., 2009. Incidence of anterior cruciate ligament injury and other knee ligament injuries: a national population-based study. Journal of science and medicine in sport 12, 622-627.

Girgis, F.G., Marshall, J.L., Monajem, A., 1975. The cruciate ligaments of the knee joint. Anatomical, functional and experimental analysis. Clinical orthopaedics and related research, 216-231.

Godest, A.C., de Cloke, C.S., Taylor, M., Gregson, P.J., Keane, A.J., Sathasivan, S., Walker, P.S., 2000. A computational model for the prediction of total knee replacement kinematics in the sagittal plane. Journal of biomechanics 33, 435-442.

Green, G.V., Berend, K.R., Berend, M.E., Glisson, R.R., Vail, T.P., 2002. The effects of varus tibial alignment on proximal tibial surface strain in total knee arthroplasty - The posteromedial hot spot. Journal of Arthroplasty 17, 1033-1039.

Grood, E.S., Suntay, W.J., 1983. A Joint Coordinate System of the Clinical Description of Three-Dimensional Motions: Application to the Knee. Journal of biomechanical engineering 105, 136-144.

Grood, E.S., Suntay, W.J., Noyes, F.R., Butler, D.L., 1984. Biomechanics of the knee-extension exercise . Effect of cutting the anterior cruciate ligament of the Knee-Extension. Journal of bone and joint surgery, 725-734.

Guess, T.M., Stylianou, A., 2012. Simulation of anterior cruciate ligament deficiency in a musculoskeletal model with anatomical knees. The open biomedical engineering journal 6, 23-32.

Guess, T.M., Thiagarajan, G., Kia, M., Mishra, M., 2010. A subject specific multibody model of the knee with menisci. Medical engineering & physics 32, 505-515.

Halloran, J.P., Clary, C.W., Maletsky, L.P., Taylor, M., Petrella, A.J., Rullkoetter, P.J., 2010. Verification of predicted knee replacement kinematics during simulated gait in the Kansas knee simulator. Journal of biomechanical engineering 132, 081010.

Halloran, J.P., Petrella, A.J., Rullkoetter, P.J., 2005. Explicit finite element modeling of total knee replacement mechanics. Journal of biomechanics 38, 323-331.

Halonen, K.S., Mononen, M.E., Jurvelin, J.S., Toyras, J., Klodowski, A., Kulmala, J.P., Korhonen, R., Year Importance of Patella, Quadriceps Forces and Depth-Wise Cartilage Structure on Knee Joint Motion and Cartilage Response During Patient-Specific Gait Cycle. In Conference Proceedings at Orthopaedic Research Society. Las Vegas, NV.

Halonen, K.S., Mononen, M.E., Jurvelin, J.S., Toyras, J., Korhonen, R.K., 2013. Importance of depth-wise distribution of collagen and proteoglycans in articular cartilage--a 3D finite element study of stresses and strains in human knee joint. J Biomech 46, 1184-1192.

Halonen, K.S., Mononen, M.E., Toyras, J., Kroger, H., Joukainen, A., Korhonen, R.K., 2016. Optimal graft stiffness and pre-strain restore normal joint motion and cartilage responses in ACL reconstructed knee. J Biomech 49, 2566-2576.

Han, S.-K., Federico, S., Epstein, M., Herzog, W., 2005. An articular cartilage contact model based on real surface geometry. Journal of biomechanics 38, 179-184.

Harris, M.D., Cyr, A.J., Ali, A.A., Shelburne, K.B., 2016. A Combined Experimental and Computational Approach to Subject-Specific Analysis of Knee Joint Laxity. American Society of Mechanical Engineers.

Hauch, K.N., Oyen, M.L., Odegard, G.M., Donahue, T.L.H., 2009. Nanoindentation of the insertional zones of human meniscal attachments into underlying bone. J Mech Behav Biomed 2, 339-347.

Heegard, J., Leyvraz, P.F., Curnier, A., Rakotomanana, L., Huiskes, R., 1995. The biomechanics of the human patella during passive knee flexion. Journal of biomechanics 28, 1265-1279.

Huberti, H.H., Hayes, W.C., 1984. Patellofemoral contact pressures. The influence of q-angle and tendofemoral contact. The Journal of bone and joint surgery. American volume 66, 715-724.

Huberti, H.H., Hayes, W.C., Stone, J.L., Shybut, G.T., 1984. Force ratios in the quadriceps tendon and ligamentum patellae. Journal of orthopaedic research 2, 49-54.

Ivester, J.C., Cyr, A.J., Harris, M.D., Kulis, M.J., Rullkoetter, P.J., Shelburne, K.B., 2015. A Reconfigurable High-Speed Stereo-Radiography System for Sub-Millimeter Measurement of In Vivo Joint Kinematics. J Med Devices 9.

Katchburian, M.V., Bull, A.M.J., Shih, Y.-F., Heatley, F.W., Amis, A.A., 2003. Measurement of patellar tracking: assessment and analysis of the literature. Clinical orthopaedics and related research, 241-259.

Kefala, V., Ali, A.A., Mannen, E.M., Shelburne, K.B., 2017. Patellofemoral kinematics of older adults during activities of daily living. Medical Engineering & Physics *in review*.

Kellis, E., Baltzopoulos, V., 1999. In vivo determination of the patella tendon and hamstrings moment arms in adult males using videofluoroscopy during submaximal knee extension and flexion. Clinical biomechanics 14, 118-124.

Kiapour, A., Kiapour, A.M., Kaul, V., Quatman, C.E., Wordeman, S.C., Hewett, T.E., Demetropoulos, C.K., Goel, V.K., 2014. Finite element model of the knee for investigation of injury mechanisms: development and validation. Journal of biomechanical engineering 136, 011002.

Komistek, R.D., Dennis, D.A., Mabe, J.A., Walker, S.A., 2000. An in vivo determination of patellofemoral contact positions. Clinical biomechanics 15, 29-36.

Komistek, R.D., Kane, T.R., Mahfouz, M., Ochoa, J.A., Dennis, D.A., 2005. Knee mechanics: a review of past and present techniques to determine in vivo loads. J Biomech 38, 215-228.

Krevolin, J.L., Pandy, M.G., Pearce, J.C., 2004. Moment arm of the patellar tendon in the human knee. Journal of biomechanics 37, 785-788.

Kurtz, S., Mowat, F., Ong, K., Chan, N., Lau, E., Halpern, M., 2005. Prevalence of primary and revision total hip and knee arthroplasty in the United States from 1990 through 2002. The Journal of bone and joint surgery. American volume 87, 1487-1497.

Kurtz, S., Ong, K., Lau, E., Mowat, F., Halpern, M., 2007. Projections of primary and revision hip and knee arthroplasty in the United States from 2005 to 2030. The Journal of bone and joint surgery. American volume 89, 780-785.

Kwak, S.D., Ahmad, C.S., Gardner, T.R., Grelsamer, R.P., Henry, J.H., Blankevoort, L., Ateshian, G.A., Mow, V.C., 2000. Hamstrings and iliotibial band forces affect knee kinematics and contact pattern. Journal of orthopaedic research 18, 101-108.

Lee, T.Q., Gerken, A.P., Glaser, F.E., Kim, W.C., Anzel, S.H., 1997. Patellofemoral joint kinematics and contact pressures in total knee arthroplasty. Clin Orthop Relat Res, 257-266.

Levy, I.M., Torzilli, P.A., Warren, R.F., 1982. The effect of medial meniscectomy on anterior-posterior motion of the knee. The Journal of bone and joint surgery. American volume 64, 883-888.

Li, G., DeFrate, L.E., Zayontz, S., Park, S.E., Gill, T.J., 2004a. The effect of tibiofemoral joint kinematics on patellofemoral contact pressures under simulated muscle loads. Journal of orthopaedic research 22, 801-806.

Li, G., Gill, T.J., DeFrate, L.E., Zayontz, S., Glatt, V., Zarins, B., 2002a. Biomechanical consequences of PCL deficiency in the knee under simulated muscle loads--an in vitro experimental study. Journal of orthopaedic research 20, 887-892.

Li, G., Suggs, J., Gill, T., 2002b. The effect of anterior cruciate ligament injury on knee joint function under a simulated muscle load: a three-dimensional computational simulation. Annals of biomedical engineering 30, 713-720.

Li, G., Zayontz, S., Most, E., DeFrate, L.E., Suggs, J.F., Rubash, H.E., 2004b. In situ forces of the anterior and posterior cruciate ligaments in high knee flexion: an in vitro investigation. J Orthop Res 22, 293-297.

Limbert, G., Taylor, M., Middleton, J., 2004. Three-dimensional finite element modelling of the human ACL: simulation of passive knee flexion with a stressed and stress-free ACL. Journal of Biomechanics 37, 1723-1731.

Lloyd, D.G., Besier, T.F., 2003. An EMG-driven musculoskeletal model to estimate muscle forces and knee joint moments in vivo. J Biomech 36, 765-776.

Lohmander, L.S., Englund, P.M., Dahl, L.L., Roos, E.M., 2007. The long-term consequence of anterior cruciate ligament and meniscus injuries: osteoarthritis. American Journal of Sports Medicine 35, 1756-1769.

Mahfouz, M., Abdel Fatah, E.E., Bowers, L.S., Scuderi, G., 2012. Three-dimensional morphology of the knee reveals ethnic differences. Clin Orthop Relat Res 470, 172-185.

Maletsky, L.P., Hillberry, B.M., 2005. Simulating dynamic activities using a five-axis knee simulator. Journal of biomechanical engineering 127, 123-133.

Maletsky, L.P., Sun, J., Morton, N.A., 2007. Accuracy of an optical active-marker system to track the relative motion of rigid bodies. Journal of biomechanics 40, 682-685.

Mannen, E.M., Ali, A.A., D.A., D., Rullkoetter, P.J., Shelburne, K.B., 2017. Patellar design influences knee kinematics of total knee arthroscopy patients in knee extension and lunge. Journal of Biomechanics *in review*.

Markolf, K.L., Gorek, J.F., Kabo, J.M., Shapiro, M.S., 1990. Direct measurement of resultant forces in the anterior cruciate ligament. An in vitro study performed with a new experimental technique. The Journal of bone and joint surgery. American volume 72, 557-567.

Markolf, K.L., Jackson, S.R., McAllister, D.R., 2012. Force measurements in the medial meniscus posterior horn attachment: effects of anterior cruciate ligament removal. Am J Sports Med 40, 332-338.

Markolf, K.L., O'Neill, G., Jackson, S.R., McAllister, D.R., 2004. Effects of applied quadriceps and hamstrings muscle loads on forces in the anterior and posterior cruciate ligaments. Am J Sports Med 32, 1144-1149.

Marra, M.A., Vanheule, V., Fluit, R., Koopman, B.H.F.J.M., Rasmussen, J., Verdonschot, N., Andersen, M.S., 2015. A Subject-Specific Musculoskeletal Modeling Framework to Predict In Vivo Mechanics of Total Knee Arthroplasty. J Biomech Eng-T Asme 137.

Mesfar, W., Shirazi-Adl, A., 2005. Biomechanics of the knee joint in flexion under various quadriceps forces. The Knee 12, 424-434.

Mesfar, W., Shirazi-Adl, A., 2006a. Biomechanics of changes in ACL and PCL material properties or prestrains in flexion under muscle force-implications in ligament reconstruction. Computer methods biomechanical biomedical engineering 9, 201-209.

Mesfar, W., Shirazi-Adl, A., 2006b. Knee joint mechanics under quadriceps--hamstrings muscle forces are influenced by tibial restraint. Clinical biomechanics 21, 841-848.

Miranda, D.L., Rainbow, M.J., Crisco, J.J., Fleming, B.C., 2013. Kinematic differences between optical motion capture and biplanar videoradiography during a jump-cut maneuver. Journal of Biomechanics 46, 567-573.

Mizner, R.L., Petterson, S.C., Stevens, J.E., Vandenborne, K., Snyder-Mackler, L., 2005. Early quadriceps strength loss after total knee arthroplasty. The contributions of muscle atrophy and failure of voluntary muscle activation. The Journal of bone and joint surgery. American volume 87, 1047-1053.

Mizner, R.L., Snyder-Mackler, L., 2005. Altered loading during walking and sit-to-stand is affected by quadriceps weakness after total knee arthroplasty. J Orthop Res 23, 1083-1090.

Mizuno, Y., Kumagai, M., Mattessich, S.M., Elias, J.J., Ramrattan, N., Cosgarea, A.J., Chao, E.Y.S., 2001. Q-angle influences tibiofemoral arid patellofemoral kinematics. Journal of orthopaedic research 19, 834-840.

Moglo, K.E., Shirazi-Adl, A., 2003. Biomechanics of passive knee joint in drawer: load transmission in intact and ACL-deficient joints. The Knee 10, 265-276.

Moissenet, F., Cheze, L., Dumas, R., 2014. A 3D lower limb musculoskeletal model for simultaneous estimation of musculo-tendon, joint contact, ligament and bone forces during gait. J Biomech 47, 50-58.

Moksnes, H., Snyder-Mackler, L., Risberg, M.A., 2008. Individuals with an anterior cruciate ligament-deficient knee classified as noncopers may be candidates for nonsurgical rehabilitation. The Journal of orthopaedic and sports physical therapy 38, 586-595.

Mootanah, R., Imhauser, C.W., Reisse, F., Carpanen, D., Walker, R.W., Koff, M.F., Lenhoff, M.W., Rozbruch, S.R., Fragomen, A.T., Dewan, Z., Kirane, Y.M., Cheah, K., Dowell, J.K., Hillstrom, H.J., 2014. Development and validation of a computational model of the knee joint for the evaluation of surgical treatments for osteoarthritis. Computer methods biomechanical biomedical engineering 17, 1502-1517.

Morris, B.A., D'Lima, D.D., Slamin, J., Kovacevic, N., Arms, S.W., Townsend, C.P., Colwell, C.W., Jr., 2001. e-Knee: evolution of the electronic knee prosthesis. Telemetry technology development. The Journal of bone and joint surgery. American volume 83-A Suppl 2, 62-66.

Nagura, T., Matsumoto, H., Kiriyama, Y., Chaudhari, A., Andriacchi, T.P., 2006. Tibiofemoral joint contact force in deep knee flexion and its consideration in knee osteoarthritis and joint replacement. Journal of applied biomechanics 22, 305-313.

Navacchia, A., Kefala, V., Shelburne, K.B., 2016a. Dependence of Muscle Moment Arms on In Vivo Three-Dimensional Kinematics of the Knee. Ann Biomed Eng.

Navacchia, A., Myers, C.A., Rullkoetter, P.J., Shelburne, K.B., 2016b. Prediction of In Vivo Knee Joint Loads Using a Global Probabilistic Analysis. J Biomech Eng 138, 4032379.

Navacchia, A., Rullkoetter, P.J., Schutz, P., List, R.B., Fitzpatrick, C.K., Shelburne, K.B., 2016c. Subject-specific modeling of muscle force and knee contact in total knee arthroplasty. J Orthop Res 34, 1576-1587.

Nebelung, W., Wuschech, H., 2005. Thirty-five years of follow-up of anterior cruciate ligament-deficient knees in high-level athletes. Arthroscopy 21, 696-702.

Neptune, R.R., Zajac, F.E., Kautz, S.A., 2004. Muscle mechanical work requirements during normal walking: the energetic cost of raising the body's center-of-mass is significant. J Biomech 37, 817-825.

Nguyen, U.S., Zhang, Y., Zhu, Y., Niu, J., Zhang, B., Felson, D.T., 2011. Increasing prevalence of knee pain and symptomatic knee osteoarthritis: survey and cohort data. Annals of internal medicine 155, 725-732.

Nha, K.W., Papannagari, R., Gill, T.J., Van de Velde, S.K., Freiberg, A.a., Rubash, H.E., Li, G., 2008. In vivo patellar tracking: clinical motions and patellofemoral indices. Journal of orthopaedic research 26, 1067-1074.

Noble, P.C., Gordon, M.J., Weiss, J.M., Reddix, R.N., Conditt, M.A., Mathis, K.B., 2005. Does total knee replacement restore normal knee function? Clin Orthop Relat Res, 157-165.

Nomura, E., Horiuchi, Y., Kihara, M., 2000. Medial patellofemoral ligament restraint in lateral patellar translation and reconstruction. The Knee 7, 121-127.

Oreskes, N., Shrader-Frechette, K., Belitz, K., 1994. Verification, validation, and confirmation of numerical models in the Earth sciences. Science 263, 641-646.

Ostermeier, S., Hurschler, C., Stukenborg-Colsman, C., 2004. Quadriceps function after TKA--an in vitro study in a knee kinematic simulator. Clinical biomechanics 19, 270-276.

Pal, S., Besier, T.F., Beaupre, G.S., Fredericson, M., Delp, S.L., Gold, G.E., 2013a. Patellar maltracking is prevalent among patellofemoral pain subjects with patella alta: An upright, weightbearing MRI study. Journal of Orthopaedic Research 31, 448-457.

Pal, S., Besier, T.F., Beaupre, G.S., Fredericson, M., Delp, S.L., Gold, G.E., 2013b. Patellar maltracking is prevalent among patellofemoral pain subjects with patella alta: an upright, weightbearing MRI study. J Orthop Res 31, 448-457.

Pal, S., Besier, T.F., Draper, C.E., Fredericson, M., Gold, G.E., Beaupre, G.S., Delp, S.L., 2012. Patellar tilt correlates with vastus lateralis: vastus medialis activation ratio in maltracking patellofemoral pain patients. J Orthop Res 30, 927-933.

Pal, S., Draper, C.E., Fredericson, M., Gold, G.E., Delp, S.L., Beaupre, G.S., Besier, T.F., 2011. Patellar maltracking correlates with vastus medialis activation delay in patellofemoral pain patients. Am J Sports Med 39, 590-598.

Pandy, M.G., Shelburne, K.B., 1997. Dependence of cruciate-ligament loading on muscle forces and external load. Journal of biomechanics 30, 1015-1024.

Patel, R.R., Hurwitz, D.E., Bush-Joseph, C.A., Bach, B.R., Jr., Andriacchi, T.P., 2003. Comparison of clinical and dynamic knee function in patients with anterior cruciate ligament deficiency. American journal of sports medicine 31, 68-74.

Pena, E., Calvo, B., Martinez, M.A., Doblare, M., 2006. A three-dimensional finite element analysis of the combined behavior of ligaments and menisci in the healthy human knee joint. Journal of biomechanics 39, 1686-1701.

Petrigliano, F.A., Musahl, V., Suero, E.M., Citak, M., Pearle, A.D., 2011. Effect of meniscal loss on knee stability after single-bundle anterior cruciate ligament reconstruction. Knee Surg Sports Traumatol Arthrosc 19 Suppl 1, S86-93.

Piazza, S.J., Delp, S.L., 2001. Three-dimensional dynamic simulation of total knee replacement motion during a step-up task. Journal of biomechanical engineering 123, 599-606.

Post, W.R., Teitge, R., Amis, A., 2002. Patellofemoral malalignment: looking beyond the viewbox. Clinics in sports medicine 21, 521-546, x.

Powers, C.M., 1998. Rehabilitation of patellofemoral joint disorders: a critical review. Journal of orthopaedic and sports physical therapy 28, 345-354.

Powers, C.M., 2003. The influence of altered lower-extremity kinematics on patellofemoral joint dysfunction: a theoretical perspective. Journal of orthopaedic and sports physical therapy 33, 639-646.

Price, A.J., Rees, J.L., Beard, D.J., Gill, R.H.S., Dodd, C.A.F., Murray, D.M., 2004. Sagittal plane kinematics of a mobile-bearing unicompartmental knee arthroplasty at 10 years. Journal of arthroplasty 19, 590-597.

Race, A., Amis, A.A., 1994. The mechanical properties of the two bundles of the human posterior cruciate ligament. J Biomech 27, 13-24.

Rullkoetter, P.J., Fitzpatrick, C.K., Clary, C.W., 2017. How Can We Use Computational Modeling to Improve Total Knee Arthroplasty? Modeling Stability and Mobility in the Implanted Knee. The Journal of the American Academy of Orthopaedic Surgeons 25 Suppl 1, S33-S39.

Rullkoetter, P.J., Fitzpatrick, C.K., Laz, P.J., Year Mechanics of anatomic and dome patellae. In International Congress for Joint Reconstruction. Kona, HI.

Salehghaffari, S., Dhaher, Y.Y., 2014. A model of articular cruciate ligament reconstructive surgery: a validation construct and computational insights. Journal of biomechanics 47, 1609-1617.

Salsich, G.B., Ward, S.R., Terk, M.R., Powers, C.M., 2003. In vivo assessment of patellofemoral joint contact area in individuals who are pain free. Clin Orthop Relat Res, 277-284.

Shalhoub, S., Maletsky, L.P., 2014. Variation in patellofemoral kinematics due to changes in quadriceps loading configuration during in vitro testing. Journal of biomechanics 47, 130-136.

Sharma, A., Leszko, F., Komistek, R.D., Scuderi, G.R., Cates, H.E., Liu, F., 2008. In vivo patellofemoral forces in high flexion total knee arthroplasty. Journal of Biomechanics 41, 642-648.

Shelburne, K.B., Pandy, M.G., 1997a. A musculoskeletal model of the knee for evaluating ligament forces during isometric contractions. Journal of biomechanics 30, 163-176.

Shelburne, K.B., Pandy, M.G., 1997b. A musculoskeletal model of the knee for evaluating ligament forces during isometric contractions. J Biomech 30, 163-176.

Shelburne, K.B., Pandy, M.G., Anderson, F.C., Torry, M.R., 2004a. Pattern of anterior cruciate ligament force in normal walking. Journal of biomechanics 37, 797-805.

Shelburne, K.B., Pandy, M.G., Torry, M.R., 2004b. Comparison of shear forces and ligament loading in the healthy and ACL-deficient knee during gait. J Biomech 37, 313-319.

Shirazi, R., Shirazi-Adl, A., Hurtig, M., 2008. Role of cartilage collagen fibrils networks in knee joint biomechanics under compression. J Biomech 41, 3340-3348.

Shoemaker, S.C., Markolf, K.L., 1986. The Role of the Meniscus in the Anterior-Posterior Stability of the Loaded Anterior Cruciate-Deficient Knee - Effects of Partial Versus Total Excision. Journal of Bone and Joint Surgery-American Volume 68A, 71-79.
Sibole, S., Bennetts, C., Borotikar, B., Maas, S., van den Bogert, A.J., Weiss, J.A., Erdemir, A., Year Open knee: a 3D finite element representation of the knee joint,. In 34th Annual Meeting of the American Society of Biomechanics. Providence, RI.

Silva, M., Shepherd, E.F., Jackson, W.O., Pratt, J.A., McClung, C.D., Schmalzried, T.P., 2003. Knee strength after total knee arthroplasty. Journal of Arthroplasty 18, 605-611.

Spoor, C., Veldpaus, F., 1980. Technical note: Rigid body motion calculated from spatial coordinates of markers. Journal of biomechanics 13, 391-393.

Stagni, R., Fantozzi, S., Cappello, A., Leardini, A., 2005. Quantification of soft tissue artefact in motion analysis by combining 3D fluoroscopy and stereophotogrammetry: a study on two subjects. Clinical biomechanics 20, 320-329.

Staubli, H.U., Schatzmann, L., Brunner, P., Rincon, L., Nolte, L.P., 1999. Mechanical tensile properties of the quadriceps tendon and patellar ligament in young adults. Am J Sports Med 27, 27-34.

Stevens-Lapsley, J.E., Balter, J.E., Kohrt, W.M., Eckhoff, D.G., 2010. Quadriceps and hamstrings muscle dysfunction after total knee arthroplasty. Clinical orthopaedics and related research 468, 2460-2468.

Stevens-Lapsley, J.E., Balter, J.E., Wolfe, P., Eckhoff, D.G., Kohrt, W.M., 2012. Early neuromuscular electrical stimulation to improve quadriceps muscle strength after total knee arthroplasty: a randomized controlled trial. Physical therapy 92, 210-226.

Stiehl, J.B., Komistek, R.D., Dennis, D.A., Keblish, P.A., 2001. Kinematics of the patellofemoral joint in total knee arthroplasty. Journal of arthroplasty 16, 706-714.

Tanska, P., Mononen, M.E., Korhonen, R.K., 2015. A multi-scale finite element model for investigation of chondrocyte mechanics in normal and medial meniscectomy human knee joint during walking. J Biomech 48, 1397-1406.

Taylor, S.J., Perry, J.S., Meswania, J.M., Donaldson, N., Walker, P.S., Cannon, S.R., 1997. Telemetry of forces from proximal femoral replacements and relevance to fixation. J Biomech 30, 225-234.

Taylor, S.J., Walker, P.S., Perry, J.S., Cannon, S.R., Woledge, R., 1998. The forces in the distal femur and the knee during walking and other activities measured by telemetry. J Arthroplasty 13, 428-437.

Van de Velde, S.K., Gill, T.J., DeFrate, L.E., Papannagari, R., Li, G., 2008. The effect of anterior cruciate ligament deficiency and reconstruction on the patellofemoral joint. American journal of sports medicine 36, 1150-1159.

van der Esch, M., Steultjens, M., Knol, D.L., Dinant, H., Dekker, J., 2006. Joint laxity and the relationship between muscle strength and functional ability in patients with osteoarthritis of the knee. Arthritis and rheumatism 55, 953-959.

Varadarajan, K.M., Gill, T.J., Freiberg, A.A., Rubash, H.E., Li, G., 2010. Patellar tendon orientation and patellar tracking in male and female knees. Journal of orthopaedic research 28, 322-328.

von Eisenhart-Rothe, R., Lenze, U., Hinterwimmer, S., Pohlig, F., Graichen, H., Stein, T., Welsch, F., Burgkart, R., 2012. Tibiofemoral and patellofemoral joint 3D-kinematics in patients with posterior cruciate ligament deficiency compared to healthy volunteers. BMC musculoskeletal disorders 13, 231.

Woo, S.L., Hollis, J.M., Adams, D.J., Lyon, R.M., Takai, S., 1991. Tensile properties of the human femur-anterior cruciate ligament-tibia complex. The effects of specimen age and orientation. Am J Sports Med 19, 217-225.

Wu, J.Z., Herzog, W., Epstein, M., 2000. Joint contact mechanics in the early stages of osteoarthritis. Medical engineering & physics 22, 1-12.

Yamaguchi, G.T., Zajac, F.E., 1989. A planar model of the knee joint to characterize the knee extensor mechanism. Journal of biomechanics 22, 1-10.

Yao, J., Snibbe, J., Maloney, M., Lerner, A.L., 2006. Stresses and strains in the medial meniscus of an ACL deficient knee under anterior loading: A finite element analysis with image-based experimental validation. J Biomech Eng-T Asme 128, 135-141.

Zhang, W., Moskowitz, R.W., Nuki, G., Abramson, S., Altman, R.D., Arden, N., Bierma-Zeinstra, S., Brandt, K.D., Croft, P., Doherty, M., Dougados, M., Hochberg, M., Hunter, D.J., Kwoh, K., Lohmander, L.S., Tugwell, P., 2007. OARSI recommendations for the management of hip and knee osteoarthritis, part I: critical appraisal of existing treatment guidelines and systematic review of current research evidence. Osteoarthritis and cartilage / OARS, Osteoarthritis Research Society 15, 981-1000.

Zheng, N., Fleisig, G.S., Escamilla, R.F., Barrentine, S.W., 1998. An analytical model of the knee for estimation of internal forces during exercise. J Biomech 31, 963-967.

APPENDIX A: SUBJECT-SPECIFIC PREDICTIONS OF MECHANICS FOR MEDIALIZED DOME AND ANATOMIC PATELLAE

Appendix A includes supplementary figures for Chapter 5, describing the individual, subject-specific trends in PF kinematics, PF contact mechanics, patellar tendon moment arm and angle for medialized dome and anatomic TKA subjects. Experimental TF and PF kinematics include excursions for additional anatomic (n=17) and dome (n=10) subjects excluded from the data presented in Chapter 5.

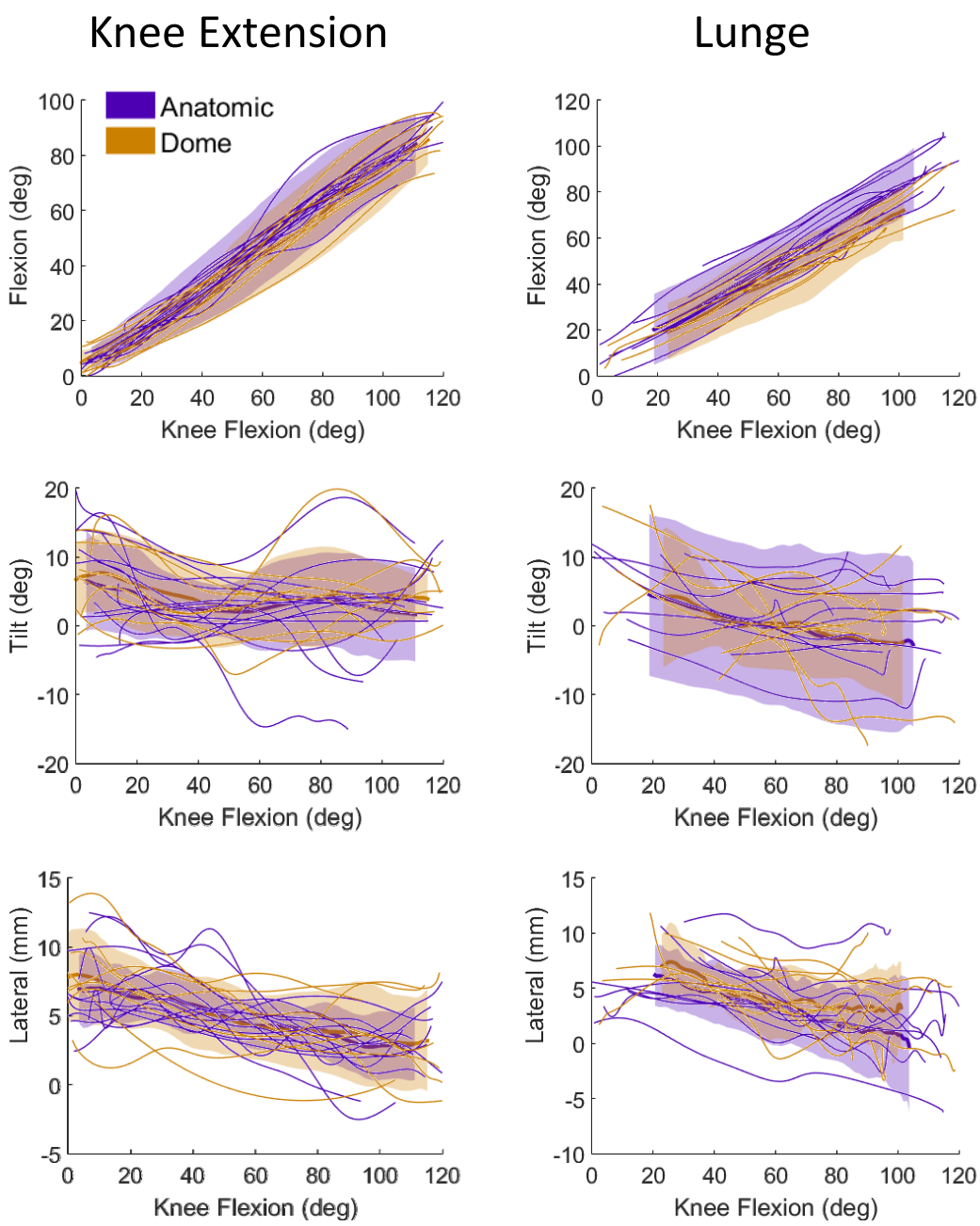

Figure A.1 Comparison of average +/- 1 standard deviation of experimental PF kinematics for medialized dome and anatomic subjects performing the knee extension and lunge. Subject-specific PF kinematics are shown using thin solid lines.

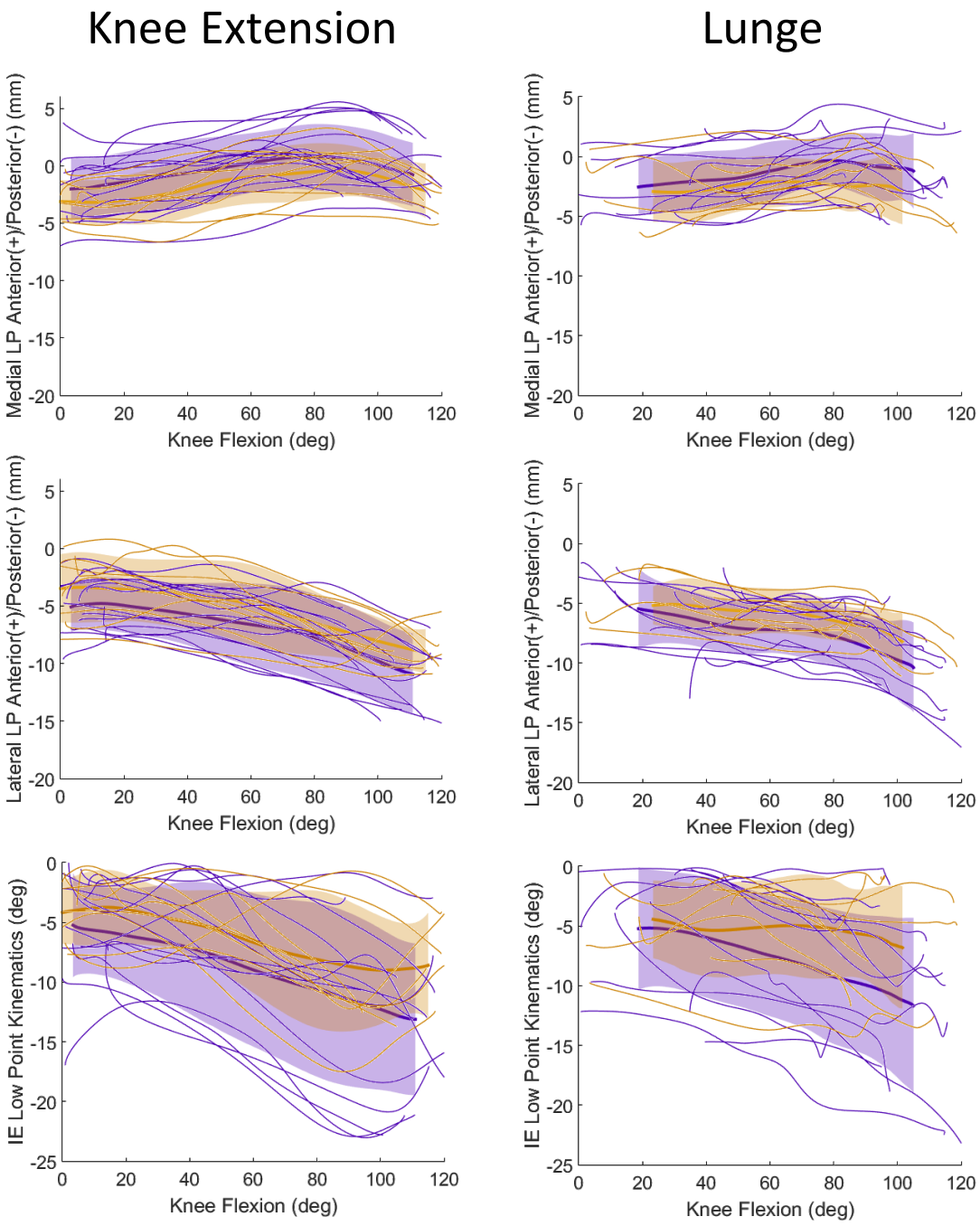

Figure A.2 Comparison of average +/- 1 standard deviation of experimental TF low point kinematics for medialized dome and anatomic subjects performing the knee extension and lunge. Subject-specific low point data are shown using thin solid lines.

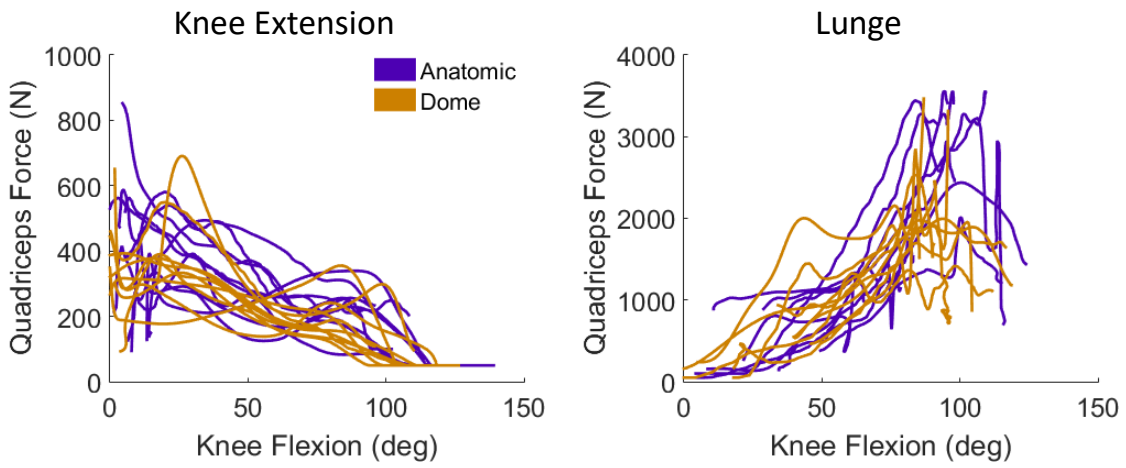

Figure A.3 Subject-specific quadriceps force predictions from musculoskeletal modeling for knee extension and lunge

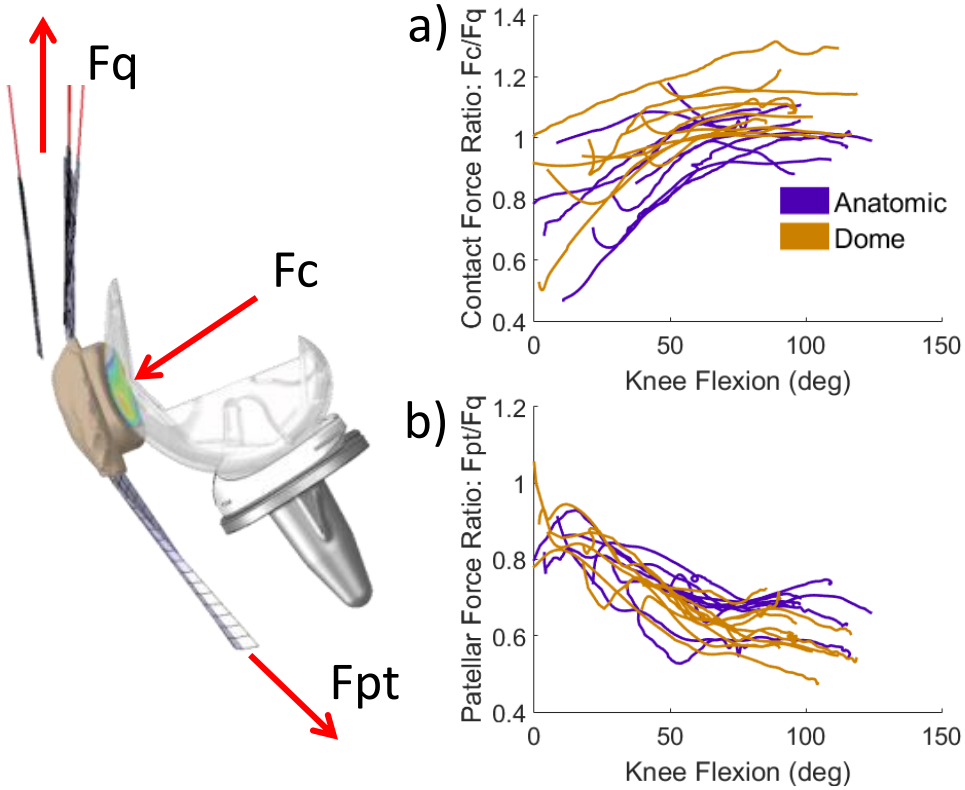

Figure A.4 Comparison of a) contact force ratio and b) patellar force ratio between medialized dome and anatomic subjects. Force ratios (right) shown for the lunge activity: Fc = contact force, Fq = quadriceps force, Fpt = patellar tendon force.

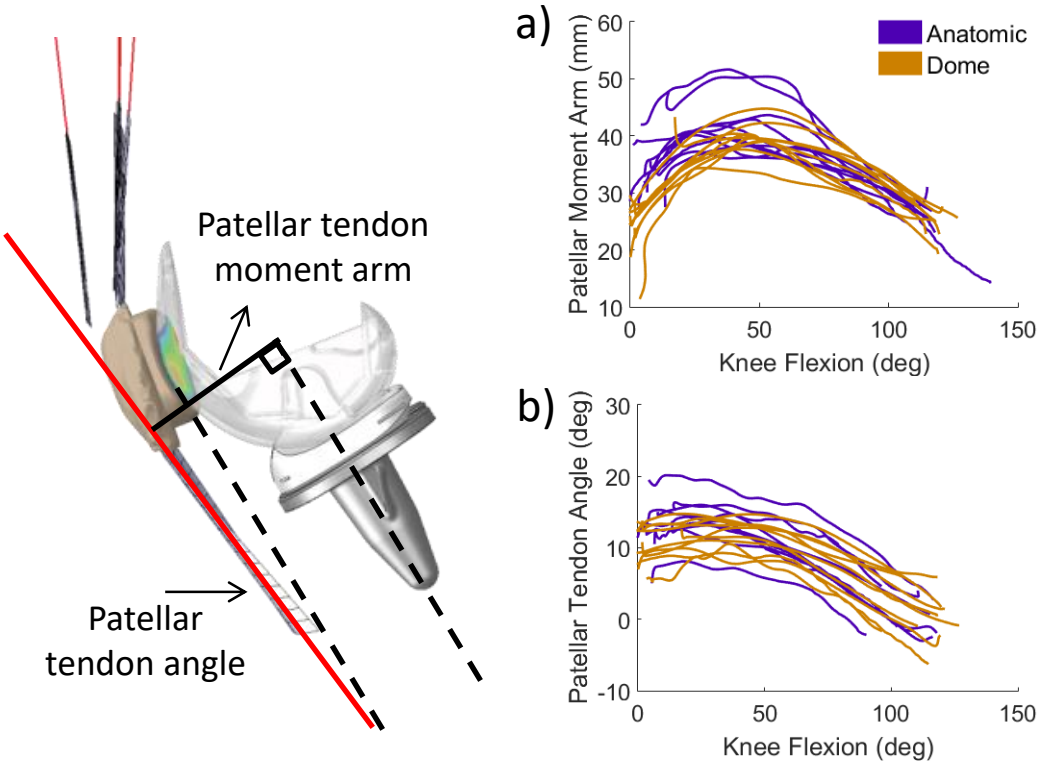

Figure A.5 Comparison of a) patellar tendon moment arm and b) patellar tendon angle between medialized dome and anatomic subjects. Results shown for knee extension only.